Resolution-Dependent Estimates of Multiple Sclerosis Lesion Loads: Evaluation of Magnetic Resonance Imaging of the Brain at 4 Tesla Versus 0.5 and 1.5 Tesla

by

Matthew K. Erskine
Department of Physiology

Submitted in partial fulfillment of the
requirements for the degree of
Master of Science

Faculty of Graduate Studies
The University of Western Ontario
London, Ontario
September 30, 1998

Abstract

Changes in brain lesion loads assessed with magnetic resonance imaging (MRI) scans, usually obtained at 0.5 or 1.5 T, are used as a measure of disease evolution in virtually all long-term natural history studies and treatment trials of multiple sclerosis. In this study, a comparison was made between the total lesion volume and individual lesions observed in typical "clinical trial" 0.5 and 1.5 T MRI scans versus high-resolution 4 T scans, representing the highest quality imaging achievable in a clinically reasonable timeframe using current technology. Lesions were quantified in 14 patients using a computer-assisted segmentation tool. The 4 T scans showed an 85% increase in total lesion volume when compared with the 0.5/1.5T scans ($n = 14$, $r = 0.875$, $p < 0.001$). In several instances, the 0.5/1.5 T scans showed individual lesions that coalesced into larger areas of abnormality in the 4 T scans. When individual lesions were directly compared ($n = 378$), 49% of those seen at 4 T were not detected at 0.5/1.5 T. These lesions were small with an average volume of 0.061 ± 0.008 cm^3 (range: 0.004 to 0.941 cm^3) and accounted for approximately 6% of the total 4 T lesion volume. The relationship between individual lesion volumes was linear ($r = 0.772$, $p < 0.001$), with a slope of 1.81 showing that the lesion volume detected at 4 T tended to increase with increasing 0.5/1.5 T volume. The 4 T voxels were less than one quarter the size of those used at 0.5/1.5 T and there were no consistent differences between the signal-to-noise ratios of the 4 T and 0.5/1.5 T images. Therefore, it appears that the increase in signal strength that accompanies the increase in field strength compensated for the loss in signal amplitude produced by the use of smaller voxels. This enabled the acquisition of images with improved in-plane and out-of-plane resolution, resulting in substantially increased lesion detectability at 4 T.

Keywords: Brain, diseases • Multiple Sclerosis • Magnetic Resonance Imaging (MRI) • Lesion Detection / Quantification • Field Strength • Image Resolution • 4 T

To My Parents

and To My Extended Family

Who have given me the support and encouragement

that has allowed me to actually live out the Erskine Family motto

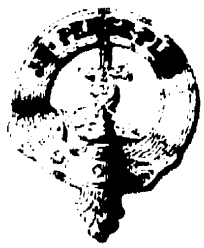

Acknowledgements

I would first like to express my sincerest appreciation to my supervisor, Dr. Steve Karlik, for his guidance, support, patience, and understanding. Although my arrival in the Karlik lab was rather serendipitous, I am extremely fortunate to have found myself working with a supervisor whose generosity and unpretentious nature endowed the lab with a collegial atmosphere that encouraged research to be carried out independently in spirited good fellowship.

My thanks also go to the members of my advisory committee, Drs. Doug Jones, Ravi Menon, and Jane Rylett for their helpful suggestions and comments. I extend a special thank you to Dr. Ravi Menon for his technical assistance with my early spectroscopy experiments.

Technical assistance and guidance on the use of the 4 T scanner was also provided by Mr. Joe Gati, Mr. Rob Bartha, and Dr. Paula Gareau. Dr. Ross Mitchell modified his image segmentation program, *Segtool*, in order to enable me to analyse my data, and Ms Lorraine Hewitt instructed me in the use of the program. To all of you, I extend a warm and heartfelt thank you.

This study would not have been possible without the cooperation of Drs. George Rice and George Ebers, who allowed me access to their patients at the London Multiple Sclerosis Clinic. I am also extremely grateful for the assistance of Ms. Debra King and Ms. Rita Schumacher who graciously assumed responsibility for the recruitment of study participants. As well, I would like to acknowledge the cooperation and understanding of the staff of the 4th floor outpatient department of the University Campus of London Health Sciences Centre, who often reorganized their patient appointments in order to accommodate unexpected changes in the scheduling of my imaging examinations.

My deepest gratitude is extended to the staff and technicians of the magnetic resonance imaging unit at the University Campus of London Health Sciences Centre for their cheerful and professional assistance. Not only did the technicians acquire all of the 0.5 T and 1.5 T imaging data used in this study, but they were always obliging, even in the wee hours of the morning, when I was underfoot as I retrieved archived data. Of course, I am equally indebted to the patients of the London Multiple Sclerosis Clinic who agreed to take part in this research. These patients freely gave of their time and spent an extended period in the confines of the imaging scanner in the hope that their efforts would eventually help others suffering from multiple sclerosis.

To the faculty, staff, and students of the Department of Physiology and the Tom Lawson Family Imaging Research Laboratories of the John P. Robarts Research Institute, I am thankful for the support, encouragement and assistance I have received on many occasions during my two years at Western. I will remember most fondly, the members of the Karlik lab and my other friends in the Department of Physiology, as well as the youth and leaders of the 31st A Cub Pack, who have made my time in London more rewarding and enjoyable.

Last, but definitely not least, I wholeheartedly thank my entire family for their continued support and encouragement. I especially thank my parents, Donald and Donna, and my grandmother, Mrs. Margaret Kelly, without whose financial assistance, I would not have been able to pursue my dream of becoming a physician.

This research was supported by the Multiple Sclerosis Society of Canada

Table of Contents

List of Tables

List of Figures

List of Appendices

List of Symbols, Abbreviations, and Nomenclature

2D	two-dimensional
3D	three-dimensional
B_0	main magnetic field
BBB	blood brain barrier
CNR	contrast-to-noise ratio
CNS	central nervous system
CPMS	chronic progressive multiple sclerosis
CSF	cerebrospinal fluid
FID	free induction decay
FOV	field of view
GM	gray matter
M	net magnetization vector
MHz	megahertz
MR	magnetic resonance
MRI	magnetic resonance imaging
MRS	magnetic resonance spectroscopy
ms	milliseconds
MS	multiple sclerosis
MT	Magnetization transfer
NAWM	normal appearing white matter
NEX	number of excitations
NMR	nuclear magnetic resonance
PDW	proton density weighted
Pixel	2D imaging unit of the MR image
RF	radio frequency
RRMS	relapsing-remitting multiple sclerosis
SNR	signal-to-noise ratio
SPMS	secondary progressive multiple sclerosis
T	Tesla
T1	longitudinal relaxation time (spin-lattice relaxation time)
T1W	T1-weighted
T2	transverse relaxation time (spin-spin relaxation time)
T2W	T2-weighted
TE	echo time
TR	repetition time (ms)
Voxel	3D volume of tissue represented by a pixel on a MR image
WM	white matter

1

Introduction

1.1 Multiple Sclerosis

1.1.1 Pathophysiology and Etiology

Multiple sclerosis (MS) is a cell-mediated autoimmune disease of the central nervous system (CNS), for which there is no effective treatment or cure. It is the most significant human demyelinating disease, affecting more than 80 per 100,000 people in Ontario (Hader *et al.*, 1988). MS usually strikes in early adult life and affects females twice as frequently as males (Ebers *et al.*, 1998). The pathological hallmark of the disease is the destruction of the myelin sheaths of neurons in the CNS. During the course of MS, the integrity of the blood brain barrier (BBB) is compromised, inflammatory cells enter the CNS, and demyelination ensues. The etiology of multiple sclerosis is not firmly established; however, it is currently hypothesized that the underlying pathogenesis of MS is related to an inappropriate class of immune response against myelin antigens

initiated by a viral infection. Environmental factors and genetic predisposition combine to influence the class of immune response and hence, the development of the disease (for review see Weiner, 1998).

1.1.2 Clinical Features

The clinical features of MS are of bewildering variability. Demyelination leads to clinical symptoms through three principal effects on the transmission of nerve impulses: a reduced conduction velocity; an increase in refractory period, or a complete blockage of transmission in severely or completely demyelinated axons. While demyelination may be partially reversible, axonal loss and reactive gliosis develop in some lesions, causing irreversible damage (McDonald *et al.*, 1970). Lesions inhibit or block neural transmission and produce a broad range of clinical symptoms, the most common of which include loss of balance, ataxia, weakness or paralysis of the limbs, blurred vision leading to partial or complete blindness, sensory and cognitive deficits, and dysfunction or incontinence of the bladder and bowel. The severity of the pathological process in multiple sclerosis depends on many variables. Present techniques, however, do not permit determination of the relative contributions of edema, inflammation, blood-brain barrier disruption, demyelination, and gliosis to clinical expression. The severity of clinical symptoms is more often related to the location of the damage than to the degree and extent of the pathological process. Some patients with severe disability due to MS carry a relatively low total volume of damaged areas, but the damage is strategically located in key areas of the nervous system, such as the brain stem, spinal cord and optic nerve (for review see Miller, 1996).

Not only is multiple sclerosis capable of producing a broad range of symptoms, the disease course, both within and between patients, is also highly variable. It varies in the same patient at different times and there is also

striking variability between patients. Early in the course of the disease, periods of disability alternate with periods of virtually complete normality. Later, there is usually an accumulation of deficit, partly due to incomplete recovery from individual relapses, and partly due to an insidious progression - the secondary progressive form of the disease. In some patients the disease runs a benign course for many years, while in others, death comes within a year of onset. There is, moreover, the mysterious and infrequent primary progressive form of the disease that progresses steadily from its inception. Although not clearly established, it is commonly believed that the aforementioned relapsing-remitting MS (RRMS) and secondary progressive MS (SPMS) are two sequential phases of the same disease, while the less common primary chronic progressive form of the disease (CPMS), that afflicts 15% of patients, may entail different pathogenic mechanisms (Paty *et al.*, 1998).

1.1.3 Epidemiology

While multiple sclerosis can lead to severe disability and often strikes at a relatively young age, the mean survival, excluding CPMS, is 35 to 40 years from the time of diagnosis (Sadovnick *et al.*, 1992). Because life span is not greatly reduced in MS, the disease has a major impact on the quality of life of both the patient and their family. It is a great psychological burden to deal with an unpredictable, incurable, and potentially disabling disease. In addition to psychological and emotional distress, multiple sclerosis commonly results in financial hardship. Less than 50 percent of patients function as wage earners or homemakers after ten years of disease (Paty *et al.*, 1998) and one study has estimated the total cost of the current MS population to US society in terms of lost wages and medical care at $29 billion a year (Inman, 1984).

1.2 The Role of Magnetic Resonance Techniques in Understanding MS

1.2.1 Magnetic Resonance Imaging and Diagnosis

Over the past 10 to 15 years, magnetic resonance (MR) techniques have had a major impact on our understanding of multiple sclerosis. In a disease with a high degree of variability of clinical signs and symptoms over time and between individuals, and with no current adequate biological markers of disease progression, MR techniques provide a direct indication of disease activity. Magnetic resonance imaging (MRI) is exquisitely sensitive for detecting brain abnormalities, particularly in the evaluation of white matter diseases like MS. In fact, MRI far outperforms any other imaging technique, and has been used to aid in the diagnosis of multiple sclerosis since 1981 (Young *et al.*, 1981). The sensitivity of MRI in detecting lesions in patients with clinically definite MS (CDMS) is 85%, compared with 25% for computed tomography (CT) (Sheldon *et al.*, 1985).

White matter consists mostly of axons with their envelope of myelin, along with two types of neuroglial cells: oligodendrocytes and astrocytes. The myelin sheath is a lamellar structure with alternating layers of lipid and protein. However, the ratio of lipid to protein is quite high (approximately 70% lipid to 30% protein), making the myelin relatively dehydrated (Rumsby, 1978). Because of the high density of myelinated axons, the water content of white matter is less than that of gray matter. This difference in water concentration allows white and gray matter to be distinguished on MR images and, as will be explained in more depth in the next chapter, is also responsible for the sensitivity of MRI for MS lesions. Inflammation and demyelination result in increased water content in MS

lesions, making them relatively easy to discern from normal-appearing white matter (NAWM). MS lesions usually appear as discrete foci with relatively well defined margins on MR images. Most are small and irregular, but larger lesions can coalesce to form large regions of diffuse abnormality, especially in periventricular white matter (Figure 1.1). It must be noted that although MRI is quite sensitive for MS lesions, it is relatively nonspecific. Thus, while positive MRI results are necessary to upgrade the diagnosis from clinically probable MS to clinically definite MS, the diagnosis is fundamentally based on clinical criteria and MRI abnormalities alone are not sufficient for a diagnosis (Miller *et al.*, 1998).

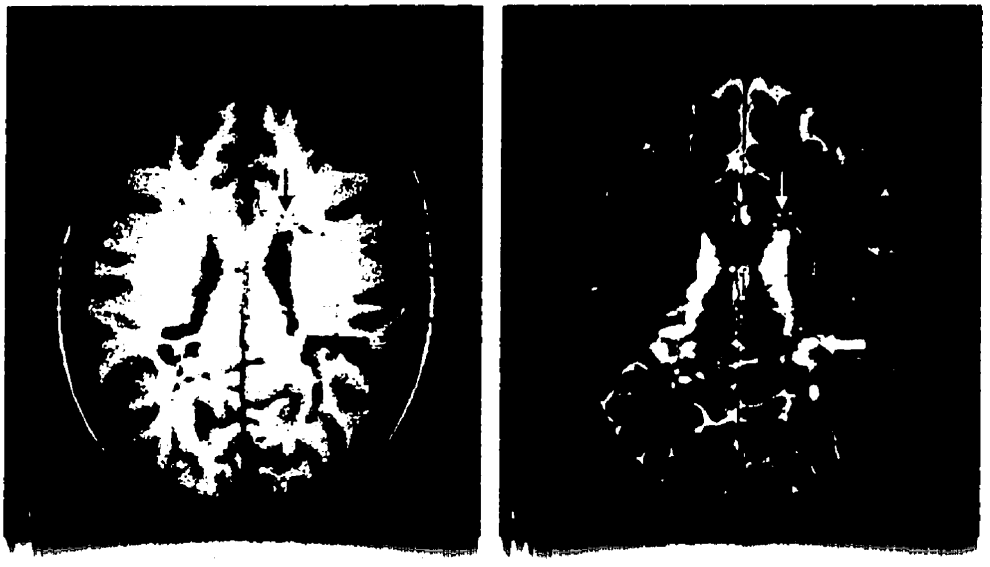

Figure 1.1 MR Images of MS Lesions

T1-weighted (a) and T2-weighted (b) images of periventricular white matter depicting small focal lesions (small arrows) and large focal areas of abnormality surrounded by diffuse lesion (large arrows).

1.2.2 Serial MRI Studies and Natural History

While MRI has an established role as an aid in the diagnosis of multiple sclerosis, serial MR studies have more recently proven their usefulness for studying the natural history of the disease. Early studies imaging post-mortem material demonstrated a good correlation between regions of diseased tissue and areas of abnormality detected by MRI (Stewart *et al.*, 1984; Ormerod *et al.*, 1987). Studies of the natural history of multiple sclerosis using T2-weighted images provided a new understanding of the disease process. Clinically silent lesions, that occurred 5 to 10 times more frequently than clinical symptoms in patients in the relapsing phase of the disease, were often seen (Isaacs *et al.*, 1988; Willoughby *et al.*, 1989). Some initial studies of contrast-enhancing lesions on T1-weighted images indicated that most new lesions begin with disruption of the BBB in relapsing-remitting and secondary progressive MS (Miller *et al.*, 1988; Bastianello *et al.*, 1990; Harris *et al.*, 1991; Thompson *et al.*, 1991; 1992; Barkhof *et al.*, 1992). The concept that BBB leakage is a consistent early feature of lesion evolution has been strengthened by recent studies that have imaged patients at weekly intervals and found that all new lesions seen on T2-weighted images are initially observed as areas of BBB disruption (Kermode *et al.*, 1990). Just as with T2 lesions, a majority of enhancing lesions on T1 images occur in clinically stable individuals (Lai *et al.*, 1996).

1.2.3 Magnetic Resonance Spectroscopy

In addition to standard imaging sequences, the examination of lesion metabolites has provided valuable information not available on images. Major advances in the understanding of the biochemical basis for the pathology of MS have resulted from the use of magnetic resonance spectroscopy (MRS). In

particular, the study of *N*-acetyl aspartate (NAA) levels provides information about axonal status (Arnold *et al.*, 1990; Davie *et al.*, 1994), and detection of abnormal lipid peaks may indicate myelin disruption (Wolinsky *et al.*, 1990). Also, a recent chemical shift imaging (CSI) study has implicated an increase in creatine with gliotic remyelination, increased choline with inflammation and myelin turnover, and decreased NAA with axonal loss or dysfunction (Pan *et al.*, 1996).

1.2.4 MR Evidence of Diffuse Disease

While MRI is very sensitive for detecting the large focal lesions that have been the hallmark of MS, the histology of multiple sclerosis reveals widespread and ubiquitous disease including diffuse astrocytic hyperplasia, patchy edema, and perivascular cellular inflammation that is not confined to white matter lesions (Adams, 1977; Allen *et al.*, 1979). Previous magnetic resonance imaging (MRI) studies have failed to show these abnormalities, presumably due to insufficient resolution (too large a voxel leads to signal averaging from the entire volume thereby obscuring small, localized abnormalities). However, studies that have examined the average spin-lattice (T1) and spin-spin (T2) relaxation rates of the protons in normal appearing white matter (NAWM) have demonstrated significantly longer relaxation times, indicating that the white matter outside detectable lesions is also abnormal (Ormerod *et al.*, 1986; Larsson *et al.*, 1988; Miller *et al.*, 1989; Armspach *et al.*, 1991). Both diffusion weighting (Larsson *et al.*, 1992) and magnetization transfer studies on large voxels have confirmed the existence of diffuse abnormalities in NAWM (Loevener *et al.*, 1995; Tomiak *et al.*, 1994; Gass *et al.*, 1994; Hiele *et al.*, 1994). These findings may be related to a fundamental change in the biochemistry of the white matter in MS associated with a change in macromolecules and myelin (Francis *et al.*, 1995; McDonald *et al.*, 1994). Confirmatory animal studies using experimental allergic encephalo-

myelitis (EAE) have shown abnormal water diffusion (Verhoye *et al.*, 1996) and macromolecule resonances in ^{1}H spectra (Zelaya *et al.*, 1996). Due to the diffuse nature of MS and the limited resolution of 0.5 and 1.5 T clinical MRI scanners, detection of these microscopic abnormalities remains problematic.

1.3 The Role of Magnetic Resonance Techniques in Managing MS

1.3.1 Prognostic Value of MRI

Notwithstanding the contributions MRI studies have made to the understanding of multiple sclerosis, the correlation between T2 lesion load and disability in established MS is disappointingly weak; typical correlations (ρ-values) have been in the range of 0.15 to 0.46 (Gass *et al.*, 1994; Filippi *et al.*, 1995; Gasperini *et al.*, 1996). These weak correlations are no doubt influenced by problems with measurement error in quantifying MRI parameters due to the clinical complexity and biological variability of the disease. The low pathologic specificity of T2 weighted abnormalities, which does not allow discrimination of demyelination and axonal damage – which may represent the greatest contribution to disability - from edema and inflammation, also helps explain the low correlations. However, it would appear that MRI exams are of prognostic value in predicting which patients presenting with monosymptomatic disease will go on to develop clinically definite multiple sclerosis.

The predictive value of changes on MR images is of considerable importance both from the standpoint of selecting patients for clinical trials focusing on the early stage of MS and on the routine management of patients as

new treatments evolve that may have their greatest effectiveness when used early in the course of the disease. Studies focusing on the number of lesions seen at the time of presentation have found that abnormal imaging results (defined as four or more T2 lesions) have a positive predictive value of patients developing CDMS within 5 years (Morrissey *et al.*, 1993). Similarly, a study looking at lesion load, rather than number, has reported a positive predictive value of 90% for developing multiple sclerosis in those with a high lesion load at presentation (Filippi *et al.*, 1994). A recent 10-year follow-up study has provided further information on the risk for long-term disability: those patients with ten or more lesions at presentation were most likely to have scores greater than three on the Expanded Disability Status Scale (EDSS) (O'Riordan *et al.*, 1996).

1.3.2 MRI and Clinical Trials

In addition to its prognostic utility, MRI has become established as a very important tool in monitoring the efficacy of potential therapies for MS. Following the seminal work on Betaseron® (Paty *et al.*, 1993), MRI assessments, usually with quantitative measurement of lesion activity, are a principal component of all current clinical trials. Serial MRI is attractive in this regard as it provides objective and direct evidence of the evolving pathological process and its modification by treatment. In 1996, a task force of the US Multiple Sclerosis Society published guidelines for the use of MR techniques in monitoring treatment (Miller *et al.*, 1996). The task force recommended that serial MRI, because of its high sensitivity for detecting asymptomatic disease in early relapsing-remitting and secondary progressive MS, be used as the primary outcome measure in exploratory studies of new therapeutic agents. It also recommended that MRI be used as a secondary outcome measure in all definitive (phase III) clinical trials. Furthermore, the task force

recommended that MRI be used to define appropriate cohorts for entry into trials aimed at preventing conversion from an isolated clinical syndrome to clinically definite multiple sclerosis.

1.4 Study Significance, Hypothesis, and Objectives

1.4.1 Significance

Magnetic resonance imaging provides an objective and direct assessment of the evolving pathology in multiple sclerosis, a devastatingly debilitating disease for which there is currently no effective treatment or cure. With the evolution of magnetic resonance technology, it is likely that MR techniques will become even more important in investigating the natural history of the disease and monitoring treatment efficacy. High field 4 Tesla (T) MRI scanners have the potential to further increase the resolution of MR images, leading to more precise lesion detection. Improved lesion detection may, in turn, result in earlier diagnosis of clinically definite MS, increased prognostic value, better understanding of the underlying pathological process of the disease. improved selection of cohorts for clinical trials and more precise monitoring of treatment effects. While the potential benefits of high field 4 T magnets include higher signal-to-noise ratio (SNR), high speed, high resolution, and the capability for MR spectroscopy and functional imaging, there is a definite cost advantage to employing middle-field-strength units. The purchase price and ongoing maintenance costs are lower for the 1.5 T scanners and the smaller magnetic field makes them easier to situate within or near existing hospital buildings. Although there is a consensus that high field magnets produce images that are subjectively better than lower field systems, this has not been proven to result in increased accuracy in the detection

of pathology (Jack *et* al., 1990; Steinberg *et* al., 1990). While a previous comparison of the diagnostic accuracy of 0.5 T and 1.5 T magnetic resonance imaging found a similar number of white matter lesions were detected in MS patients regardless of magnetic field strength used (Lee *et al.*, 1995), to date, no comparison has been made between lesion detection at high (4 T) and mid fields (1.5 and 0.5 T).

1.4.2 Hypothesis

It is hypothesized that high-resolution 4 Tesla MRI exams, representative of the highest quality imaging achievable in a clinically reasonable timeframe with current technology, will result in an increased detectable lesion load when compared with standard clinical MRI exams performed at 1.5 and 0.5 Tesla.

1.4.3 Objectives

The objective of this research was to first determine the increase in the number of lesions, lesion volumes, and total lesion load detected at 4 T as compared to 0.5 and 1.5 T. Subsequently, the manner in which the total lesion load increased was to be investigated. Specifically, the relative contribution of small lesions that are not detected at 0.5 and 1.5 T versus the effect of more precise in-plane and out-of-plane edge detection of larger lesions seen at all field strengths was investigated. Finally, keeping in mind the large number of uncontrolled variables, the cause of any increase in total lesion load was to be explored. Does the increase in lesion load result primarily from improved image resolution due to decreased slice thickness, smaller pixel size, and higher SNR at 4 T, or from improved contrast-to-noise ratios produced by the imaging parameters used at the higher field?

1.5 Thesis Outline

The first chapter introduced multiple sclerosis, the eventual treatment or cure for which will hopefully be facilitated in some small part by this research. Included was an overview of the current state of magnetic resonance research into MS, followed by the significance of the study, guiding hypothesis, and overall objectives for this investigation. The second chapter consists of a description of the theory and practice of magnetic resonance imaging as it applies to this project. The rationale for the study can be found in chapter three, while a description of my methods, as well as the results of my research, and discussion of significant results, limitations and possible sources of error are located in chapters four, five and six, respectively. The final chapter summarizes and suggests the future direction of the work, and indicates where the methodology could be changed in order to improve the overall results. Finally, Appendix A provides information on the ethics approval of this research.

2

Magnetic Resonance Imaging

2.1 Historical Perspective

Nuclear magnetic resonance was discovered in 1946 (Bloch *et al.*, 1946; Purcell *et al.*, 1946). Felix Bloch of Stanford and Edward Mills Purcell of Harvard had worked together during World War II on an anti-radar project for the U.S. government. After the war, they returned to their respective laboratories, where they independently and almost simultaneously discovered the phenomenon of nuclear magnetic resonance (NMR). They were jointly awarded the Nobel Prize for Physics in 1952. NMR quickly developed into an important spectroscopic method for chemists, physicists, and biochemists to determine the structure of complex molecules (Friebolin, 1993). The first reported use of NMR signals to produce images was published by Dr. Paul Lauterbur in 1973 (Lauterbur, 1973). His work sparked the development of magnetic resonance imaging (MRI), a noninvasive technique that provides detailed images of the human body with unprecedented soft tissue contrast.

2.2 Principles of Magnetic Resonance

A basic understanding of the principles of magnetic resonance is necessary in order to understand how MRI machines operate, how to obtain the best possible images, and consequently, why imaging at 4 T instead of 0.5 or 1.5 T should allow for improved detection of MS lesions. Since an in-depth treatment of the physics underlying magnetic resonance is beyond the scope of this thesis, what follows is an elementary description of the fundamental principles of magnetic resonance and their applications to imaging.

2.2.1 Production of Net Magnetization

Magnetic resonance is based on the interaction between an external magnetic field and the nucleus of an atom that possesses spin. Nuclear spin (I), or more precisely, nuclear spin angular momentum, is one of the intrinsic characteristics of an atom. Depending on their atomic weight and atomic number, nuclei can possess integer values of spin, half-integer values, or zero spin. Only nuclei that possess spin can interact with magnetic fields. In biological systems, hydrogen (^1H) is the most abundant such nucleus (the body consists largely of H_20), and is therefore a natural choice for probing the body with MR techniques. Due to their large gyromagnetic ratio (γ), hydrogen atoms also produce the largest MR signals. A hydrogen nucleus, being a solitary proton, behaves in certain respects like a tiny bar magnet. This magnetism is an intrinsic property of the proton and can be thought of in analogy with Faraday's law: moving electrical charges produce magnetic fields. A bar magnet has a north and south pole, or more precisely, one end of the magnet has a greater positive magnetic field than the other end. A magnitude and direction to the magnetic field can be defined. A

Figure 2.1 A spinning Proton Generates a Magnetic Field

The spinning proton in the hydrogen nucleus produces a magnetic field and behaves as if it were a small bar magnet. It can be represented by a vector, as can any magnetic field.

hydrogen atom, or proton, can be viewed as a vector having an axis of rotation with a definite orientation and magnitude to this axis (Figure 2.1). This orientation of the nuclear spin vector and how it changes due to the experimental manipulations that the nucleus undergoes provide the basis for the MR signal.

Under normal conditions, the magnetic vectors representing hydrogen nuclei in body tissue are randomly orientated. Performing a vector addition of these spin vectors produces a zero sum, that is, no net magnetization is observed in the tissue (Figure 2.2). When the tissue is placed in a strong magnetic field ($\mathbf{B_0}$), the individual protons will begin to precess about the field. The protons will be tilted slightly away from the axis of the field, but the axis of rotation will be parallel to $\mathbf{B_0}$. This precession occurs because of the interaction of the magnetic field with the moving positive charge of the nucleus. The rate or frequency of precession is proportional to the strength of the magnetic field and is

expressed by the Larmor equation:

$$\omega_0 = \gamma \mathbf{B_0}/2\pi \qquad [2\text{-}1]$$

Where ω_0 is the Larmor frequency in megahertz (MHz), $\mathbf{B_0}$ is the magnetic field strength in Tesla that the proton experiences, and γ is the gyromagnetic ratio for hydrogen in $s^{-1}T^{-1}$. Thus, for hydrogen, the Larmor frequency is 42.577 MHz/T. While the protons are all aligned parallel to the main magnetic field $\mathbf{B_0}$, some will be pointing in the same direction, while those with higher energy, will be pointing in the opposite, antiparallel, direction (Figure 2.3). The energy difference between these two states, ΔE, increases with increasing $\mathbf{B_0}$ and γ:

$$\Delta E = h\gamma B_0 \qquad [2\text{-}2]$$

where h is Planck's constant, 6.626×10^{-34} J•s. Because the orientation parallel to $\mathbf{B_0}$ is of lower energy, there will be more protons in that orientation than in the antiparallel, higher energy orientation. The exact number of protons in

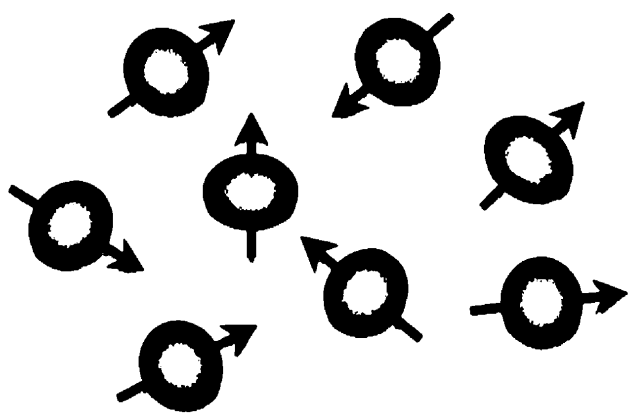

Figure 2.2 Randomly Oriented Nuclei

Hydrogen atoms, each behaving as a small magnet, are randomly oriented under normal conditions.

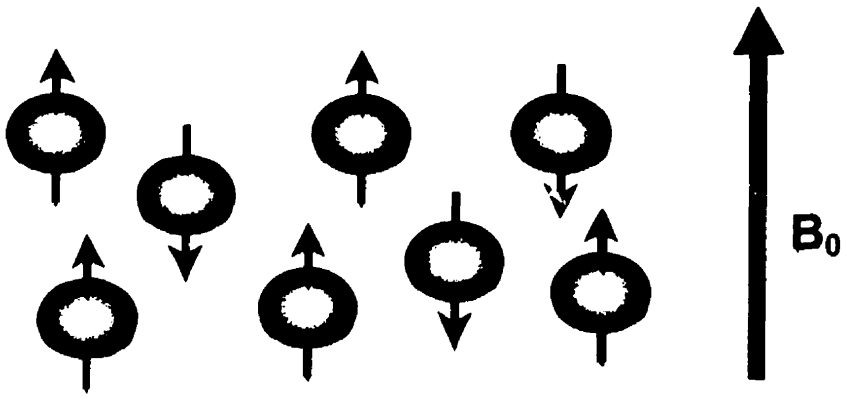

Figure 2.3 Nuclei in the Presence of a Magnetic Field

In an applied magnetic field, these small magnets align themselves in the direction of the field, with more pointing along the field than against it.

each energy level is governed by a distribution known as the Boltzman distribution:

$$N_{UPPER}/N_{LOWER} = e^{-\Delta E/kT} \qquad [2\text{-}3]$$

Where N_{UPPER} and N_{LOWER} are the number of protons in the upper and lower energy levels, respectively, T is the absolute temperature in Kelvin of the volume of tissue, and k is Boltzman's constant, $1.381 \times 10^{-23} J \cdot K^{-1}$. This unequal number of protons in each energy level means that the vector sum of spins will be non-zero and will point parallel to the magnetic field. In other words, the tissue will become magnetized in the presence of $\mathbf{B_0}$ with a value **M**, known as the net magnetization. The orientation of this net magnetization will be in the same direction as $\mathbf{B_0}$ and will be constant will respect to time (Figure 2.4). This arrangement with **M** aligned along the magnetic field is the normal, or equilibrium, state for the protons. It is the lowest energy configuration and the arrangement to which the protons will naturally try to return following any perturbation, such as energy absorption. This induced magnetization, **M**, is the

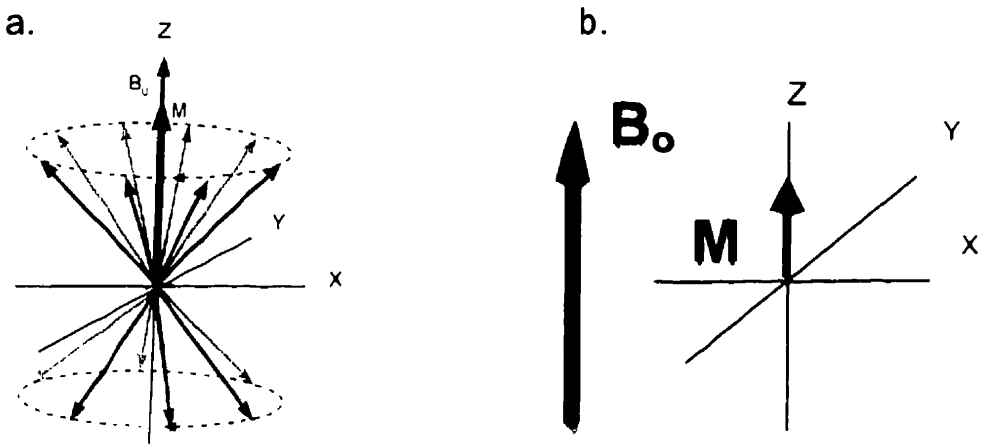

Figure 2.4 Individual spin vectors and Resultant Net Magnetization Vector

Microscopic (a) and macroscopic (b) diagrams of a collection of protons in the presence of an external magnetic field. Each proton precesses about the magnetic field tracing out two cones, one with a positive z component and one with a negative z component. Because there are more protons in the upper cone, there will be a nonzero vector sum, **M**, of constant magnitude and parallel to $\mathbf{B_0}$.

source of signal for all MR experiments. Consequently, all other things being equal, the greater the field strength $\mathbf{B_0}$, the greater the value of **M** and the greater the MR signal (Figure 2.5).

2.2.2 Excitation: Resonance Absorption

The MR experiment, in its simplest form, can be considered to be a re-emission phenomenon. Energy that will be absorbed is applied to the patient. A short time later, this energy will be reemitted, detected, and processed. The strong, static magnetic field $\mathbf{B_0}$, aligns the protons in the body, establishing an equilibrium magnetization **M**. To observe this magnetization (i.e., to image the body), the equilibrium must be disrupted. The simplest manipulation of **M** involves the application of a short burst, or pulse, of radiofrequency (RF) energy. During the pulse, the protons absorb a portion of the energy at a

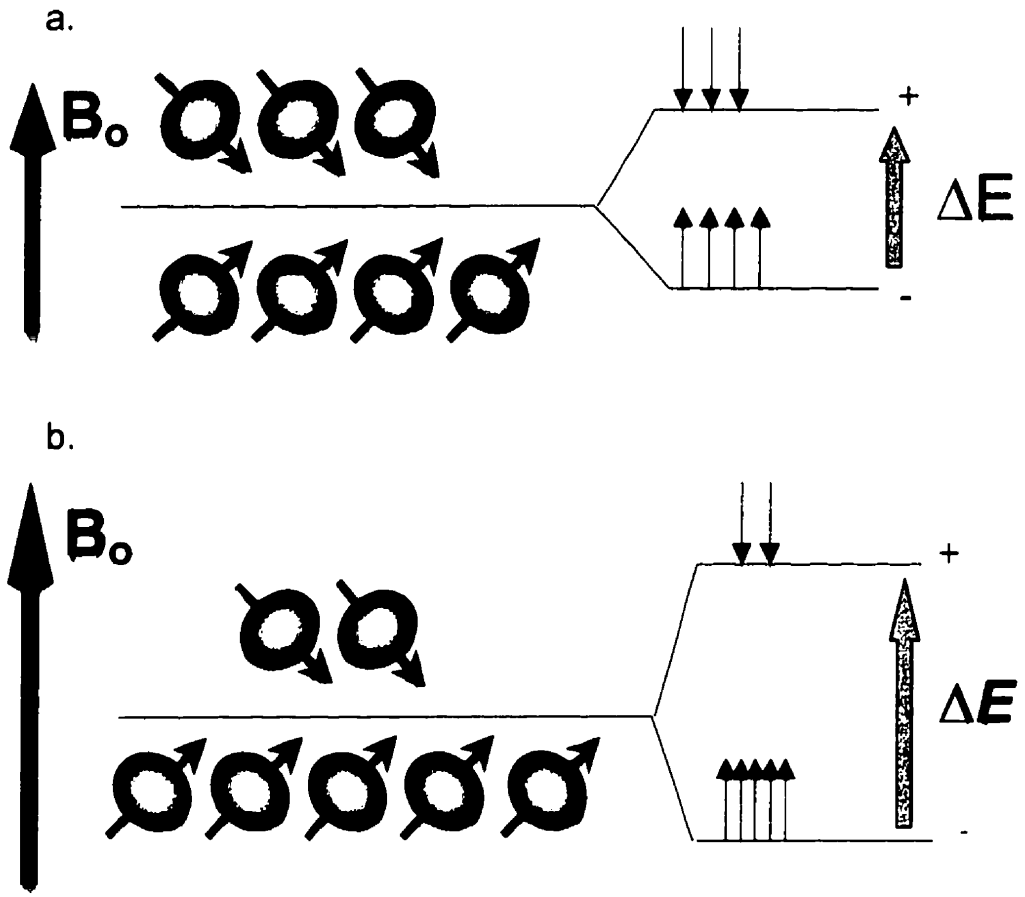

Figure 2.5 The Net Magnetization Vector Increases with Field Strength

The degree of alignment of protons with an applied magnetic field $\mathbf{B_0}$ depends on the strength of the field. With a weak field (a), the energy difference ΔE between the parallel and antiparallel states is small, so protons tend to distribute nearly equally between the two alignments. With a stronger field (b), more protons tend to align in the lower energy parallel orientation, resulting in a larger net magnetization **M**.

particular frequency known as their resonance frequency, which is determined according to the Larmor equation [2-1]. Following the pulse, the protons reemit the energy. The RF pulse represents the first step of a process by which **M** is transformed into a useable MR signal. Unlike any individual spin, which, when measured, can have only two alignments, the net magnetization of a group of

protons, **M**, may be oriented in any direction. By convention, the direction of the main field $\mathbf{B_0}$ is called the z axis or the longitudinal axis. The plane perpendicular to the main field is called the x-y plane or transverse plane. Spins can be detected only when their magnetization is in the transverse plane.

The dynamics of spins are fairly simple: spins precess precisely at the Larmor (or resonance) frequency of the applied magnetic field. In the classic view, the spins are tipped out of equilibrium by applying a second, oscillating, RF magnetic field, $\mathbf{B_1}$. This magnetic field is produced by a set of wires called the transmitter coil, which is designed and oriented so that its $\mathbf{B_1}$ is perpendicular to $\mathbf{B_0}$. When the RF pulse is applied, the effect of its $\mathbf{B_1}$ field is to cause **M** to rotate away from its equilibrium alignment along the z axis (Figure 2.6). The angle by

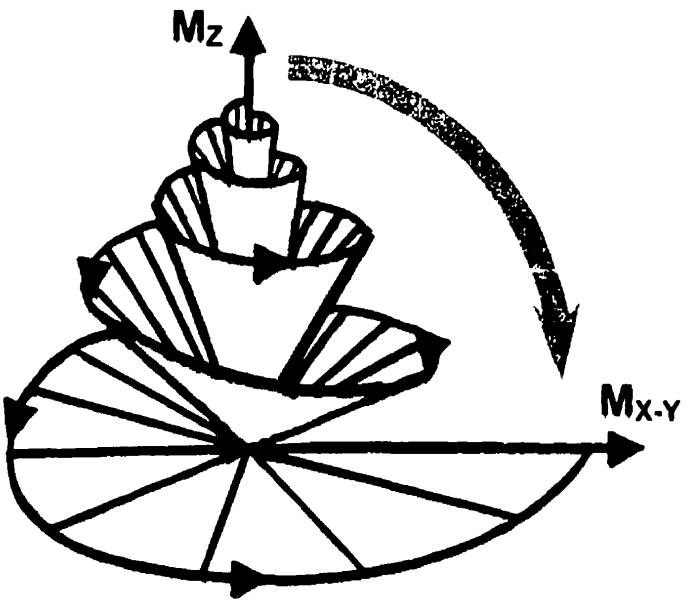

Figure 2.6 Effect of a 90° RF Pulse

The effect of a 90° pulse on the net magnetization is to tilt **M** into the transverse plane. The combination of the tilt produced by the RF pulse with the precession of the spins results in a complex spiraling motion. Note that as **M** is rotated by 90°, the $\mathbf{M_Z}$ component is reduced to zero and $\mathbf{M_{XY}}$ becomes equal to **M**.

which the RF pulse rotates **M** off the z axis is called the flip angle (for example, 90° or 180°). The flip angle increases with the amplitude and duration of the RF pulse. Any flip angle can be applied, depending upon the pulse sequence used in any given imaging method. Once the magnetization is in the transverse plane, **M** precesses about the direction of the main field. The rotation of the component of **M** in the transverse plane induces a voltage across the ends of a properly designed receiver coil. This voltage will decay with time as more and more of the excited protons give up their absorbed energy by a process known as relaxation. The induced voltage, the MR signal, is known as the FID, or free induction decay. The FID signal, which is analog in nature, is measured with an analog-to-digital converter (ADC) to produce a digital version of the signal for storage and postprocessing by a computer. The magnitude of the signal depends on the value of **M** immediately prior to the RF pulse (Figure 2.7).

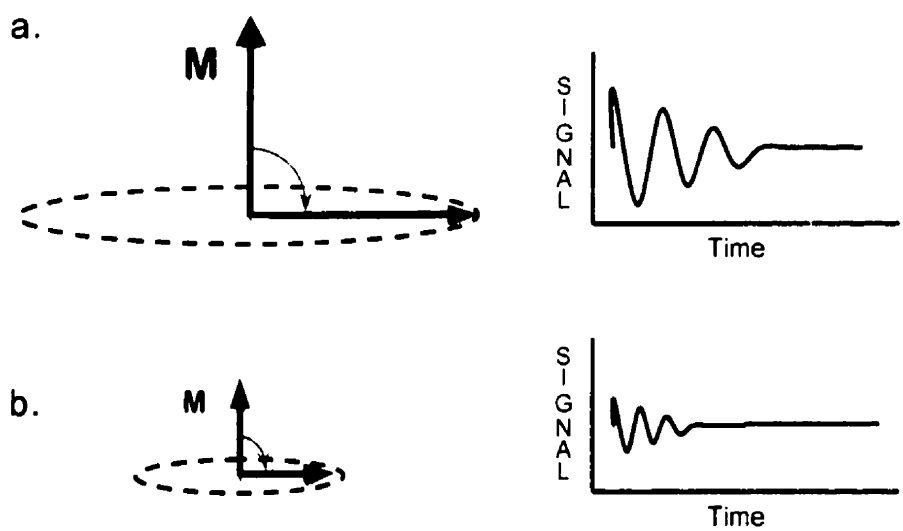

Figure 2.7 M is Translated into Signal Strength by a RF pulse.

With a large longitudinal magnetization (a), signal strength is large. With a small **M** (b), signal strength is reduced.

2.2.3 Relaxation

Equal in importance to resonance absorption in MR is the concept of relaxation. In resonance absorption, RF energy is absorbed by the protons when it is broadcast at the correct frequency. Relaxation is the process by which protons release this energy and return to their original configuration. While an individual proton is excited, relaxation times are measured for an entire sample and are average measurements. Two relaxation times can be measured, known as T1 and T2.

T1 is the time required for the z component of **M** to return to 63% of its original value following an excitation pulse. It is also known as the spin-lattice relaxation time or longitudinal relaxation time. T1 relaxation is the mechanism by which protons give up their energy to return to their original configuration parallel to $\mathbf{B_0}$. If a 90° pulse is applied to **M**, there will be no longitudinal magnetization following the pulse. As time goes on, a return of the longitudinal magnetization will be observed as the protons release their energy (Figure 2.8).

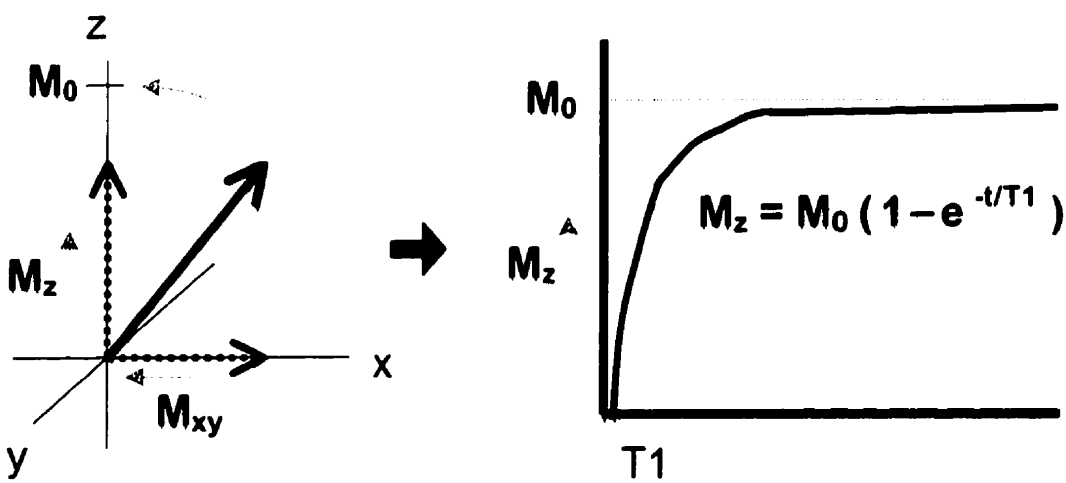

Figure 2.8 Recovery of Longitudinal Magnetization

$\mathbf{M_0}$ represents z magnetization at equilibrium. T1 is the longitudinal relaxation time constant. The equation for $\mathbf{M_z}$ is for a 90° tip of **M** after it has reached its $\mathbf{M_0}$ equilibrium value.

The return of magnetization follows an exponential growth process, with T1 being the time constant for the growth. After three T1 time periods, **M** will have returned to 95% of its value prior to the excitation pulse. The term spin-lattice refers to the fact that the excited proton, or spin, loses its energy to its surroundings, or lattice, rather than to another spin. The energy no longer contributes to spin excitation. For practical reasons, the time between successive RF pulses is usually insufficient for complete T1 relaxation. **M** will not be completely restored to its original value. Application of a second RF pulse will rotate **M** into the transverse plane, but with a smaller magnitude than following the first RF pulse (see Figure 2.7). After a few repetitions, **M** will return to the same magnitude prior to each RF pulse. In other words, **M** achieves a steady state value that depends on the time between excitation pulses, or repetition time (TR), and how efficiently the protons give up their energy (T1 relaxation time). To produce this steady state prior to data collection, additional RF pulses are applied immediately prior to the main imaging pulses. The signal produced by these steady state or dummy pulses is not usually recorded.

As mentioned, T1 relaxation measures energy transfer from an excited proton to its surroundings. The key to this energy transfer is the presence of some type of molecular motion (e.g., vibration, rotation) in the vicinity of the excited proton with an intrinsic frequency ω_1, that matches the resonant frequency ω_0. The closer ω_0 is to ω_1, the more readily the motion will absorb the energy and the more frequently this energy transfer will occur, allowing the collection of protons to return to its equilibrium state sooner. In tissues, molecular rotations or tumbling of proteins typically have a low frequency. Therefore, at lower resonance frequencies (lower $\mathbf{B_0}$), there is a better match between ω_L and ω_0, a more efficient energy transfer will occur, and T1 will be shorter. This is the basis for the frequency dependence of T1, namely that T1

increases with increasing $\mathbf{B_0}$.

T2 is the time required for the transverse component of **M** to decay to 37% (1/e) of its initial value. It is also known as the spin-spin relaxation time or transverse relaxation time. At equilibrium, **M** is oriented only along the z ($\mathbf{B_0}$) axis and no portion of **M** is in the xy plane. The coherence, or uniformity, of the protons is entirely longitudinal. Absorption of energy from a 90° pulse causes **M** to rotate entirely into the xy plane, so that the coherence is in the transverse plane. At the end of the pulse, each proton precesses at the same frequency ω_0 and is synchronized at the same point or phase of the precessional cycle. Since a nearby proton of the same type will have the same molecular environment and the same ω_0, it will readily absorb the energy that is being released. Spin-spin relaxation refers to this energy transfer from an excited proton to another nearby proton. The absorbed energy remains as spin excitation rather than being transferred to the surroundings as in T1 relaxation. This proton-proton energy transfer can occur many times as long as the protons are close to one another and remain at the same ω_0. Intermolecular and intramolecular interactions such as vibrations or rotations will cause ω_0 to fluctuate. This will produce a gradual, irreversible loss of phase coherence to the spins as they exchange energy and reduce the magnitude of the transverse magnetization (Figure 2.9). As time elapses, this coherence disappears completely only to reform in the longitudinal direction as T1 relaxation occurs and protons reorient themselves along $\mathbf{B_0}$. This loss of coherence is what causes the MR signal (FID) to decay. As the spins lose coherence, the value of **M** in the xy plane decreases toward zero. This dephasing time T2 is always less than or equal to T1.

There are several causes for a loss of transverse coherence to **M**. One is the movement of adjacent spins due to molecular vibrations or rotations, which is responsible for spin-spin relaxation, or *true* T2. Another cause arises from the

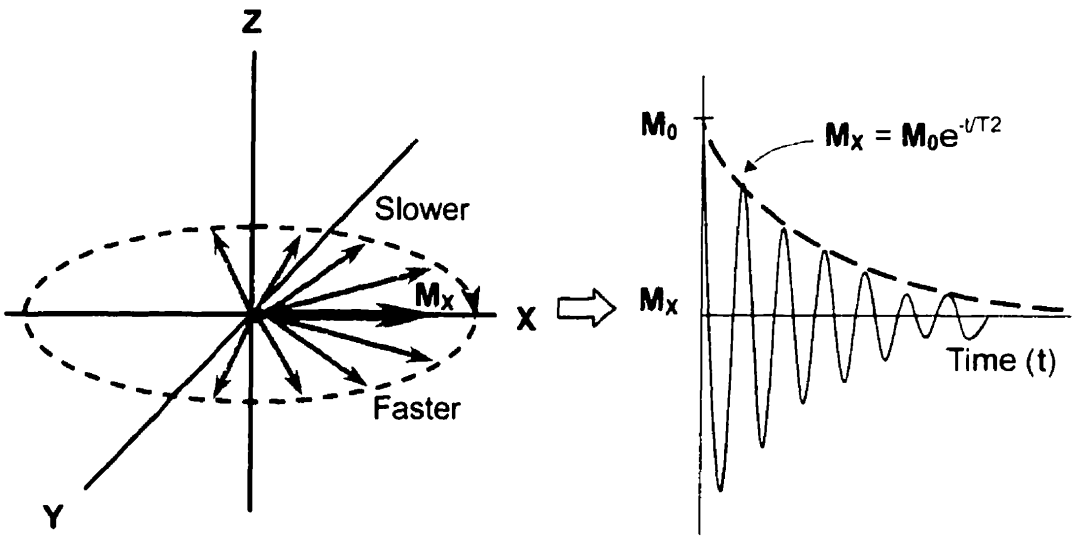

Figure 2.9 Dephasing of Transverse Magnetization

Spins begin to exchange energy resulting in a loss of phase coherence. The transverse magnetization, and hence, the MR signal, decays at an exponential rate with a time constant T2. The equation shown for $\mathbf{M}_X$ is for a 90° flip of **M** after it has reached its $\mathbf{M}_0$ equilibrium value.

fact that a proton never experiences a magnetic field that is perfectly uniform or homogenous. As the proton precesses, it experiences a fluctuating local magnetic field, causing a change in ω_0 and a loss in transverse phase coherence. This nonuniformity in $\mathbf{B}_0$ comes from two principle sources: main field inhomogeneity caused by imperfections in the magnet or extraneous magnetic fields, and sample-induced inhomogeneity resultant from differences in the magnetic susceptibility, or degree of magnetization, of adjacent tissues (e.g., bone, tissue, air). The total transverse relaxation time, T2*, includes the effects of this local field nonuniformity as well as spin-spin interactions. Due to the combined dephasing effects of both factors, T2* is always shorter than the T2 relaxation time. Since T2 relaxation involves energy transfer to other spins, not to the surrounding lattice, it is relatively independent of field strength.

2.3 Images and Image Quality

2.3.1 Overview: Image Resolution, Contrast, and SNR

The magnets used for most clinical MRI range in strength from 0.5 to 2.0 T, where one Tesla = 10,000 Gauss. By comparison, the magnetic field of the Earth is approximately 0.5 Gauss. The highest magnetic field strength currently approved for use in humans is 4 T, and there are presently six such MR scanners in the world, although none are yet in routine clinical use. Since magnetic resonance images are used to make and confirm medical diagnoses and there is a high demand for MRI services, it is important to obtain the highest quality images possible in a limited amount of time. There is a consensus that high field magnets produce images that are subjectively better than lower field magnets, however this has not been shown to improve the diagnostic utility of MRI (Jack *et* al., 1990; Steinberg *et* al., 1990; Lee *et* al., 1995). Spatial resolution, contrast-to-noise ratio (CNR), and signal-to-noise ratio (SNR) are all critical parameters that determine the likelihood of detecting pathologic changes on MR images. All of these parameters interact with each other and with the total examination time. The length of time it takes to complete an imaging exam is very important. If it takes too long to achieve a certain level of image quality, patients are unable to remain motionless and the superior resolution or SNR is wasted.

Spatial resolution of an image determines the viewer's ability to discern two points as separate and distinct. Small two dimensional (2D) units of the image are called pixels. The pixel and the thickness of the slice of tissue being imaged combine to determine a three-dimensional (3D) volume of tissue (voxel) within the patient. It is this three-dimensional voxel that emits the RF signals that are then mapped onto a two-dimensional image (Figure 2.10). Resolution is

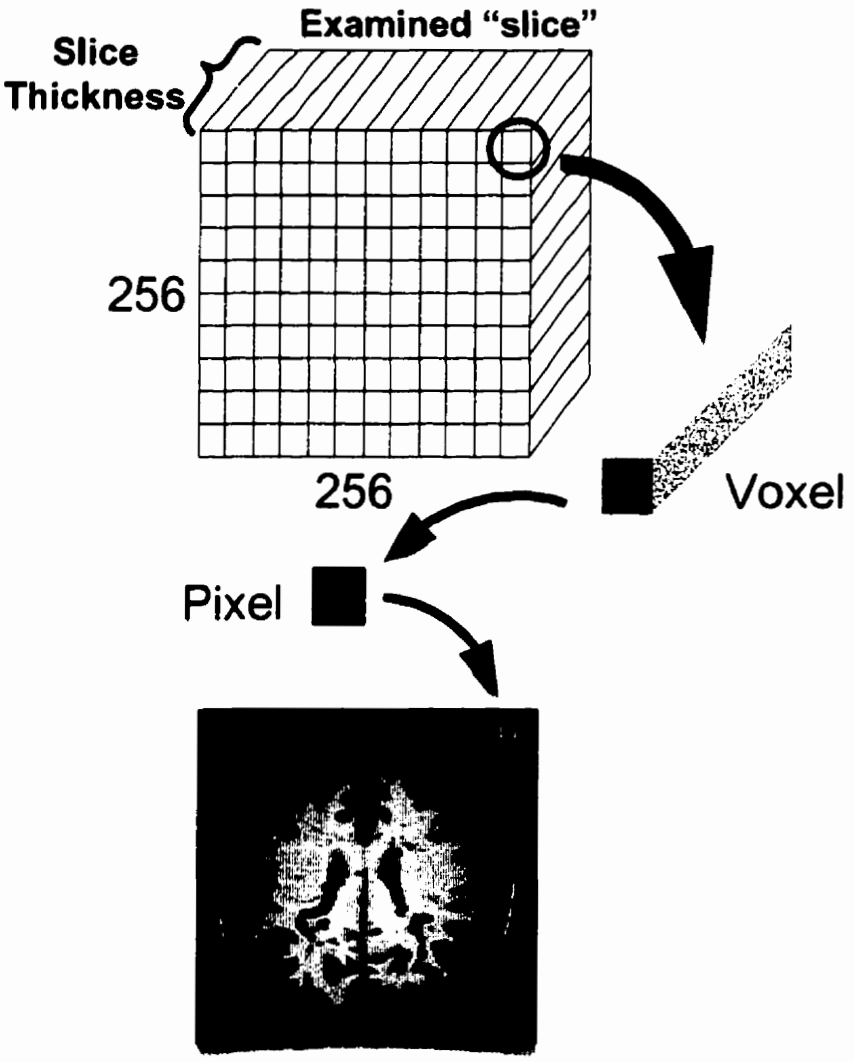

Figure 2.10 MRI Matrix, Pixels, and Voxel

The MR image of the examined slice is composed of a matrix of 65,536 pixels (256 x 256) of varying intensity, each representing the average MR signal from one voxel of tissue.

determined by the voxel size. A large voxel may contain several small structures, however the pixel on the MR image will be formed using the average signal from that voxel, causing these structures to become indistinguishable from one another. This is commonly referred to as partial volume effect or volume averaging. Volume averaging leads to a loss of both in-plane (Figure 2.11)

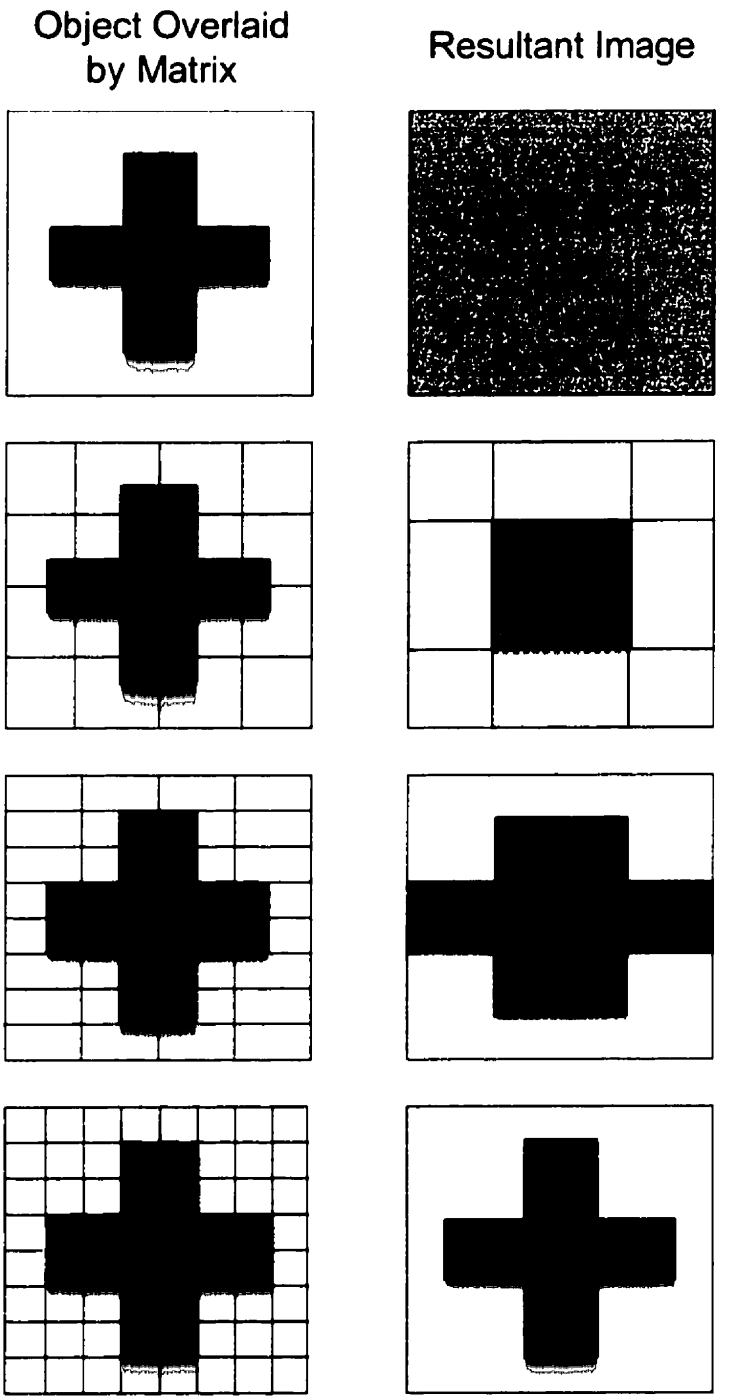

Figure 2.11 Effect of Matrix Size on In-Plane Resolution

As the number of pixels increases, and therefore the size of each pixel decreases, the shape of the cross produced becomes closer to that of the actual object. Signal averaging produces varying signal intensity depending on the percentage of each pixel filled by the object.

and out-of-plane resolution (Figure 2.12). Small voxels, on the other hand, allow separate structures to be differentiated as they will contribute their MR signal to separate pixels. Voxel size is dependent on slice thickness, the area being imaged, or field of view (FOV), and image matrix, which determines the number of pixels for the given area. A larger slice thickness will increase the voxel size and decrease out-of-plane resolution. Increasing the FOV increases the pixel size, which decreases the in-plane resolution. Increasing the matrix increases the number of pixels for a given FOV, thereby increasing the in-plane resolution.

The intensity of each pixel of the MR image depends upon the magnitude of the RF signal detected within the voxel it represents. High signal intensity will produce hyperintense (bright) pixels and low signal intensity results in hypointense (dark) pixels. The ease with which a signal can be detected in a voxel is measured in terms of the ratio of the proton signal in the voxel to the standard deviation of noise in the image (Henkelman, 1985). Noise is the background RF produced by the random motion of conductive ions in the patient's body (thermal noise), as well as from the electrical noise of the MR scanner, and, in poorly shielded rooms, radio and television signals. A high SNR results in a sharp image, whereas a low SNR will result in a grainy image. Many factors may have an effect on SNR. For instance, a higher magnetic field will result in higher SNR in a given voxel due to the larger net magnetization vector produced by the increased population difference between high and low energy spins. Low bandwidth pulse sequences produce images with a higher SNR than high bandwidth pulse sequences. Increased noise will obviously lower the signal-to-noise ratio. Both receiver coil sensitivity, determined by its design, and the distance between the coil and the tissue producing the signal will effect SNR. As spatial resolution is increased, the SNR decreases in direct proportion to the voxel volume due to the smaller number of protons per voxel. Finally, SNR

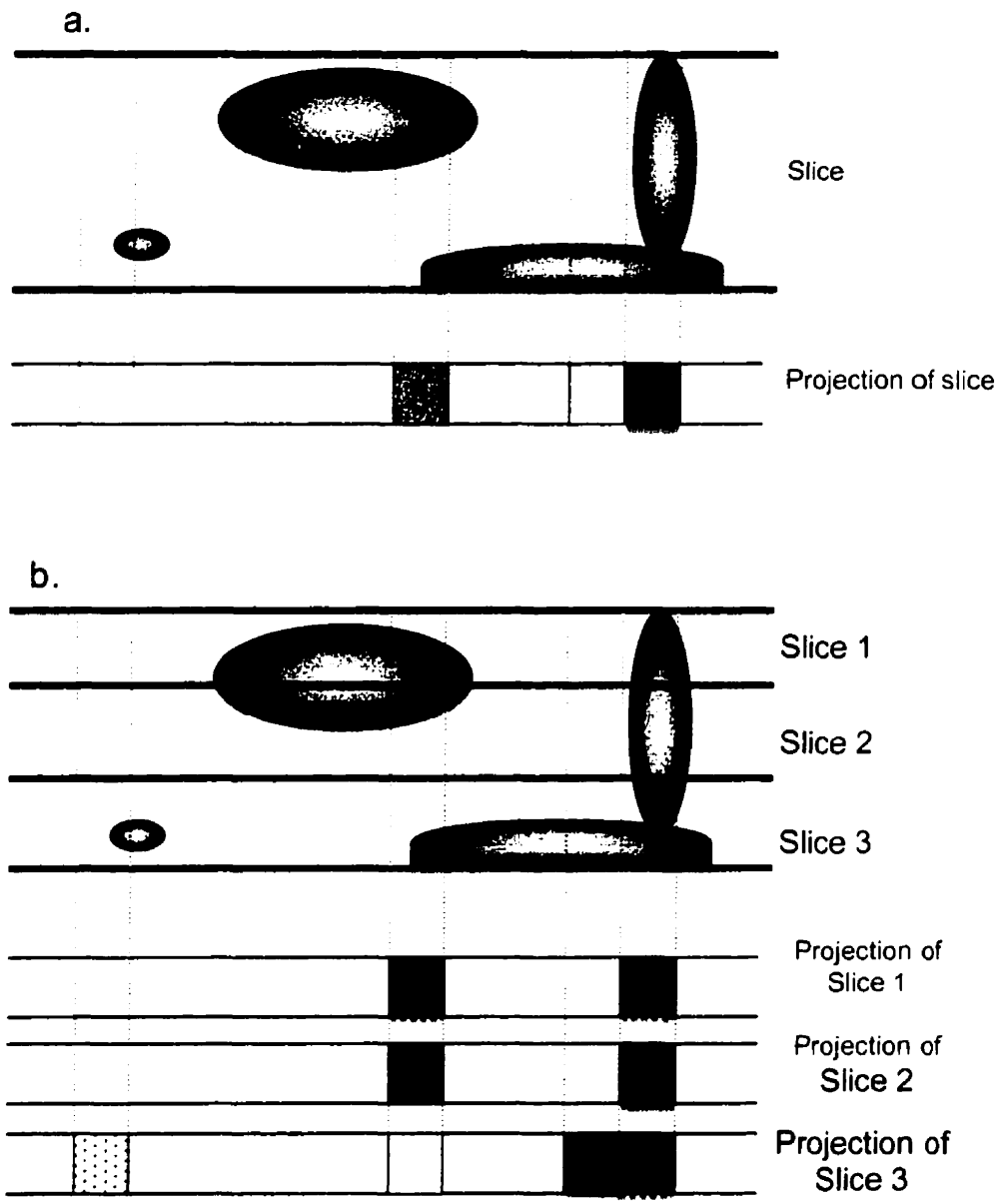

Figure 2.12 Effect of Slice Thickness on Out-of-Plane Resolution

With a thick slice (a), a structure that does not extend through the entire slice is either missed or detected at reduced intensity compared with a structure (or combination of structures) that does extend through the slice. Here the slice contains four structures, and some representative pixel boundaries (·····) define regions that are filled to greater or lesser extents by the structures. The resultant signal intensity on the slice projection represents the extent to which the structure fills the sensitive area. If the tissue is divided into three slices (b), the ability to discriminate between fine structures is enhanced.

depends on the pulse sequence and timing of the pulse sequence used, and the T1 and T2 relaxation rates of the tissues being imaged. For random noise, the amount of noise relative to signal decreases as the square root of the averaging time. That is, quadrupling the time during which the signal is measured doubles the resulting SNR. Thus, SNR can be increased by increasing the number of times that the signal from each voxel is averaged (NEX) before the image is formed. Every four additional repetitions, when averaged with the previous acquisitions, result in a doubling of SNR.

Perhaps more important for diagnostic imaging than SNR is the contrast-to-noise ratio (CNR). CNR is the difference in SNR between two adjacent tissues. Thus, CNR determines the detectability of differences between the voxels of different tissues. It is this difference that provides the ability to differentiate between diseased and normal-appearing tissue on MR images. The disparity in SNR between tissues, or image contrast, may be manipulated through the selection of scan parameters and pulse sequences.

2.3.2 Signal Strength

The amplitude of the RF signal used to construct MR images has a major bearing on the quality of the images produced. The factors that effect signal strength can be divided into two basic categories: instrumental parameters, and imaging sequence parameters. These parameters determine the noise and signal amplitudes intrinsic to the recorded FIDs. Instrumental parameters include magnetic field strength ($\mathbf{B_0}$) and RF coil design, while repetition time (TR), echo time (TE), and flip angle are important pulse sequence parameters.

As previously described, when a patient is placed in a strong magnetic field ($\mathbf{B_0}$), the hydrogen nuclei in their body align either parallel or anti-parallel to the field. As it requires less energy, more spins align parallel to the field

than antiparallel. The excess of spins aligned parallel to the field results in the creation of a net magnetization vector (**M**). Since, according to the Boltzman distribution (Equation 2-3), the difference in spin population between the high and low energy state is proportional to the energy difference between them (ΔE), and furthermore, since ΔE is directly proportional to field strength (Equation 2-2), the net magnetization vector, and therefore the SNR, increases with increasing field strength.

The MR signal that is created when the net magnetization vector is tipped into the transverse plane is detected by a RF receiver coil. Noise from the body is also detected by the coil, therefore it is desirable to match the size of the receiver coil to the region of interest. A small head coil that is almost completely filled by the patient's head provides a better SNR for brain imaging compared with a larger coil because it is less sensitive to thermal noise arising from tissues outside the brain and it can be placed closer to the protons of the brain, thereby detecting a stronger signal.

While the field strength and coil sensitivity are determined by the design of the instruments themselves, the repetition time, echo time, and flip angle used in a given pulse sequence are selected by the operator. Repetition time (TR), measured in milliseconds (ms), is defined as the time from the application of one excitation RF pulse to the application of the next RF pulse. The TR determines the degree to which **M** recovers along the z axis. If the TR is equal to the T1 relaxation time of a tissue, 63% of **M** will have recovered. As the TR is increased, more regrowth of **M** is allowed to occur between pulses, consequently the signal amplitude increases. The TR therefore determines the amount of MR signal available from a given tissue (Figure 2.13). When the longitudinal relaxation (T1) of brain tissue and cerebral spinal fluid (CSF) are compared, brain has a shorter T1 relaxation time than CSF. Thus, when TR is short, **M** of brain

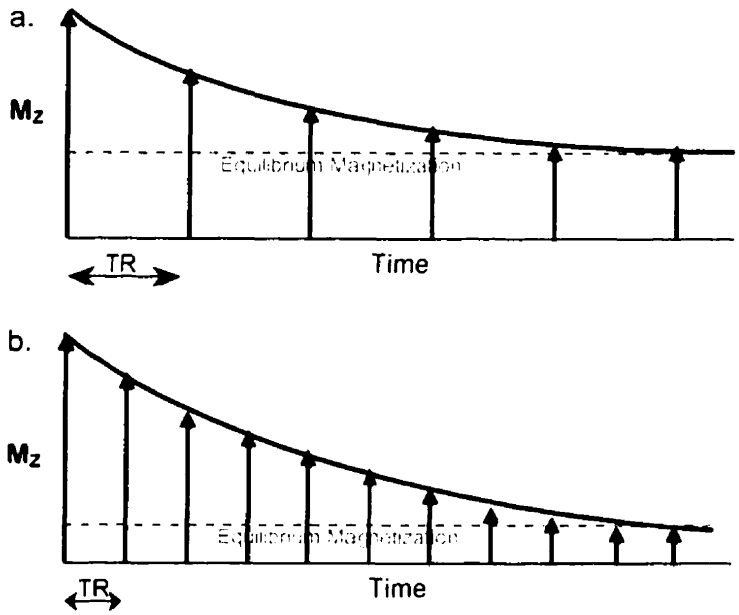

Figure 2.13 Effect of TR on Net Magnetization

After several RF pulses, an equilibrium is attained between TR and T1 relaxation. With a long TR (a), the equilibrium magnetization is large. With a short TR (b), the equilibrium magnetization is smaller.

tissue will have recovered more fully than that of CSF, resulting in a large difference in the signal intensities of the two tissues. As the TR is increased, the disparity between the signal intensities, and thus the contrast between brain tissue and CSF, is decreased (Figure 2.14). In general, as the TR is increased, T1 contrast is decreased, and SNR and scan time are increased.

If, for example, the T1 of gray matter was 800 ms and the T1 of CSF was 2000 ms and a TR of 800 ms was selected, the gray matter would recover 63% of **M** while the CSF would recover much less. The gray matter would therefore appear bright, while the CSF would be darker. If the TR was decreased to 400 ms, there would be less time for longitudinal recovery in both tissues, resulting in an overall decrease in SNR. If the TR was increased to 2000 ms there would be sufficient time for 90% recovery of the gray matter signal and 60% recovery of the CSF signal. This would produce an overall increase in SNR, however, **M** for gray

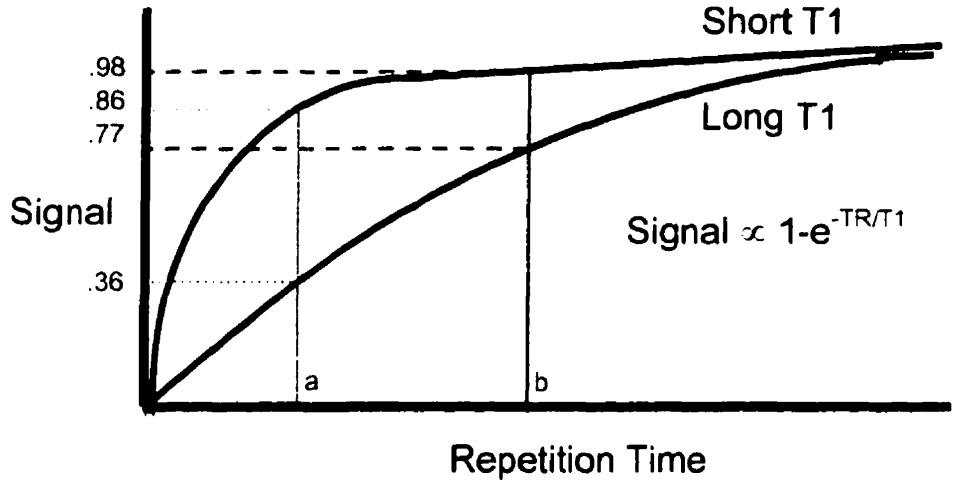

Figure 2.14 Graph of Signal Intensity Changes as a Function of TR

If a short repetition time is used (a), the tissue with a short T1 will have a relative signal intensity of 86% while the tissue with a long T1 will have a relative intensity of 36%. If the TR is lengthened (b), the signal intensity of the tissue with the short T1 increases to 98% while that of the tissue with a long T1 increases to 77%. All signals increase with longer TR. The relative brightness of tissues with short T1 values is increased by using a shorter TR.

matter and CSF would then be dependent to a larger degree on relative proton density, not T1 relaxation times, and the image will be less T1-weigted. To obtain a T1-weighted (T1W) image, both a short echo time (TE) and a short TR are required. A short TE minimizes the T2 relaxation effects and allows the signal intensities, and thus image contrast, to be based on the T1 values of the tissues. For a proton density weighted image, a long TR and a short TE are used. The long TR minimizes the T1 effects and the short TE minimizes the T2 effects. The signal intensity is therefore dependent on the tissue proton density.

The echo time (TE), measured in milliseconds, is the time between the middle of the excitation pulse to the peak of the signal induced in the receiver coil. TE determines the amount of dephasing of the transverse magnetization that is allowed to occur before the MR signal is recorded, and thus, controls the

amount of T2-weighting in an image. A tissue with a short T2 that is imaged using a long TE will appear dark due to the complete dephasing of its MR signal. **M** from a tissue with a long T2 will not have dephased as much and will produce signal and appear brighter. As the TE is increased, SNR is decreased and the CNR is increased as the image becomes more T2 dependent. However only those tissues with long T2 relaxation times will have high signal on images using long TEs. Therefore, a TE must be selected that gives both good SNR and CNR (Figure 2.15). The TE controls T2 contrast, but does not affect T1 contrast.

The flip angle, as determined by the RF pulse amplitude and duration, controls the angle to which **M** is tipped into the transverse plane. Spin echo imaging sequences use flip angles of 90° while gradient echo acquisitions typically employ flip angles less than 90°. The flip angle combined with the selection of TR will determine the T1-weighting of the tissue. Low flip angles

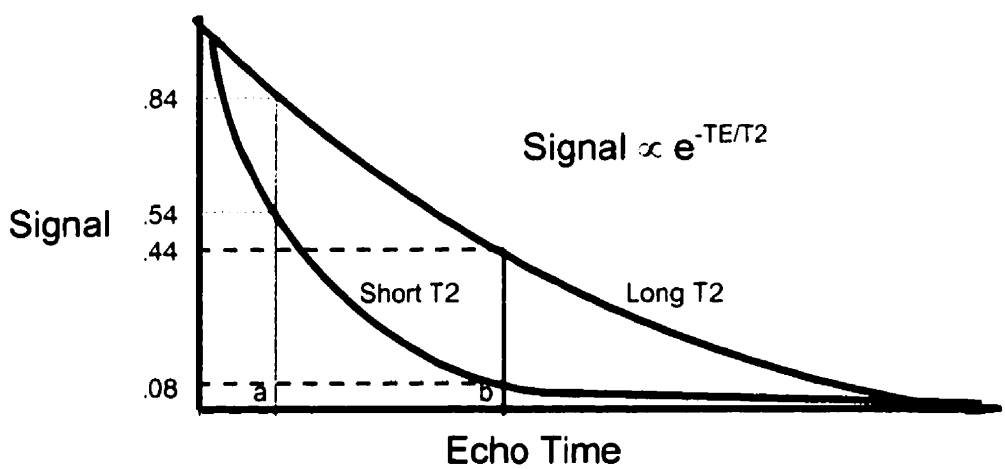

Figure 2.15 Graph of Signal Intensity Changes as a Function of TE

If a short echo time is used (a), tissue with a short T2 will have a relative signal intensity of 54%, and that of tissue with a long T2 will be 84%. If the TE is increased (b), the signal from the tissue with a short T2 drops to 8% and the signal of the tissue with a long T2 is reduced to 44%. Increasing the TE decreases the total signal and will therefore decrease SNR. The relative brightness of tissues with long T2 values is increased by using a longer TE.

allow most of **M** to remain in the longitudinal plane. Consequently, short TRs may be used, thereby decreasing the scan time. The amplitude of the resultant signal will be proportional to the proton density of the tissue being imaged, as T1 relaxation will have little effect on **M**.

2.3.3 Imaging Options

While field strength, receiver coil design, TR, TE, and flip angle rely on intrinsic differences in the magnetic properties of tissue to manipulate MR signal intensity and image contrast, the quality of the image produced for any given combination of the above hardware and pulse sequence options depends heavily on the image parameters selected by the operator. These parameters, which include the matrix size, field of view (FOV), slice thickness, number of excitations (NEX), and receiver bandwidth, do not alter the amplitude of the MR signal produced by individual protons, rather they determine how the signal is acquired and processed to form the final image.

The matrix size determines the number of pixels within a predetermined field of view. If the FOV remains constant and the matrix size is increased, the size of the pixels is decreased. This results in better resolution and less volume averaging within the pixel. However, increasing the matrix size also lowers SNR and increases the scan time. SNR is proportional to the voxel size, so as the matrix increases, SNR decreases. Each row of data along the phase encoded direction of a MR acquisition is formed from a separate FID. Thus, if when the matrix is increased, the number of rows in the image is increased, the scan time will increase as well. Changing the number of rows in the frequency encoded direction does not typically affect scan time.

The FOV establishes the two-dimensional area that will be imaged. The FOV divided by the matrix determines the size of the pixels and voxels and, therefore, it will affect the image resolution. FOV also affects the SNR because the signal amplitude from each voxel decreases with voxel size. Slice thickness determines the anatomy imaged in the third dimension. Along with pixel size, the slice thickness determines voxel size. Thus, if the pixel size remains constant, SNR will increase with slice thickness as the number of protons within each voxel increases. However, as slice thickness increases, spatial resolution in the out-of-plane direction decreases leading to increased partial volume effects.

The loss of SNR that accompanies an increase in image resolution can be offset by an increase in the number of excitations (NEX) averaged to produce each image. Since the noise in the image is random while the signal is not, the signal amplitude grows more rapidly with each additional average than does the noise. As previously described, quadrupling the NEX will double the SNR, however, it will also have the effect of increasing the scan time by a factor of four. Three-dimensional imaging allows the entire imaging volume to be excited while 2D imaging excites a single slice at a time. Consequently, with 3D imaging the MR signal comes from the entire "slab", rather than from just a single slice. The number of slices required determines the number of times the slab will be sampled, hence, the SNR increases with the number of slices imaged with a 3D acquisition. This increase in the number of samplings is comparable to increasing the NEX per slice in a 2D imaging sequence. Thus, a 64-slice volume acquired with a 3D sequence is comparable to collecting 64 NEX per slice with a 2D sequence.

Finally, the SNR of an image is affected by receiver bandwidth. Setting the receiver bandwidth determines the range of frequencies the system will use to map the image. The receiver bandwidth determines how many frequencies

will be used across the FOV, and thus, across each pixel. A wide bandwidth includes more thermal noise with the signal, whereas a narrow bandwidth reduces the amount of noise picked up by the receiver. While decreasing the bandwidth will increase the SNR, the readout time will also be increased, thus the minimum TE increases.

There are a great number of parameters that can be altered in order to produce a MR image. Each will change the quality of the image in a variety of ways, but resolution and SNR can always be increased at the expense of increasing the overall scan time (Table 2.1). Standard clinical imaging protocols for the examination of MS patients at 0.5 and 1.5 T sacrifice in-plane and out-of-plane resolution in order to obtain images with high SNR in a reasonable period of time. The increase in net magnetization produced by a 4 T MRI scanner allows high-resolution images to be acquired in a time frame comparable to that used in clinical MR exams while maintaining similar image contrast and SNR.

Table 2.1 Scanning Parameter Effect on Image Acquisition

Parameter	Value	SNR	Resolution	Scanning Time
TR	High	↑	—	↑
	Low	↓	—	↓
NEX	High	↑	—	↑↑
	Low	↓	—	↓
Matrix	Large	↓	↑↑	↑
	Small	↑	↓↓	↓
FOV	Large	↑	↓	—
	Small	↓	↑	—
Slice Thickness	Thick	↑	↓	—
	Thin	↓	↑	—
Slice Spacing	Narrow	↓	↓	—
	Wide	↑	↑	—
Bandwidth	Narrow	↑	↑	↑
	Wide	↓	↓	↓

3

Rationale

Magnetic resonance imaging provides an objective and direct assessment of the evolving pathology in multiple sclerosis, a devastatingly debilitating disease for which there is currently no effective treatment or cure. With the evolution of magnetic resonance technology, it is likely that MR techniques will become even more important in investigating the natural history of the disease and monitoring treatment efficacy. High field 4 Tesla (T) MRI scanners have the potential to further increase the resolution of MR images, leading to more precise lesion detection. Improved lesion detection may, in turn, result in earlier diagnosis of clinically definite MS, increased prognostic value, better understanding of the underlying pathological process of the disease, improved selection of cohorts for clinical trials and more precise monitoring of treatment effects. The advantages of 4 T magnets, which include high speed and/or high resolution, and the capability for MR spectroscopy and functional imaging, are made possible by the increase in signal-to-noise ratio that results from the use of a stronger magnetic

field. As field strength increases, so too does the energy difference between high and low energy spins, resulting in a greater population difference between spin states at 4 T. Consequently, the net magnetization produced in a given sample placed within a 4 T field is larger than that that would be produced at commonly used fields of 0.5 or 1.5 T. This increase in net magnetization is manifest as an increase in the intrinsic SNR of MR signals at 4 T.

Although there is a consensus that high field magnets produce images that are subjectively better than lower field systems, this has not been proven to result in improved accuracy in the detection of pathology, and despite the potential benefits of high field imaging, there is a definite cost advantage to employing middle-field-strength units. The purchase price and ongoing maintenance costs are lower for the 1.5 T scanners and the smaller magnetic field makes them easier to situate within, or near, existing hospital buildings. Thus, driven by both economic and patient-care implications, the issue of optimal magnetic resonance field strength has received a great deal of attention. Clinical evaluation studies (Bilaniuk *et al.*, 1984a; Bilaniuk *et al.*, 1984b; Crooks *et al.*, 1984; Posin *et al.*, 1985; Hansson *et* al., 1989; Seidenwurn *et al.*, 1989; Jack *et al.*, 1990; Steinberg *et al.*, 1990, Orrison *et* al., 1991; Lee *et al.*, 1995) as well as theoretical and laboratory based studies (Bottomley *et al.*, 1978; Crooks *et al.*, 1982; Hart *et al.*, 1983; Chen *et al.*, 1986; Hoult *et al.*, 1986, Rinck *et al.*, 1988) addressing this subject at low field strengths (0.35 – 1.5 T) have been published. A broad consensus has never been reached, however, due in large part to the logistic and economic hurdles inherent in conducting clinical studies comparing field strength.

In order to evaluate the increase in lesion detectability that results from the use of high-resolution 4 T MRI exams representative of the highest quality imaging achievable in a clinically reasonable timeframe using current technology,

a clinical study comparing MR imaging of the brain at 0.5/1.5 T and 4 T was conducted at the University of Western Ontario. Fourteen patients with multiple sclerosis were studied, and, using three MR scanners, each patient was imaged at 0.5 or 1.5 T as well as at 4 T. The resulting paired image series were evaluated based on the number and volume of white matter lesions detected on the high-resolution 4 T images versus the standard resolution low field images.

4

Methods

4.1 Subjects

Twenty-five outpatients (17 women and 8 men) with clinically definite multiple sclerosis were recruited from the MS Clinic of the London Health Sciences Centre. Six patients had relapsing-remitting multiple sclerosis and nineteen patients had secondary progressive multiple sclerosis. Their mean age was 41.6 years (range, 25-58 years), and the mean duration of disease was 8.4 years (range, 1-28 years). The subjects had an average Expanded Disability Status Scale (EDSS) score of 3.9 (range, 0-6.5). Written informed consent was obtained from all of the patients before inclusion in the study, which was conducted with the approval of the University of Western Ontario's Review Board for Health Sciences Research Involving Human Subjects.

Of the twenty-five patients originally recruited to participate, eleven were eliminated from the study because of claustrophobia, bladder incontinence, technical problems, failure to keep the imaging appointment, or because

corresponding 0.5 or 1.5 T images were not available. Thus, MR imaging data were available for fourteen patients. Patients were asked to undergo the 4 T MR examination just prior to, or immediately following, their regularly-scheduled 1.5 T imaging exam. In some cases the two examinations occurred on separate days, however, the 4 T exams were always completed within forty-eight hours of the 1.5 T exams. Eight patients were imaged according to the above protocol (Group 1). Due to scheduling constraints and limits on the availability of appropriate study patients, however, additional patients, who had previously been imaged at either 1.5 or 0.5 T, were recruited to be imaged at 4 T. Of this second group of patients, two had been scanned at 1.5 T (Group 2) and four at 0.5 T (Group 3). The mean period of time elapsed between the two imaging sessions was 5 months (range, 3-8 months) for the 1.5 T patients, and 11.6 months (range, 3-27 months) for the patients first imaged at 0.5 T. The demographic and clinical data for each participant is summarized in Table 4.1.

4.2 0.5 T and 1.5 T Imaging

The 0.5 T and 1.5 T imaging was performed on two GE Signa™ scanners (GE Medical Systems, Milwaukee, WI) at the University Campus of London Health Sciences Centre (LHSC-UC). Both machines have similar configurations, with transmit-receive quadrature head coils, shielded gradients, and digital RF transmitter and receiver electronics. The 0.5 and 1.5 T images were acquired by the technicians in the Department of Diagnostic Radiology and Nuclear Medicine of LHSC-UC, either as part of the patients' ongoing care, or as part of a concomitant, though unrelated, clinical trial. Axial images through the brain were obtained in the oblique plane with the corpus callosum as an internal landmark,

Table 4.1 Summary of Patient Information

	Patient:	Age:	Duration of Disease (years):	Diagnosis:	EDSS Score:	Therapy:
Group 1	JAD	44	4	SPMS	3.5	Betaseron
	KLM	48	2	SPMS	3.5	Betaseron
	BAB	43	14	SPMS	3.5	Betaseron
	RCS	40	11	SPMS	5.5	Betaseron
	MMA	46	20	SPMS	4	Betaseron
	JET	35	14	SPMS	6	Betaseron
	DLM	42	6	SPMS	3	Betaseron
	ARM	44	2	SPMS	3	Betaseron
2	BNC	49	11	SPMS	4.5	none
	DAT	44	10	SPMS	6.5	none
3	DLH	33	4	RRMS	1.5	Rebif
	RED	48	7	SPMS	3	Cladribine
	BHB	47	13	SPMS	3	none
	CMT	31	1	RRMS	3.5	Betaseron
Excluded	RJL	44	7	SPMS	6	Betaseron
	CVW	54	28	SPMS	6	Betaseron
	MMD	36	6	SPMS	5	none
	MCC	45	6	SPMS	3.5	Betaseron
	LB	38	5	SPMS	3	Betaseron
	RSS	31	3	SPMS	5.5	Betaseron
	LKQ	34	8	RRMS	0	none
	TLW	42	12	SPMS	6.5	none
	CLP	38	3	RRMS	1.5	Betaseron
	JGH	58	6	RRMS	3.5	none
	MMM	25	7	RRMS	3	none

with slices angled along the inferior aspect of the genu and splenium of the corpus callosum. In most cases, the 0.5/1.5 T exam consisted of the acquisition of T2-weighted and proton density weighted images using a dual echo spin echo sequence, as well as pre- and post-gadolinium T1-weighted images.

The imaging parameters for the eight patients who underwent MRI exams at 1.5 T and 4 T with an inter-exam interval of less than 48 hours (Group 1) were

as follows: The T2-weighted and proton density weighted images were acquired using a dual echo spin echo pulse sequence with a TR of 2000 ms and a TE of 30 ms for the early echo and 80 ms for the late echo. Thirty 5 mm thick contiguous slices were acquired using a matrix size of 256 by 192 to cover a 22 cm by 16 cm field of view. Only a single excitation was used for each slice. The T1-weighted images were acquired using a conventional spin echo sequence with at TR of 550 ms and a TE of 13 ms. The slice thickness, matrix size, and FOV were identical to those used for the T2W/PDW images. Two excitations were averaged to produce the image of each slice. The T2W/PDW imaging required 11 minutes while the T1W imaging was completed in 6 minutes, for a total imaging time of 17 minutes.

The following parameters were used to acquire the images from the two patients who underwent scanning at 1.5 T and 4 T with a mean inter-scan interval of 5 months (Group 2): T2W/PDW images of patient DAT were acquired with a dual echo spin echo pulse sequence using a TR of 2400 ms and a TE of 30 ms and 80 ms for the early and late echoes, respectively. Fifty 3 mm thick contiguous slices were imaged using a matrix of 256 by 192 over a 24 cm by 18 cm FOV, with 1 NEX per slice. T1W images of the patient were not used in this study, as they were acquired using a 5 mm slice thickness and, therefore, could not be matched to, and analysed with, the T2W images. The T2W/PDW imaging required a total of 18 minutes to complete. T2W/PDW images of patient BNC were acquired with a dual echo spin echo pulse sequence using a TR of 10000 ms and a TE of 17 ms and 102 ms for the early and late echoes, respectively. Forty-two 3 mm thick contiguous slices were imaged using a matrix of 256 by 128 over a 24 cm by 24 cm FOV, with 1 NEX per slice. These images were acquired in 21 minutes. No T1W images were acquired from this patient.

Finally, images from the patients scanned at 0.5 T (Group 3) were

obtained using the following parameters: T2W/PDW images were acquired from all four patients using a dual echo spin echo pulse sequence. TR values ranged from 2800 ms to 3100 ms, while early echo TEs were either 30 ms or 32 ms, and late echo TEs were either 85 ms or 90 ms. In all cases, slices were imaged using a matrix size of 256 by 192, over a FOV of 22 cm by 16 cm, with one NEX per slice. The time required to acquire the images ranged from 9 to 10 minutes. Patient DLH was scanned using twenty-four 5 mm thick slices with an inter-slice gap of 0.5 mm, while patients RED, and CMT were imaged using twenty-three 4 mm thick slices and inter-slice gaps of 2 mm. Twenty-two slices, each one being 4 mm thick with an inter-slice gap of 2 mm, were used to image patient BHB. No T1W images were obtained for these patients.

4.3 4 T Imaging

The 4 T imaging was performed on a ^{UNITY}*INOVA*™ MR scanner (Varian Associates, Palo Alto, CA and Siemens Medical Systems, Erlangen, Germany) located in the A.M. Cuddy Wing of the Imaging Research Laboratories of the John P. Robarts Research Institute, London, Ontario. The system uses actively shielded whole body gradients and digital RF transmitter and receiver electronics. Transmission and reception of RF signal were achieved using a custom-made 27cm diameter quadrature birdcage head coil (Keller, *et al.*, 1997). Axial images through the brain were obtained in the oblique plane with the corpus callosum as an internal landmark, with slices angled along the inferior aspect of the genu and splenium of the corpus callosum as in the 0.5 and 1.5 T images. The 4 T exam consisted of the acquisition of T1- and T2-weighted images. The T2W images were obtained using a conventional spin echo sequence, and a 3D magnetization

prepared ultrafast gradient recalled echo sequence was used to acquire the T1W images (Lee J, *et al.*, 1995).

All subjects were imaged according to the following protocol: After the patient was placed in the magnet, the field homogeneity was optimized by manually shimming on the MR signal from the entire head using a simple pulse-acquire sequence. The proton signal amplitude was maximized and the full-width-half-maximum line-width was minimized using an iterative approach. Next, the 90° pulse power was calibrated by incrementing the pulse amplitude until the maximal signal strength had been achieved. Scout images were then acquired with a magnetization prepared fast low angle shot (mpFLASH) gradient echo sequence. A TR of 12 ms, TE of 6 ms and a flip angle of 22° were used for all scout images to acquire a 256 by 128 matrix over a FOV of 24 cm by 24 cm. First an axial image was obtained and used to plan a slice along the interhemispheric fissure. The resultant slice parameters were then transferred into a new experiment file and used to obtain a coronal image. Using the coronal image, a slice was planned along the interhemispheric fissure and down the middle of the cervical spine. The slice parameters were once again transferred into a new experiment file and used to acquire a sagittal image. The center slice for the imaging sequences was planned using this sagittal image with the inferior aspect of the genu and splenium of the corpus callosum as internal landmarks as previously described. An error in the manufacturer's software caused difficulties when planning such multiple-oblique imaging planes. Consequently, an additional mpFLASH image of the center slice was acquired and the slice planning parameters were manually adjusted to correct for any unwanted rotation present in the prescribed imaging plane. These final parameters were transferred to two experiment files in order to acquire the actual imaging data.

T2W images were acquired first, followed by T1W images. The T2W

images were obtained using a conventional spin echo sequence with a TR of 4000 ms and a TE of 70 ms. These sequence timings were selected based on the results of research which compared images of guinea pig brain obtained from the 1.5 T and 4 T scanners used in the current study (Gareau *et al.*, 1998). Gareau and colleagues found that a TR of 5000 ms at 4 T was necessary in order to achieve a similar degree of T1 relaxation as obtained with a TR of 3000ms at 1.5 T (Gareau, personal communication). Since the 0.5 and 1.5 T images used in this study were acquired with a TR between 2000 ms and 3000 ms, it was decided that a 4 T TR of 4000 ms would allow a similar degree of relaxation to occur between excitation pulses, while keeping the scan time reasonable. Thirty-nine contiguous 2.2 mm slices were acquired using a matrix of 512 by 256 over a FOV of 22 cm by 22 cm. Two excitations were averaged to produce each image. A three-dimensional magnetization-prepared fast low-angle shot (mpFLASH3d) sequence was used to obtain the T1W images. A TR of 11.8 ms and a TE of 6 ms were employed in conjunction with an 11° flip angle. A 512 by 256 matrix covering a 22 cm by 22 cm FOV was used to image a 128 mm slab of tissue, which was divided into sixty-four contiguous 2.2 mm thick slices during post-processing. The T2W imaging required 34 minutes while the T1W imaging was completed in 5 minutes, for a total imaging time of 37 minutes. The 0.5/1.5 T and 4 T imaging parameters are summarized in Table 4.2.

4.4 Lesion Identification and Quantification

Once acquired, all images were transferred via Ethernet to a Sun SPARCstation 4 (Sun Microsystems, Mountainview, CA) for processing. 0.5 T and 1.5 T images were converted from GE format to VFF format with 8 bits of

Table 4.2 Summary of Imaging Parameters

Field Strength	Group	Patient	Sequence	TR/TE (ms)	# of Slices	Slice Thick. (mm)	Slice Gap (mm)	FOV (cm)	Matrix	NEX	Voxel (mm3)	Duration (min)	Relative SNR*
1.5 T	1	All	Spin Echo	2000/30/80	30	5	0	22 x 16	256 x 192	1	3.6	11	2.2
				550/30						2		6	n/a
1.5 T	2	BNC		10000/17/102	40	3	0	24 x 24	256 x 128	1	5.3	21	1
		DAT		2400/30/80	50	3	0	24 x 18	256 x 192	1	2.6	18	1.8
0.5 T	3	BHB		3000/32/90	22	4	2	22 x 16	256 x 192	1	2.9	10	1
		CMT		2800/30/85	23	4	2				2.9	9	
		DLH		3100/32/90	24	5	0.5				3.6	10	
		RED		2800/32/85	23	4	2				2.9	9	
4 T	All	All	Spin Echo	4000/70	39	2.2	0	22 x 22	512 x 256	2	0.8	34	1
			mpFLASH3d	11.8/6	64					1		5	n/a

*Relative mean SNR of T2W WM normalized using the mean SNR (23.2) of WM from four T2W images acquired at 0.5 T.

dynamic range. 4 T images were converted from raw FID files into ".sdt" format image files using *Stimulate* (Strupp, 1996). As with the 0.5 and 1.5 T images, the 4 T .sdt files were then converted into 8 bit VFF files for display and further processing. Next T1- and T2-weighted (or PD- and T2- weighted in the case of the Group 2 1.5 T data and Group 3 0.5 T data) three dimensional image sets were created from each exam by stacking all of the T1W and T2W images, respectively (Mitchell *et al.*, 1994). In the case of the 4 T exams, where there was a greater number of T1W images covering a larger anatomic volume than that covered by the T2W images, the excess T1W slices were not converted to VFF format and were not included in the 3D image sets.

The three-dimensional image sets produced by stacking the images acquired at 0.5/1.5 and 4 T were then analysed with the aid of the computer-assisted image segmentation program, *Segtool* (Figure 4.1) (Mitchell *et al.*, 1994). This method uses the computer to outline lesions from a manually selected starting point, followed by manual editing. The program employs an algorithm based on multispectral analysis that provides interactive assistance to a knowledgeable operator and acts locally upon individual lesions. A *k*-nearest-neighbor cluster classification is applied to differentiate the intensity characteristics of a single lesion from that of surrounding tissue, after which the lesion voxels are identified by the computer and then edited manually by the operator (Mitchell *et al.*, 1994). The lesion identification/quantification procedure required three steps for each exam that was analysed.

In the first step, regions of cerebrospinal fluid and normal-appearing white matter in multiple locations from a number of slices were identified. Sample regions were selected from different locations and different slices in order to incorporate intensity variations due to RF inhomogeneities. In effect, this step "taught" the computer the typical intensity characteristics of both NAWM and

CSF. In the next step, lesions were identified on each slice of the exam, on a slice by slice basis, using the mouse. The 3 pixel by 3 pixel region around the point identified by a mouse click was used by the system to analyse the T1 and T2 (or PD and T2) intensity distribution of the lesion. This intensity information was then used by the system to label the pixels within the lesion, beginning with the pixel identified by the mouse click, and working outwards toward the edges of the lesion. All lesion-labeled pixels are highlighted on the MR image for visual verification by the operator. In the final step, the computer-determined area of each lesion was corrected using manual outlining to add or remove lesion-labeled pixels to the lesion area. While most lesion areas required minor manual adjustment, errors in image registration between the T1W and T2W images arising from patient movement during the course of the imaging exam necessitated more extensive operator intervention in some cases.

The author was not blinded as to the field strength used to acquire the images under analysis. Given the obvious differences in the in-plane and out-of-plane resolution of the 4 T images compared to the 0.5/1.5 T images, such a procedure would not have been possible. To prevent knowledge of a given patient's lesion profile gained from analysing the images acquired at one field strength from influencing lesion identification at the other field strength, the analysis of the two sets of images from each patient were conducted at least one week apart. Each image set was also reviewed following the initial identification process in order to reduce intraobserver variability. Images were checked for missed abnormalities and inaccurately or mistakenly identified lesions. This review was always conducted at least twenty-four hours after the initial identification session.

Once both the initial lesion identification and the subsequent review had been completed on both sets of images from each patient, lesion-to-lesion

comparison began. Images acquired at both high and low field were displayed simultaneously on the computer monitor in order to facilitate the designation of corresponding lesions. Once "matching" lesions were identified, they were selected by the operator and assigned a new highlight colour. The 3D connected-component labeling features of *Segtool* made it possible to identify a lesion that extended through multiple slices by simply clicking on the lesion-labeled tissue in any one of those slices. Areas directly above or below the selected tissue that had previously been identified as lesion would be automatically assigned the new highlight colour. This technique worked well in some cases, but operator verification, and, under certain circumstances, operator intervention were required: The thick slices and, in some cases, the relatively large inter-slice gaps used in the 0.5/1.5 T exams complicated three-dimensional connectivity analysis. Depending upon the shape and three-dimensional orientation of a lesion, and those of neighbouring lesions, areas of abnormality could conceivably be mistakenly reassigned, or missed. For instance, two separate lesions that happened to be positioned one over the other in adjacent slices would be wrongly identified as a single lesion, whereas a single elongated lesion oriented at some angle to the perpendicular of the image plane may not be recognized as a single structure. Multiple focal lesions that bordered areas of diffuse abnormality in the out-of-plane direction also complicated the determination of connectivity in the third dimension. In these cases, the operator had to subjectively differentiate between true connectivity in the out-of-plane direction versus confluency due to partial volume effects.

Once corresponding lesions had been re-coloured on all of the slices in which they appeared, the volume of the lesion in each image set was determined by summing the number of re-coloured pixels on each slice. The total number of pixels comprising the lesion at each field strength were then recorded and later

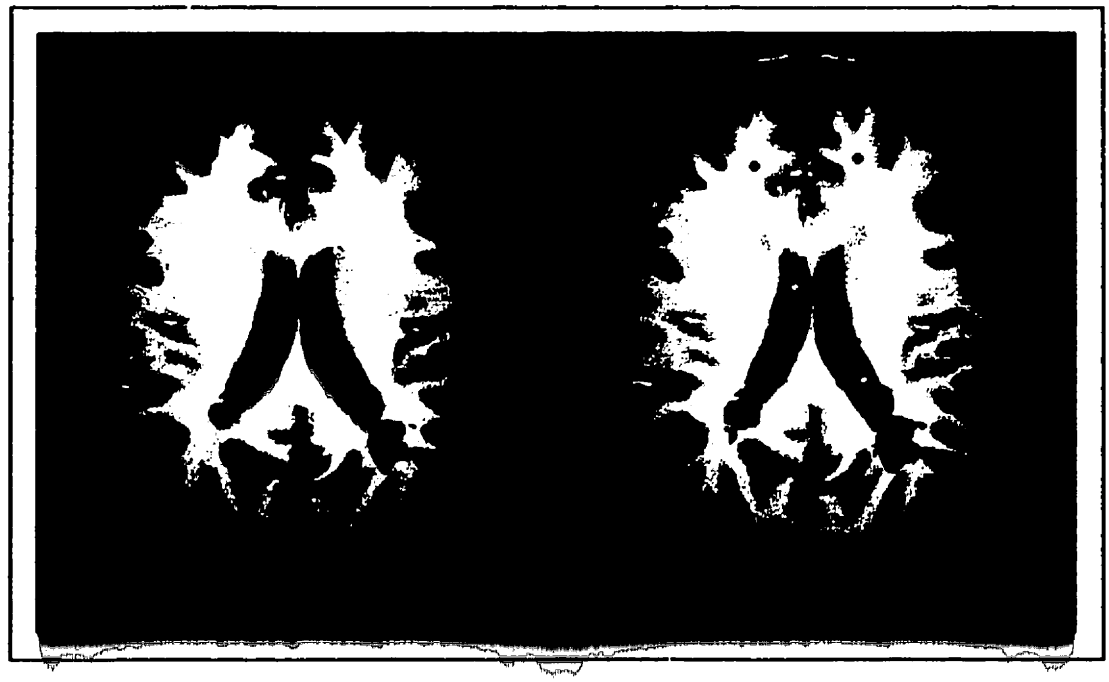

Figure 4.1 T1W Image Before and After Segmentation

Regions of CSF (yellow) and NAMW (purple) were used to train the computer algorithm. All lesions were then identified and marked with the aid of the computer (green). Next, lesions were selected and analysed one at a time (red) and once analysed, were recoloured to prevent double counting (blue).

multiplied by the voxel volume to obtain the total estimated lesion volume. Once the total number of pixels identified as abnormal in a given lesion at each field strength had been recorded, the lesions were re-labeled to prevent any lesion-pair from being counted more than once. In some cases, due to the difference in slice thickness and inter-slice gaps used at the high and low fields, single lesions or confluent areas of diffuse abnormality identified on the 4 T scans appeared as separate lesions or separate areas of abnormality on the 0.5/1.5 T scans. In such cases, based on the knowledge acquired from the higher resolution 4 T images, the separate lesions detected at 0.5/1.5 T were considered a single lesion or area of abnormality, and their pixels were summed in order to permit

comparison with the 4 T data. Because the 0.5/1.5 T imaging exams covered a greater volume of brain tissue than the 4 T exams, only those 0.5/1.5 T slices that were included in the anatomy scanned at 4 T were used in the analysis. No low-field data are available for the anatomy missed due to inter-slice gaps present in group 3 patients, thus there is a difference in the total volume of tissue analysed at 0.5 and 4 T in this group. Small areas of apparent abnormality detected at 4 T but of uncertain cause – for example, possible small blood vessels – were not included in the analysis. Once data analysis had been completed, lesion identification was verified by an expert observer (SJK).

4.5 Statistical Analysis

Product-moment correlation analysis was used to investigate the relationship between the number of lesions detected, the total lesion load, and the individual lesion volumes measured at 0.5/1.5 T and 4 T. In order to verify that all patient data came from the same population, covariance analysis was used to compare the slopes of the correlation lines from each data set, thereby validating the calculation of a single correlation coefficient for the pooled data. When differences in lesion volume measured at high field versus low field were examined on a patient by patient basis, or by patient group, significance was tested using a Mann-Whitney Rank Sum test. With one exception, a one way ANOVA was employed to examine differences between image SNR and CNR. Post hoc comparisons were performed using Dunnett's test to determine differences between the 4 T images and the images acquired at 0.5 and 1.5 T. Mean CSF-lesion CNR comparison on T1-/PD-weighted images, however, was performed using a Kruskall-Wallis test, as the data were not normally distributed.

Dunn's test was used for post hoc analysis in this case. In all cases, a 95% confidence limit was used to determine significance.

5

Results

When data from 13 patients were compared, a 65% increase in the number of lesions detected at 4 T as compared to 0.5 and 1.5 T was found. (The diffuse nature of the lesions detected in patient BAB made a comparison of lesion number meaningless for this patient.) Analysis of the individual data sets gave a correlation coefficient of 0.872 ($p < 0.001$, DF = 12) and the slope of the correlation line was 1.572, indicating that the number of lesions detected at 4 T tends to increase with the number of lesions detected at lower fields (Figure 5.1). No substantial change occurred in the correlation results when the data were analysed separately based on the time elapsed between high-field and low-field imaging exam and the strength of the low-field exam. Analysis of the grouped data sets gave *r* values of 0.902 (n = 7 patients, p = 0.005) and 0.981 (n = 4 patients, p = 0.019) for groups 1 and 3, respectively, with correlation line slopes of 1.912 and 1.610 ($F = 1.96$, $F_{0.05(1),1,7} = 5.59$). Correlation analysis could not be performed on data from Group 2, as this group consisted of only two patients.

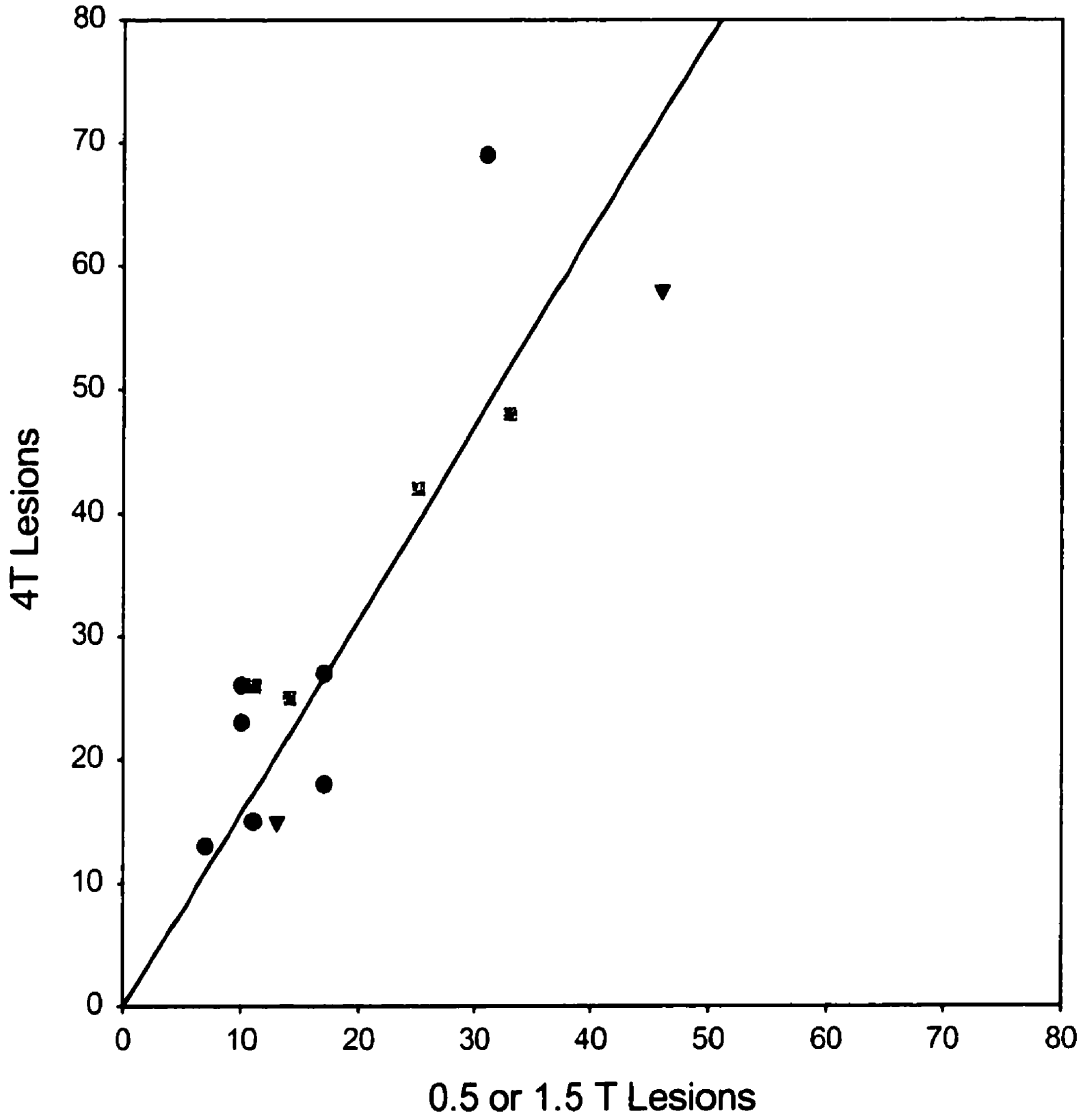

Figure 5.1 Number of Lesions Detected: 4 T Versus 0.5 and 1.5 T

The number of lesions detected in each patient at 1.5 T (<48 hours elapsed between exams) (●), 1.5 T (> 1 month elapsed between exams) (▼), and 0.5 T (> 1 month elapsed between exams) (■) are plotted against the number seen at 4 T. When the data from all 13 patients was compared there was a 65% increase in the number of lesions detected at 4 T versus 0.5/1.5 T. As demonstrated by the correlation line, the relationship between individual lesion volumes was linear ($R=0.872$, $P<0.001$, $DF = 12$), with a slope of 1.572 showing that the number of lesions detected at 4 T increases with the number of lesions detected at the lower fields.

As with the number of lesions detected, individual lesion volumes also tended to increase at 4 T when compared to 0.5 and 1.5 T values. A total of 378 lesions from 12 patients were compared. (The data from BAB and KLM were excluded due to the diffuse nature of lesions and the difference in the angle between the imaging planes at high and low field, respectively. These factors made the positive identification and accurate quantification of corresponding lesions on the 1.5 and 4 T images difficult and unreliable.) The relationship between lesion volumes was linear with a correlation coefficient of 0.772 ($p < 0.001$, DF = 377). The slope of the correlation line was 1.808, indicating that the lesion volume detected at 4 T tends to increase with that detected at lower field (Figure 5.2). Analysis of the lesions according to patient group produced similar results to those obtained from the analysis of all lesions as a single group. Correlation of the grouped data gave *r* values of 0.734 (n = 136 lesions, $p < 0.001$), 0.943 (n = 88 lesions, $p < 0.001$) and 0.777 (n = 154 lesions, $p < 0.001$) for groups 1, 2 and 3, respectively. The slopes of the correlation lines for the three groups were 1.684, 2.518, and 1.720, respectively ($F = 0.70$, $F_{0.05(1),2,372} \approx 3.02$). Forty-nine percent of the lesions seen in these 12 patients at 4 T were not detected at 0.5/1.5 T. These lesions were small with an average volume ± SE of 0.061 ± 0.008 cm^3 (range, 0.004 – 0.940 cm^3). Conversely, 20% of the lesions identified at 0.5/1.5 T were not identified at 4 T. Like their 4 T counterparts, these undetected lesions were small (mean volume, 0.076 ± 0.019 cm^3; range, 0.007 – 0.710 cm^3). It is also important to note that 22% of the lesions seen at both high and low field had measured volumes that were higher at 0.5/1.5 T than at 4 T.

Examples of lesions that were only detected at 4 T (Figures 5.3 and 5.5), or that appeared larger (Figure 5.3) or more diffuse (Figure 5.4) at the higher field are provided below. Also included are examples of lesions that were identified at

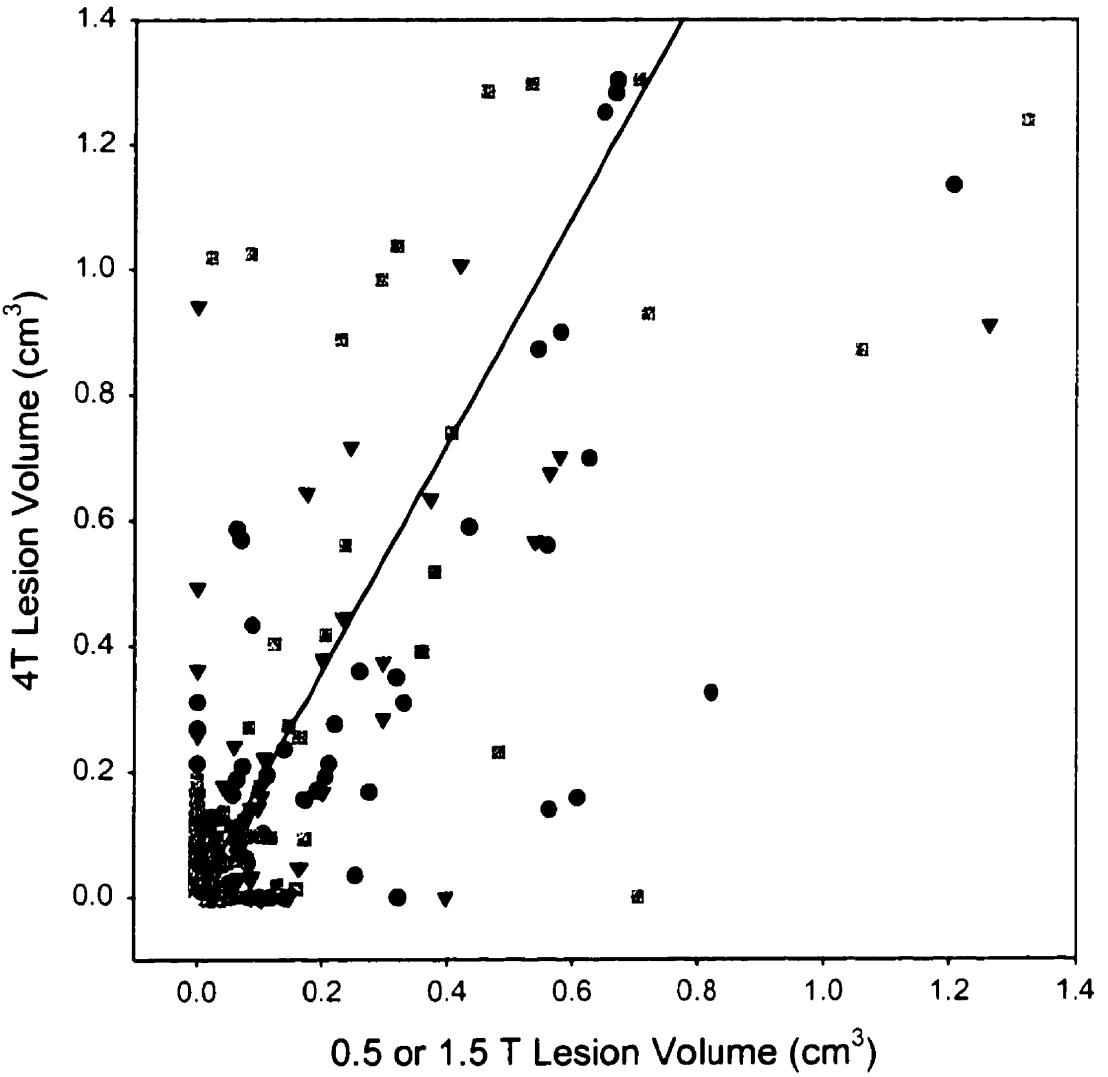

Figure 5.2 Individual Lesion Volumes: 4 T Versus 0.5 and 1.5 T

Individual lesion volumes as measured at 1.5 T (<48 hours elapsed between exams) (●), 1.5 T (> 1 month elapsed between exams) (▼), and 0.5 T (> 1 month elapsed between exams) (■) are plotted against volumes measured from a 4 T exam. When individual lesions were directly compared (n=378), 49% of those seen at 4 T were not detected at 0.5/1.5 T. These lesions were small with an average volume ± SE of 0.061 ± 0.008 cm^3 (range: 0.004 – 0.941 cm^3). As demonstrated by the correlation line, the relationship between individual lesion volumes was linear (R=0.772, P<0.001, DF = 377), with a slope of 1.808 showing that the lesion volume detected at 4 T tends to increase with that detected at lower field. However, 22% of the lesions measured were larger at 0.5/1.5 T than at 4 T, and 20% of the lesions seen at 0.5/1.5T were missed at 4 T. Like their 4 T counterparts, these undetected lesions were small (mean volume ± SE: 0.076 ± 0.019 cm^3; range: 0.0073 – 0.706 cm^3).

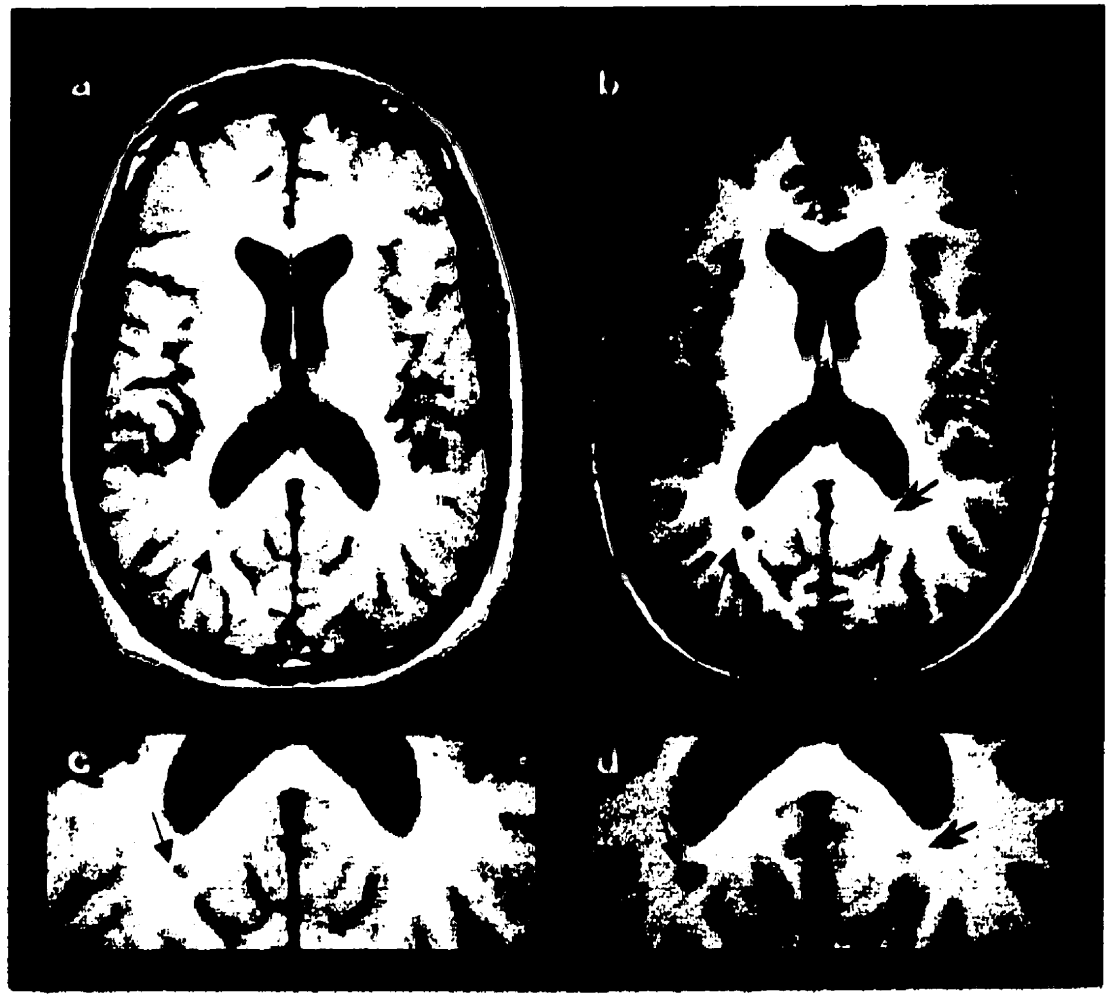

Figure 5.3 Lesion that Appears Larger at 4 T than at 1.5 T and Lesion Detected at High Field but not at Low Field

T1-weighted images (a and b) and enlarged regions of interest (c and d) acquired at 1.5 T (left) and 4 T (right) from patient RCS. These images show a lesion that appears smaller at 1.5 T (➔ ,a and c) than at 4 T (➔ ,b and d). Also visible on the 4 T image is a lesion that is not detected at 1.5 T (➔ ,b and d).

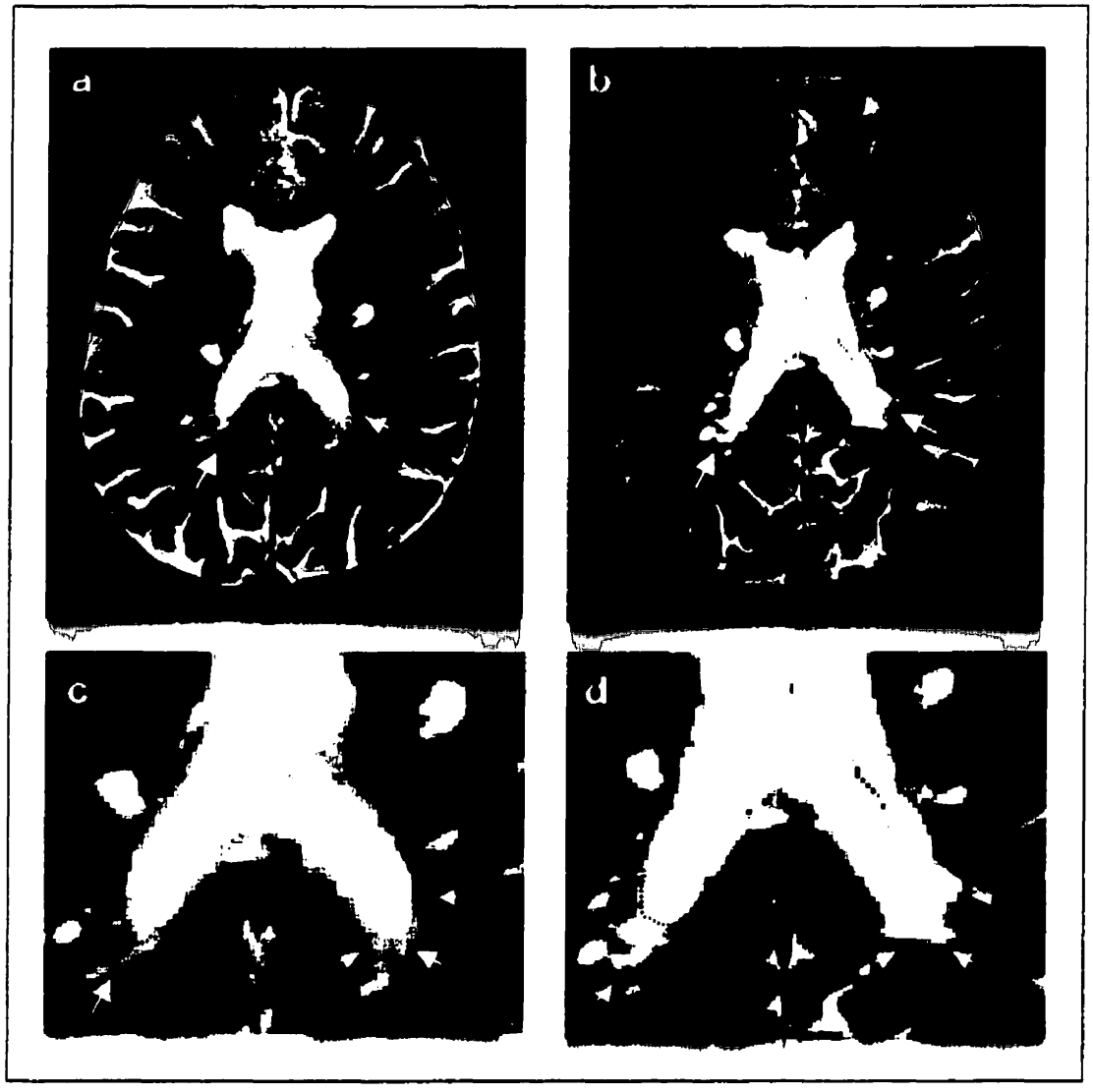

Figure 5.4 Lesions that Appears Focal at 0.5 T Become Diffuse at 4 T

T2-weighted images (a and b) and enlarged regions of interest (c and d) acquired at 0.5 T (left) and 4 T (right) from patient BHB. These images depict lesions that appear focal at 1.5 T and become a region of diffuse abnormality when viewed at 4 T(◌). The posterior edge of the right lateral ventricle also appears to be surrounded by confluent lesion at 4 T.

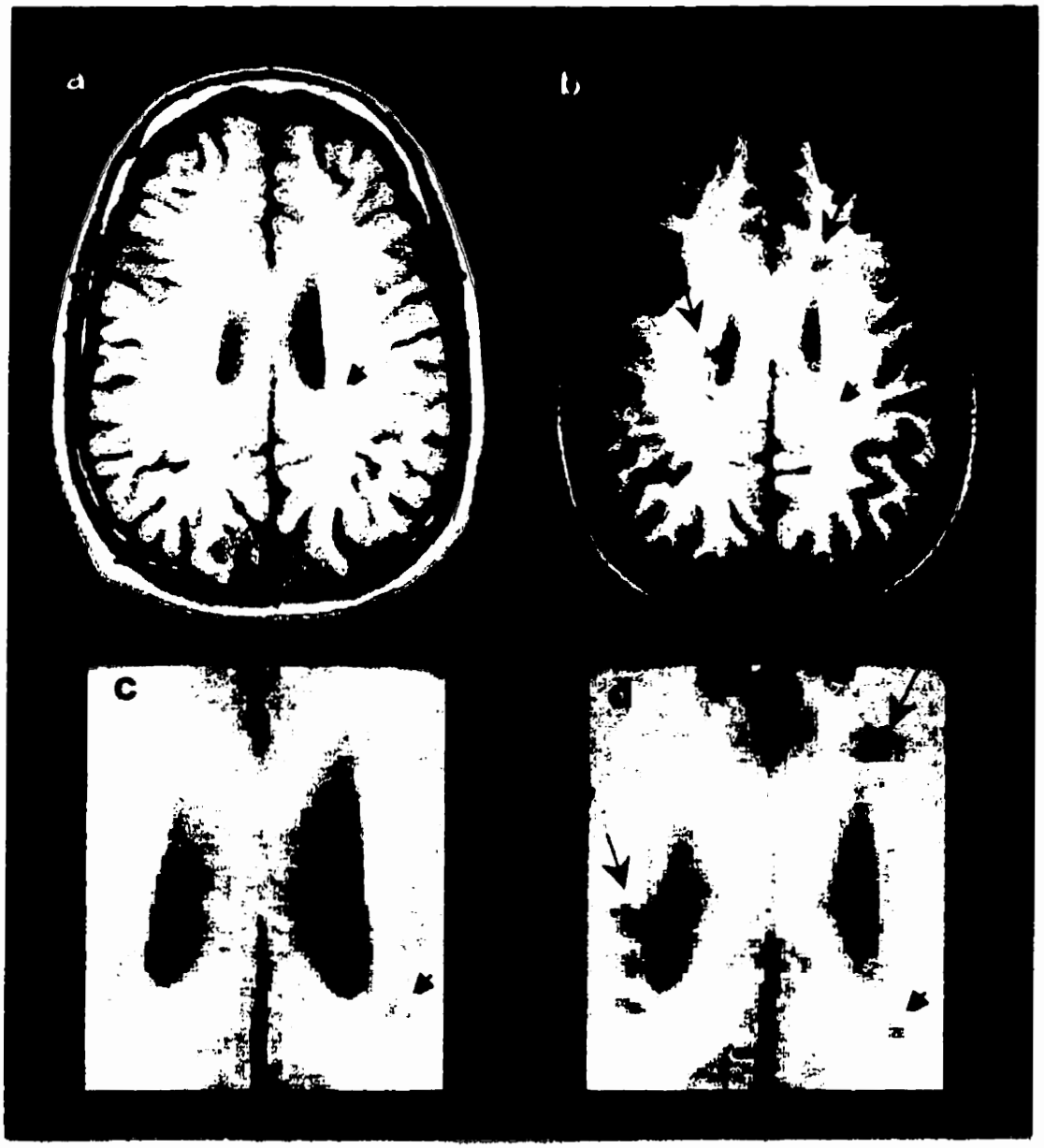

Figure 5.5 4 T Lesions that are not Seen at 1.5 T and a Lesion that Appears Smaller and More Focal at 4 T.

T1-weighted images (a and b) and enlarged regions of interest (c and d) acquired at 1.5 T (left) and 4 T (right) from patient RCS. These images reveal four lesions that can be identified at 4 T but not at 1.5 T (large arrows). Also visible is a lesion that appears smaller and more focal at 4 T than at 1.5 T. (small arrows).

low field but missed at 4 T (Figure 5.6), or that appeared larger (Figures 5.5 and 5.7) or more diffuse at the lower fields (Figures 5.8 and 5.9). As explained previously, the identification of individual lesions was complicated when focal lesions appeared to merge resulting in areas of confluent abnormality (Figure 5.10). In such cases it was necessary for the observer to make subjective

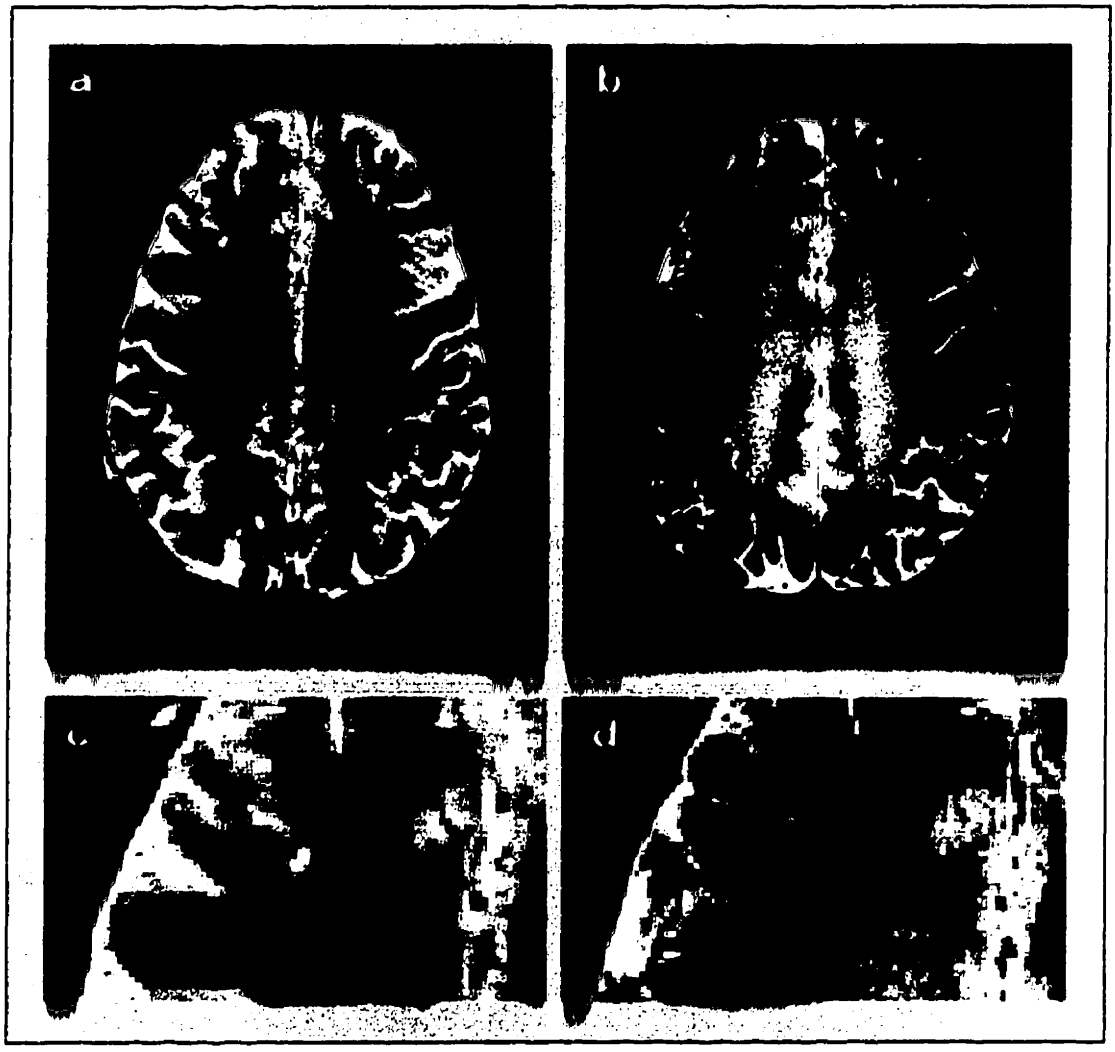

Figure 5.6 Lesion Detected at 0.5 T that is not Visible at 4 T

T2-weighted images (a and b) and enlarged regions of interest (c and d) acquired at 0.5 T (left) and 4 T (right) from patient DLH. These images display a lesion that can be identified at 0.5 T but not at 4 T.

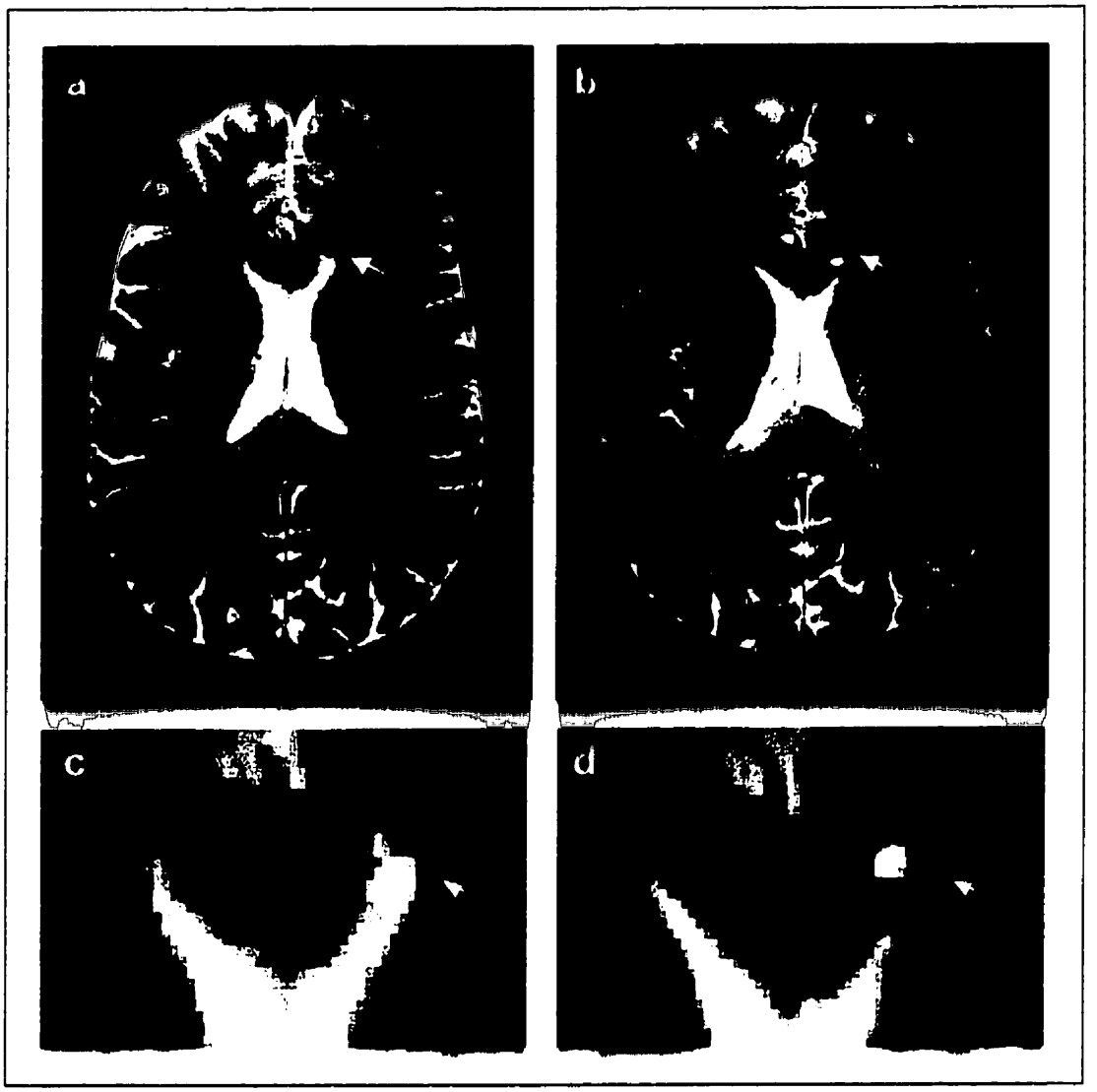

Figure 5.7 Lesion that Appears Larger at 1.5 T than at 4 T

T2-weighted images (a and b) and enlarged regions of interest (c and d) acquired at 1.5 T (left) and 4 T (right) from patient DAT. These images show a lesion that looks larger when viewed at 1.5 T than it does on the 4 T image.

judgments as to the identification of a lesion as distinct or part of a diffuse abnormality. While lesion identification is inherently subjective, only lesions that were identified with certainty by the observer were used in this study.

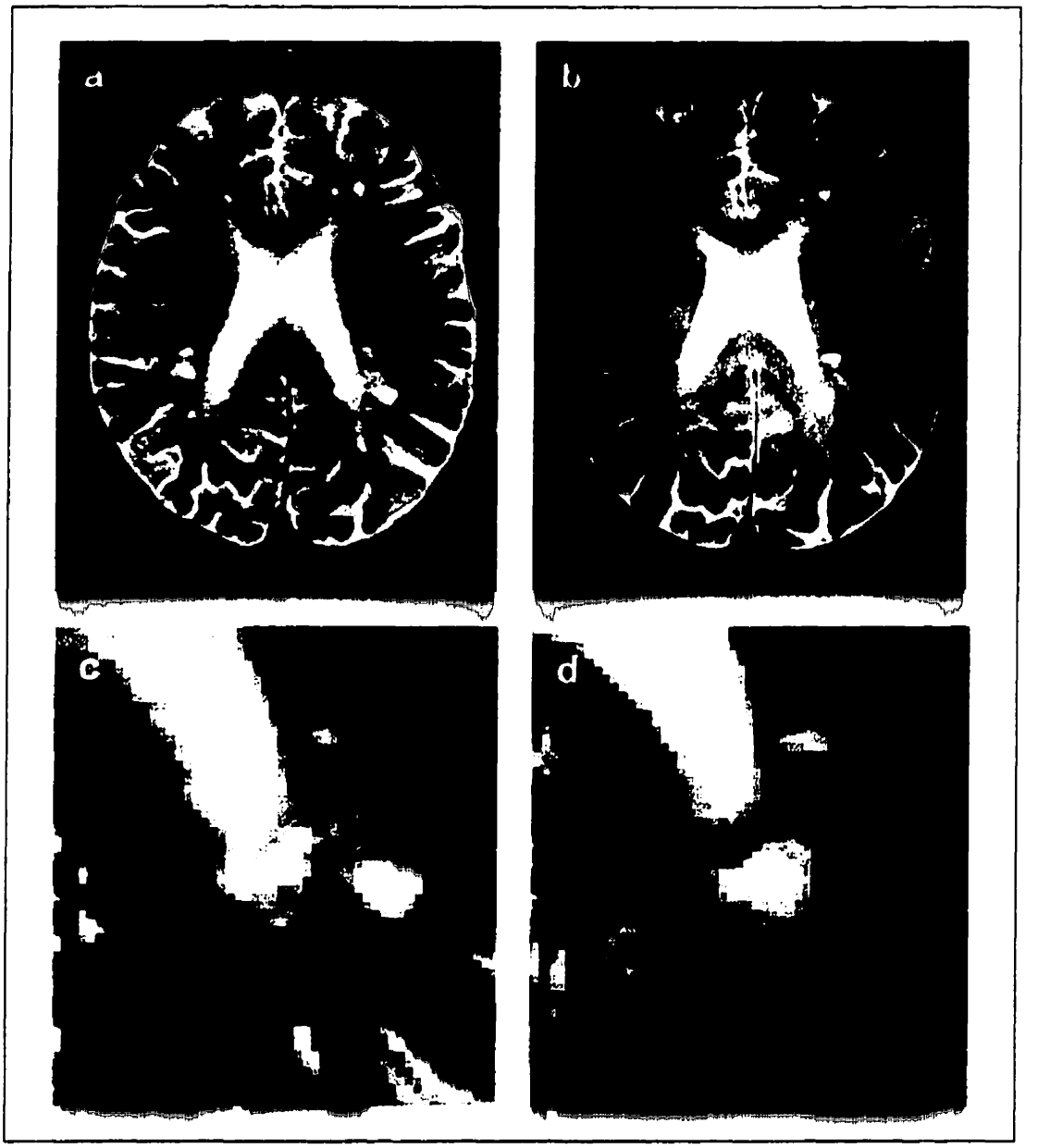

Figure 5.8 Diffuse Area of Abnormality at 0.5 T Appears as Three Focal Lesions at 4 T

T2-weighted images (a and b) and enlarged regions of interest (c and d) acquired at 0.5 T (left) and 4 T (right) from patient RED. The 4 T image depicts three focal lesions that look like a diffuse area of abnormality when viewed on the 0.5 T image.

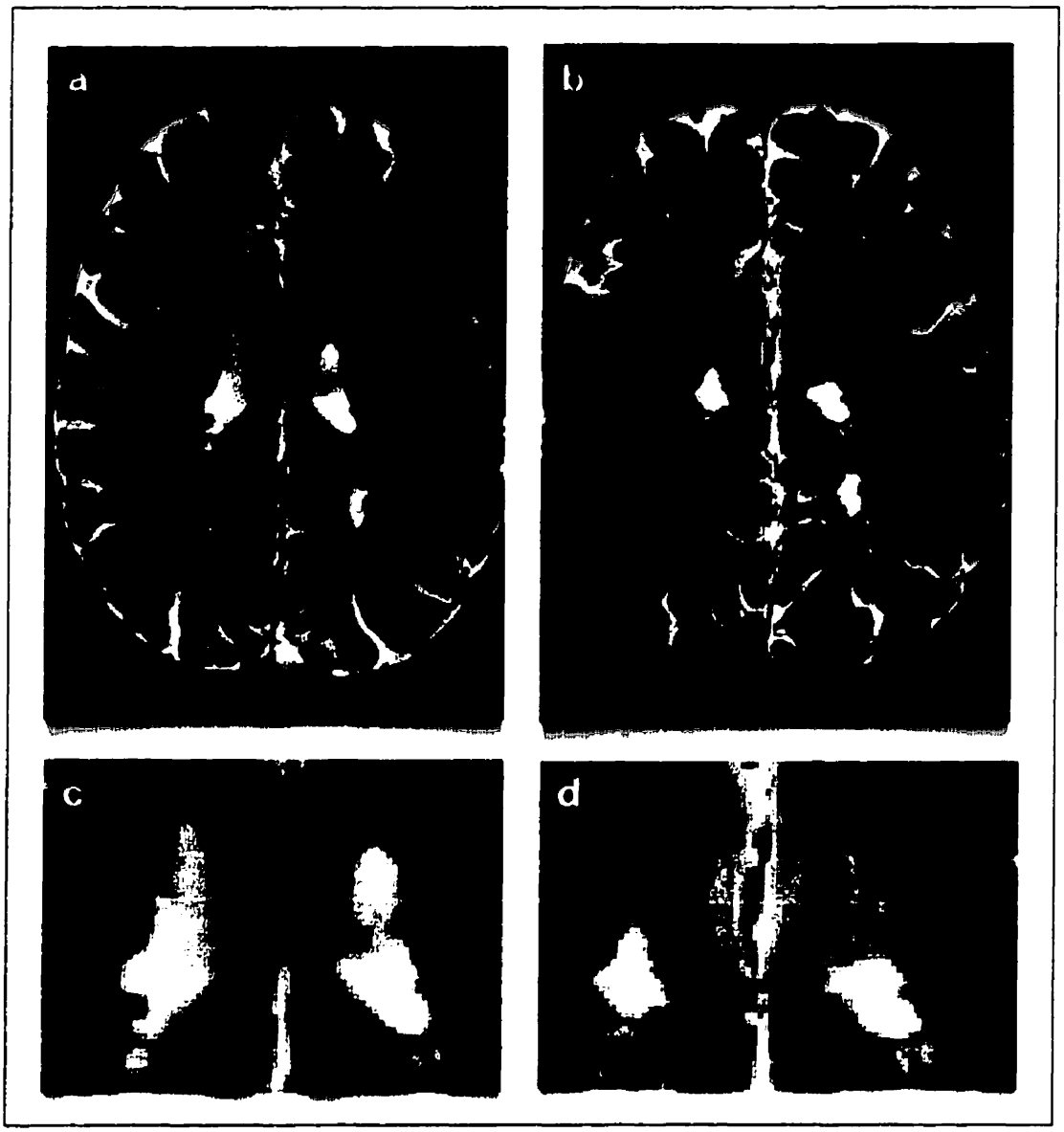

Figure 5.9 Periventricular Lesions Appear More Focal at 4 T

T2-weighted images (a and b) and enlarged regions of interest (c and d) acquired at 1.5 T (left) and 4 T (right) from patient DLM. The 4 T image displays two periventricular lesions that look larger and more diffuse on the 1.5 T image due to volume averaging with the lateral ventricles.

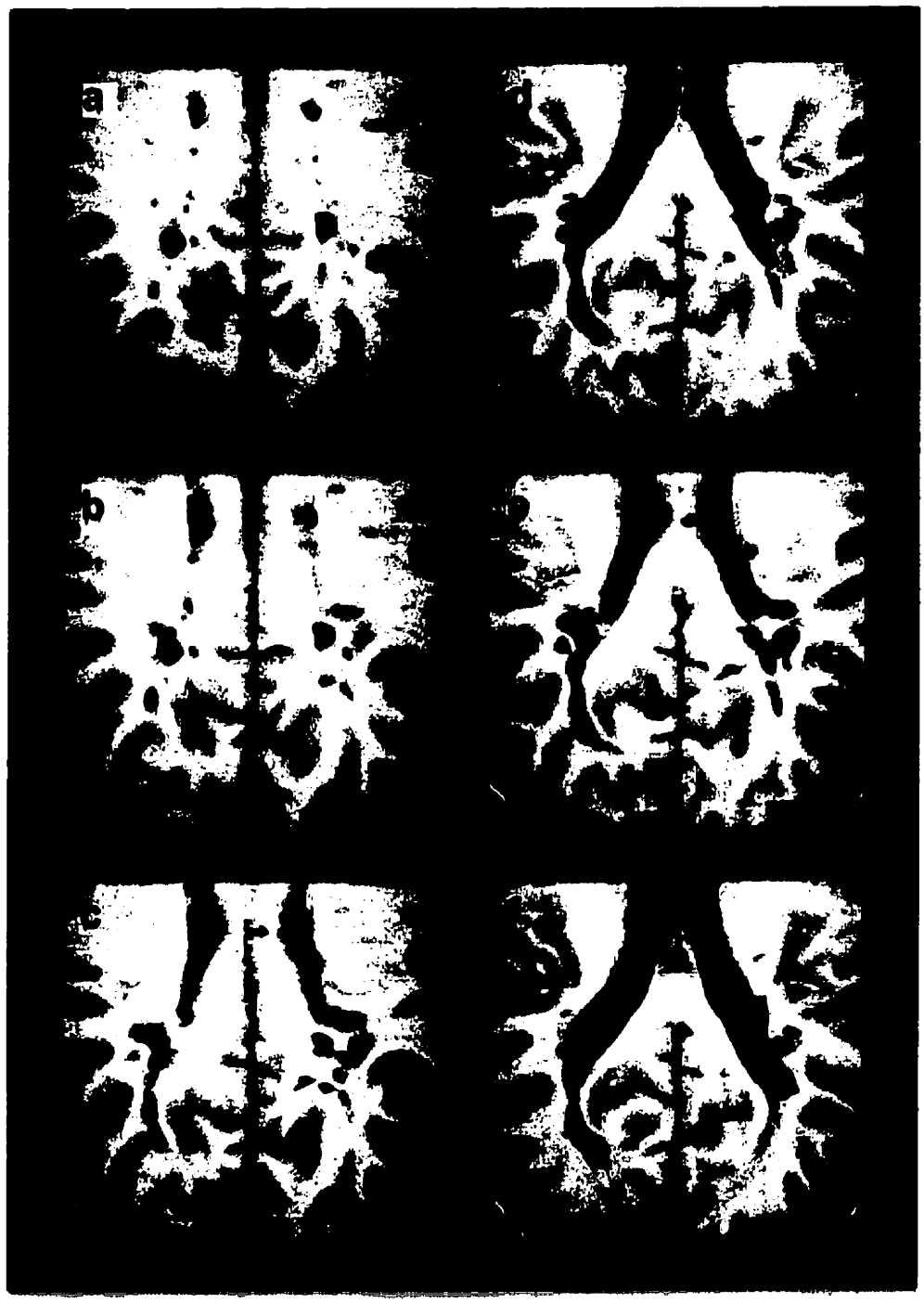

Figure 5.10 Focal Lesions Combine to Form Confluent Abnormality

These six consecutive T1-weighted images acquired at 4 T demonstrate how focal lesions often merge to form confluent areas of abnormality, thereby complicating the identification and comparison of individual lesions.

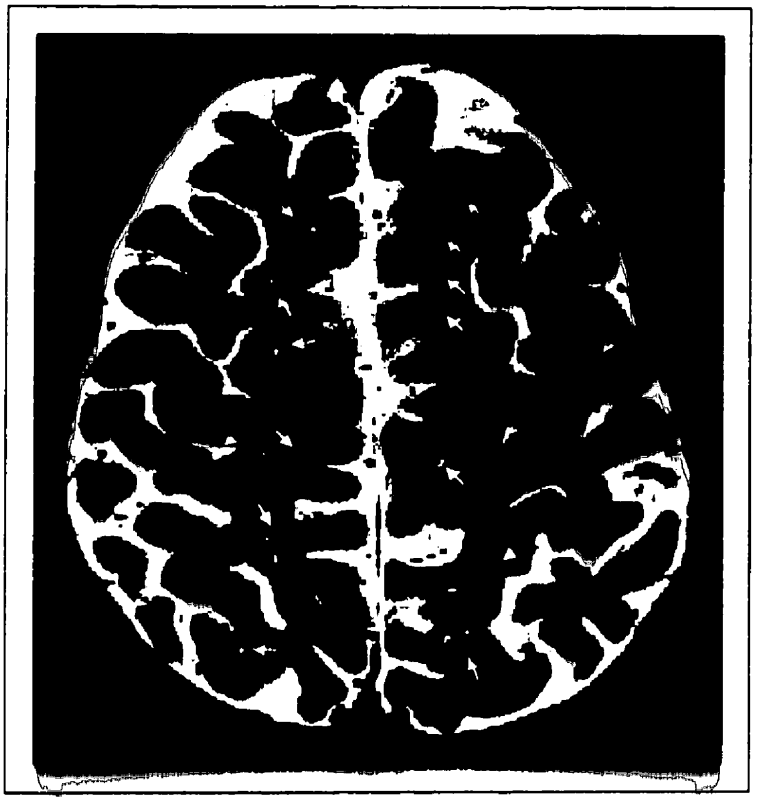

Figure 5.11 Small Areas of Apparent Abnormality of Uncertain Cause

This 4 T T2-weighted image shows enlarged Virchow-Robin spaces (→) of uncertain origin that were not included in the data analysed for this study.

Small areas of apparent abnormality detected at 4 T but of uncertain cause were not included in the analysis (Figure 5.11).

A significant progressive increase in the total lesion load measured at 4 T with increasing 0.5/1.5 T lesion load was found. Data from all 14 patients were compared and demonstrated an 84% increase in the total lesion load measured at 4 T versus 0.5/1.5 T. The relationship between the lesion load measurements at high and low field strength was linear with an r value of 0.875 ($p < 0.001$, DF = 13). The slope of the correlation line was 1.817 showing that the total lesion load detected at 4 T tends to increase with increasing 0.5/1.5 T lesion load. (Figure 5.12). As with the lesion number and volume data, a strong positive correlation

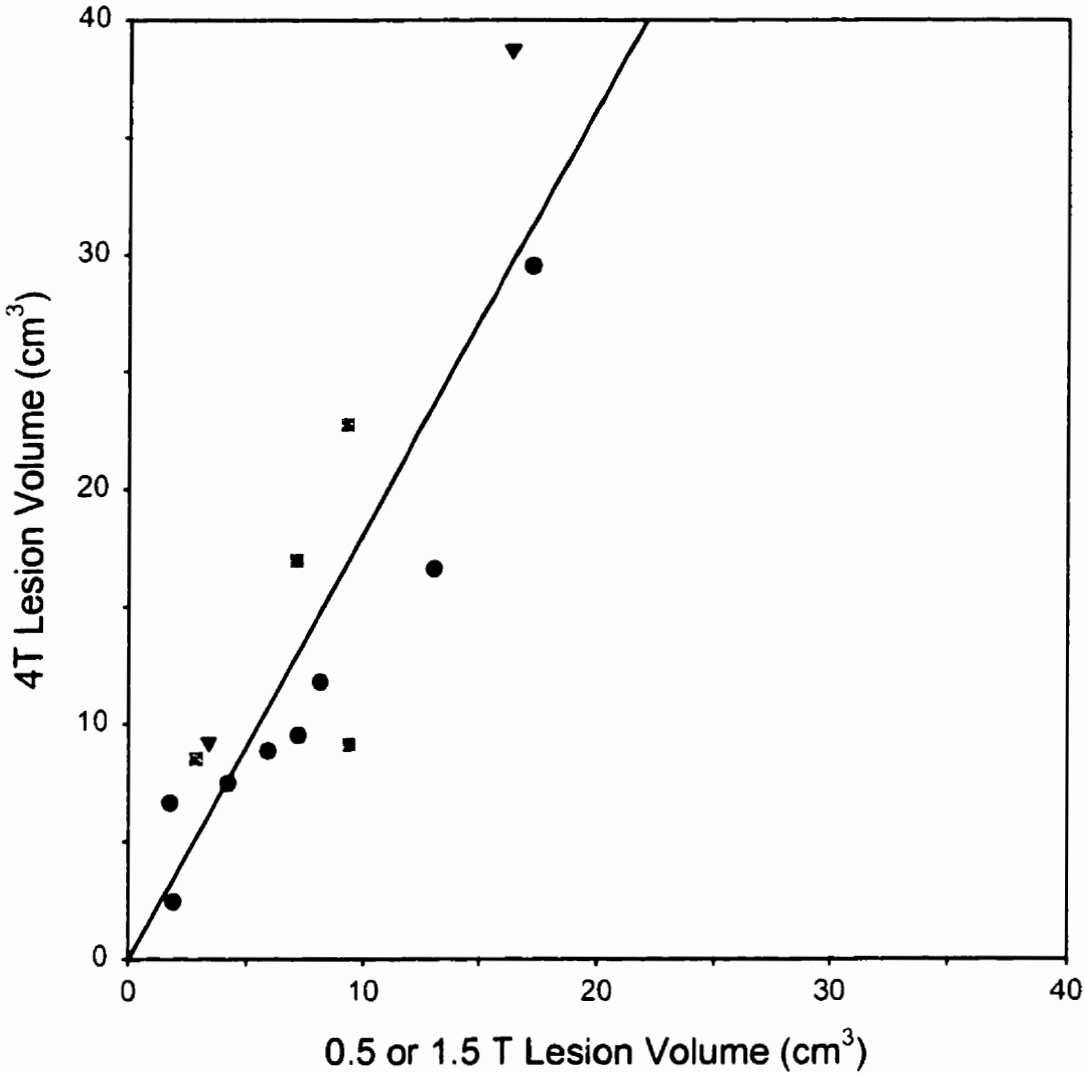

Figure 5.12 Total Lesion Load: 4 T Versus 0.5 and 1.5 T

The total lesion load detected in each patient at 1.5 T (< 48 hours elapsed between exams) (●), 1.5 T (> 1 month elapsed between exams) (▼), and 0.5 T (> 1 month elapsed between exams) (■) is plotted against the total lesion load measured at 4 T. When the data from all 14 patients was compared there was an 84% increase in the total lesion load detected at 4 T versus 0.5/1.5 T. As demonstrated by the correlation line, the relationship between the lesion loads was linear ($R=0.875$, $P<0.001$, $DF = 13$), with a slope of 1.817 showing that the total lesion load detected at 4 T tends to increase with increasing 0.5/1.5 T lesion load.

was also obtained when lesion loads from Group 1 patients were considered separately ($r = 0.958$, $p < 0.001$, $b= 1.540$). However, the moderate positive correlation between the 0.5 T and 4 T data ($r = 0.503$, $b = 1.903$) did not reach statistical significance. All data was determined to originate from the same population ($F = 3.10$, $F_{0.05(1),1,8} = 5.32$). Only two sets of lesion load values were available from Group 2, thus correlation analysis was not performed on this group.

When analysed on a per patient basis, the increase in the number of lesions detected at 4 T was variably present in all patients for whom data were available (Figure 5.13). The number of lesions seen at 4 T but not identified at 0.5 or 1.5 T, expressed as the percentage of the total number of 4 T lesions, ranged from 6% to 62%. The mean value for all patients was 40%, while lesions that were identified at 4 T but not seen at lower fields comprised 47% of the total number of lesions of Group 1 patients, and 19% and 41% for Groups 2 and 3, respectively (Figure 5.14).

Change in total lesion load was also investigated on a per patient and per group basis. An increase in the total lesion load measured at 4 T as compared to that measured at 0.5 or 1.5 T was seen in 13 of 14 subjects (Figure 5.15). The percentage increase in 4 T lesion load ranged from 28% to 282%, with the exception of patient CMT whose 4 T lesion load was 2% less than that measured at 0.5 T. On average, the 4 T lesion load was 57% greater than that detected at 1.5 T in Group 1 patients, and increased over the lower field by 144% and 101% in Group 2 and Group 3 patients, respectively. When all patients were consider together, the mean increase in 4 T lesion load was 84% (Figure 5.16).

Lesion-to-lesion volume comparisons at high and low field, as well as the number and size of lesions identified at only one field strength, were graphed for each patient for whom data were available. One such graph from each patient

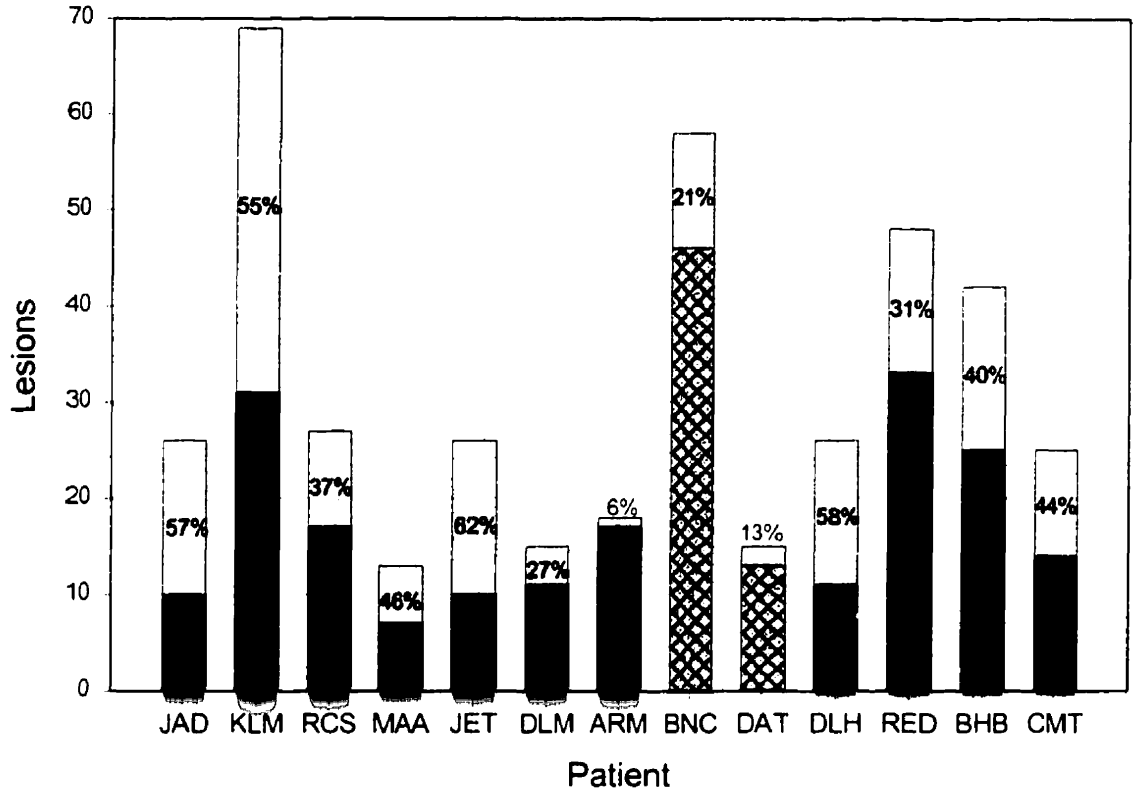

Figure 5.13 Per Patient Increase in the Number of Lesions Identified at 4 T

Graph of the number of lesions detected at 4 T and the percentage of those lesions that were not seen at 0.5/1.5 T. The light gray area of each bar ( ) represents the number of lesions not detected at 0.5 or 1.5 T, while the lower portions of the bars represent lesions detected at 1.5 T in Groups 1 ( ) and 2 ( ), and at 0.5 T in Group 3 ( ), respectively. An increase in the number of lesions identified at 4 T as compared to 0.5/1.5 T is variably present in all patients for whom data were available.

group is presented here as an example of the data obtained (Figure 5.17). The pooled data were also analysed and graphed (Figure 5.18). While a majority of the lesions identified at both high and low field in each patient have larger measured volumes at 4 T, some lesions do appear smaller at the higher field. However, in all but two subjects, the total volume of lesions seen at both field strengths is higher at 4 T than at the lower field. Lesions that were missed at 0.5/1.5 T but identified at 4 T are present in every patient and the reverse is true

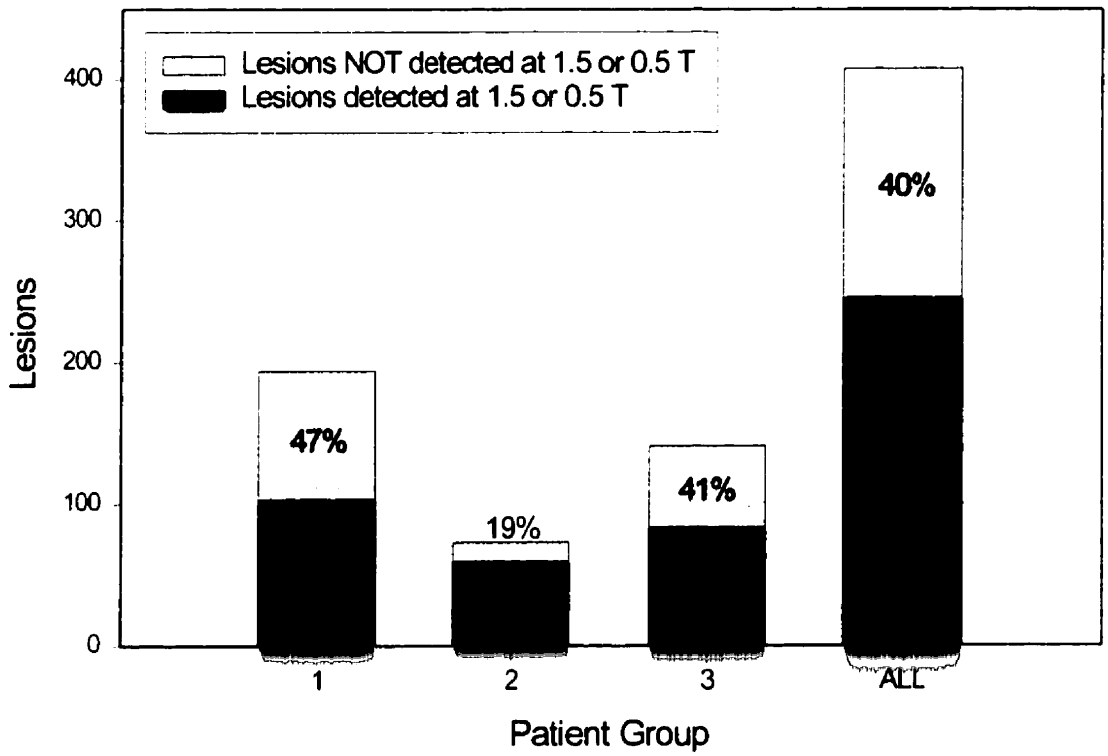

Figure 5.14 Per Group Increase in the Number of Lesions Identified at 4 T

Graph of the number of lesions detected at 4 T and the percentage of those lesions that were not seen at 0.5/1.5 T. An increase in the number of lesions identified at 4 T as compared to 0.5/1.5 T is variably present in all patient groups.

in all but two subjects. In all cases there was a greater number and total volume of lesions seen only at 4 T than lesions seen only at 0.5/1.5 T. When analysed on a group by group basis, the total volume of the lesions identified at both field strengths is always greater at 4 T than at 0.5/1.5 T. Likewise, in Groups 1, 2 and 3, the number and total volume of lesions seen only at 4 T exceeds the number and total volume of lesions detected only at the lower field.

The increase in the lesion load measured at 4 T was found to be principally attributable to the generally larger 4 T volumes of lesions detected at

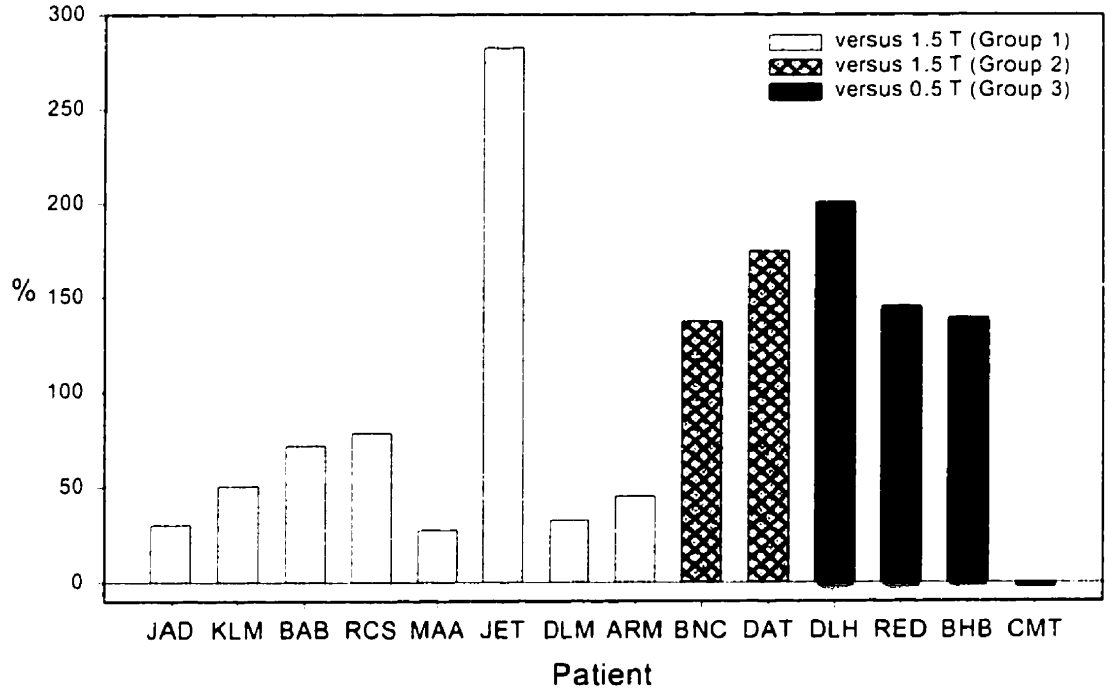

Figure 5.15 Per Patient Increase in 4 T Lesion Load

An increase in the total lesion load measured at 4 T, displayed as the percent increase in the 0.5/1.5 T value, is variably present in all patients except CMT.

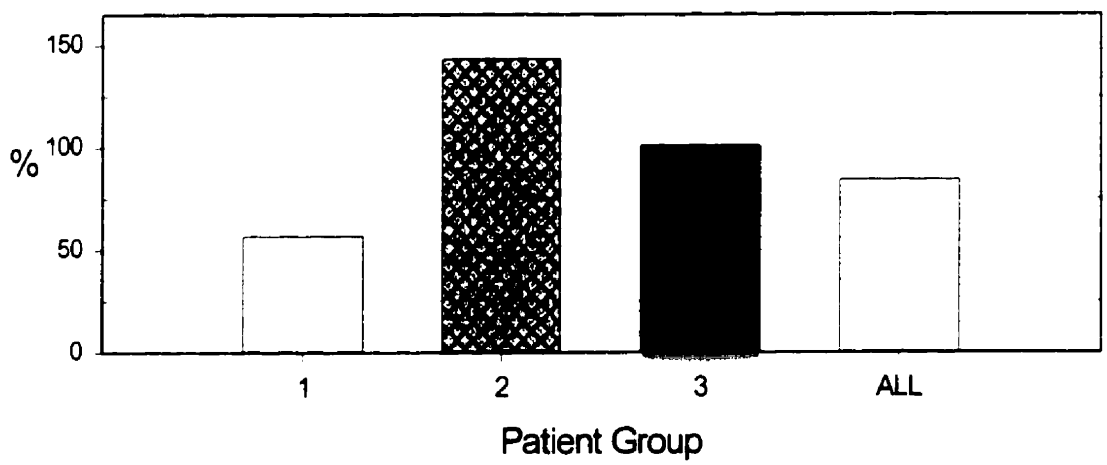

Figure 5.16 Per Group Increase in 4 T Lesion Load

An increase in the total lesion load measured at 4 T, displayed as the percent increase in the 0.5/1.5 T value, is variably present in all patient groups.

a.

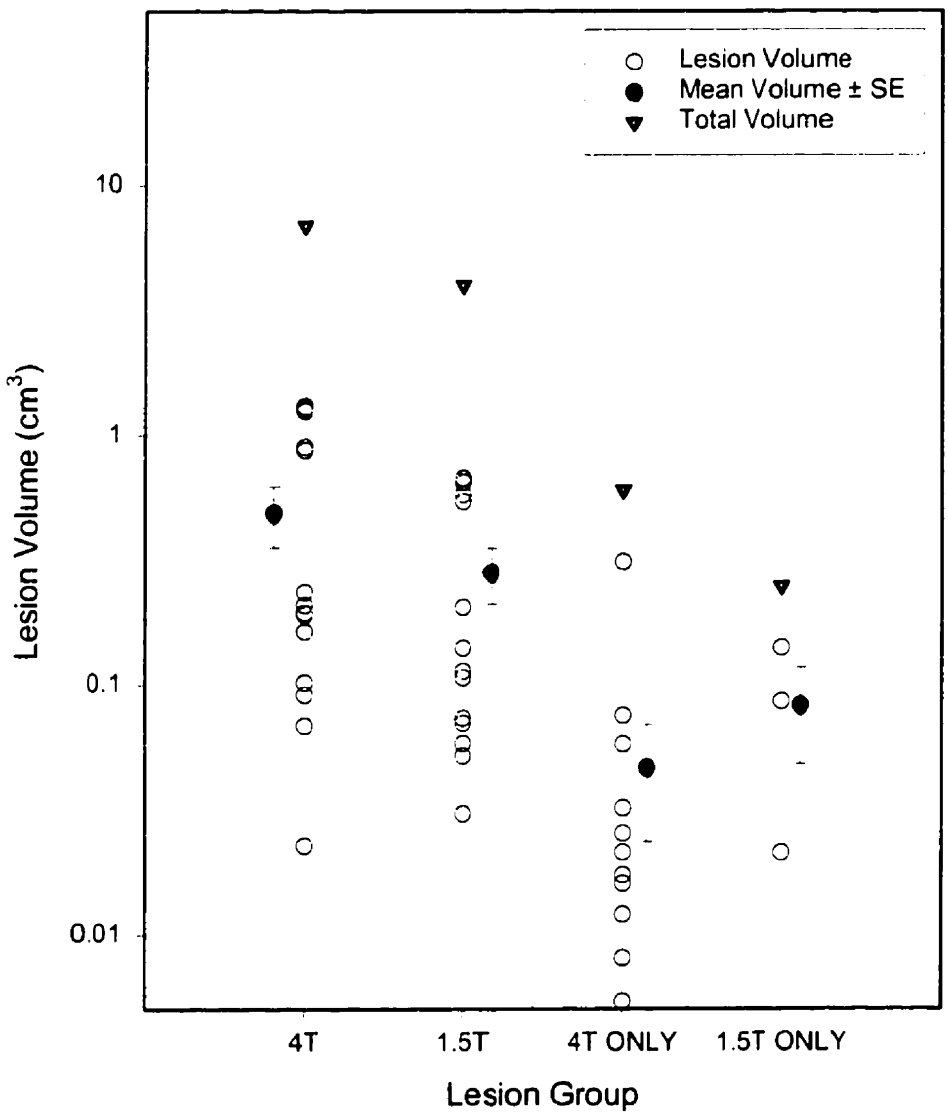

Figure 5.17 Individual Lesion Volumes at High and Low Field as Measured in Three Patients

(a) Comparison of the 4 T volumes and 1.5 T volumes of 14 lesions seen at both field strengths in patient RCS (group 1), as well as of the volumes of the lesions seen only at 4 T and the volumes of the lesions seen only at 1.5 T. Although the volume of some individual lesions decreased when measured at 4 T as compared to 1.5 T, there was a 74% increase in both the mean volume (0.492 ± 0.135 cm^3 vs. 0.283 ± 0.072 cm^3) and total volume (6.890 cm^3 vs. 3.961 cm^3) of lesions measured at 4 T. A total of 13 lesions, with a mean volume of 0.047 ± 0.023 cm^3 and a total volume of 0.604 cm^3, were detected at 4 T and missed at 1.5 T. Three lesions, with a mean volume of 0.082 ± 0.034 cm^3 and a total volume of 0.247 cm^3 were not identified at 4 T and seen only at 1.5 T.

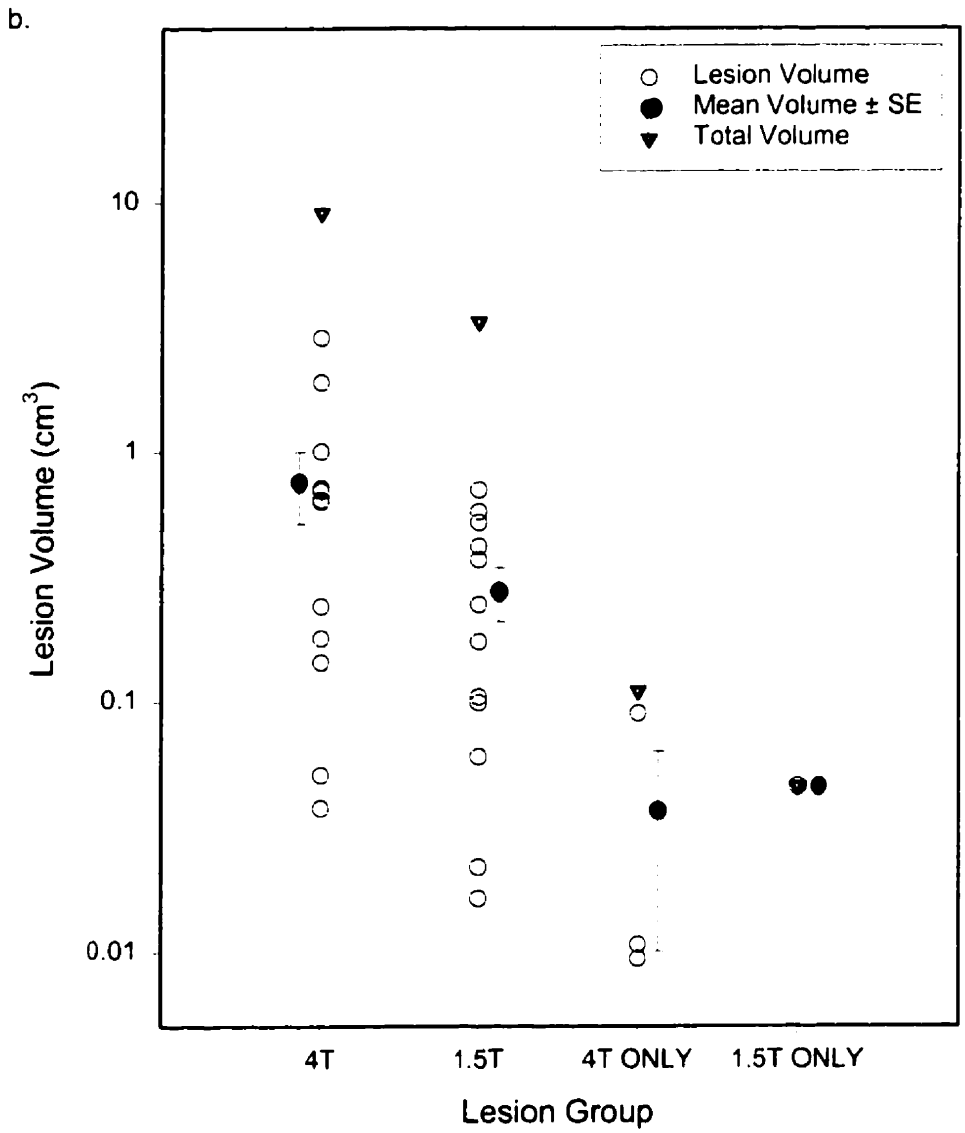

Figure 5.17 (Continued): (b) Comparison of the 4 T volumes and 1.5 T volumes of 12 lesions seen at both field strengths in patient DAT (group 2), as well as of the volumes of the lesions seen only at 4 T and the volumes of the lesions seen only at 1.5 T. There was a 175% increase in both the mean volume (0.761 ± 0.244 cm^3 vs. 0.277 ± 0.069 cm^3) and total volume (9.131 cm^3 vs. 3.322 cm^3) of lesions measured at 4 T. A total of 3 lesions, with a mean volume of 0.037 ± 0.027 cm^3 and a total volume of 1.110 cm^3, were detected at 4 T and missed at 1.5 T. One lesion, with a volume of 0.046 cm^3 was not identified at 4 T and seen only at 1.5 T.

c.

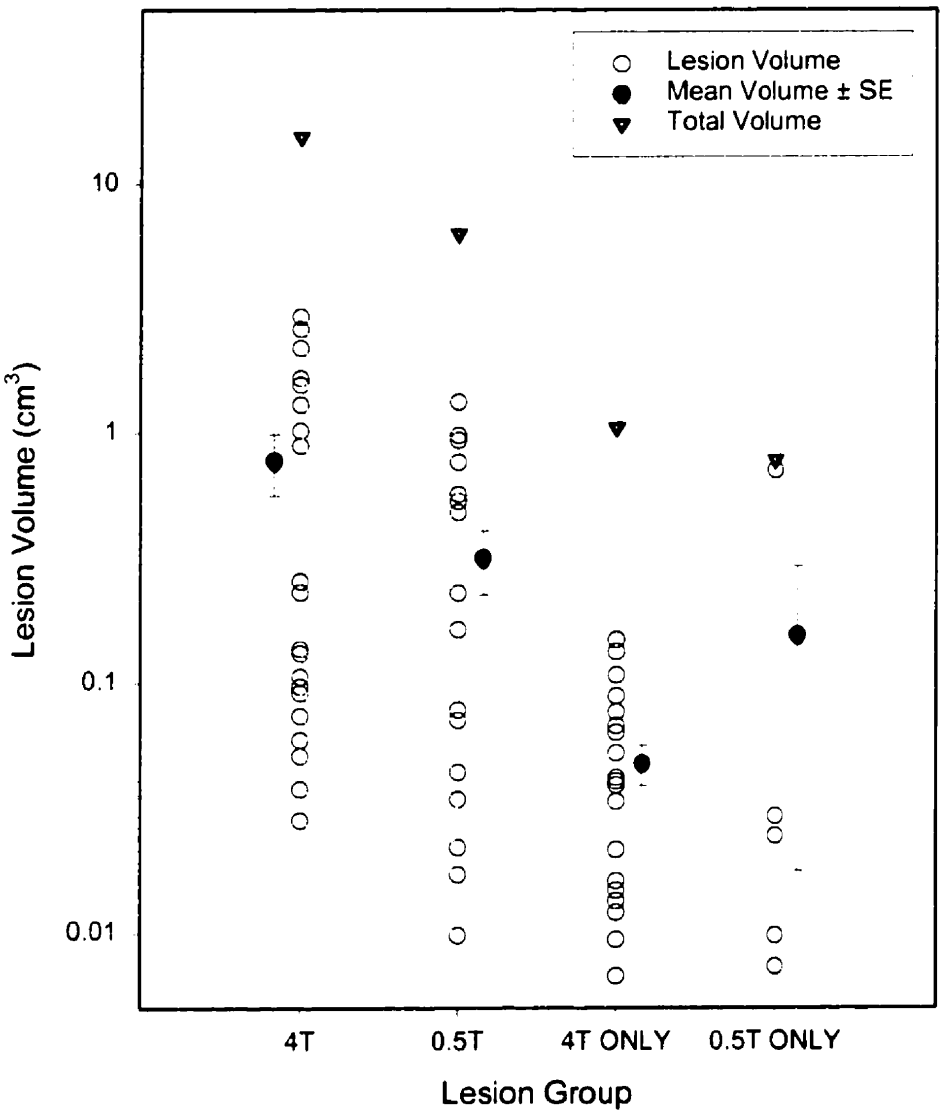

Figure 5.17 (Continued): (c) Comparison of the 4 T volumes and 0.5 T volumes of 20 lesions seen at both field strengths in patient BHB (group 3), as well as of the volumes of the lesions seen only at 4 T and the volumes of the lesions seen only at 0.5 T. Although the volume of some individual lesions decreased when measured at 4 T as compared to 0.5 T, there was a 144% increase in both the mean volume (0.773 ± 0.213 cm^3 vs. 0.316 ± 0.090 cm^3) and total volume (15.461 cm^3 vs. 6.328 cm^3) of lesions measured at 4 T. This difference was statistically significant (Mann-Whitney, p=0.036). A total of 22 lesions, with a mean volume of 0.048 ± 0.008 cm^3 and a total volume of 1.046 cm^3, were detected at 4 T and missed at 0.5 T. Five lesions, with a mean volume of 0.155 ± 0.138 cm^3 and a total volume of 0.776 cm^3 were not identified at 4 T and seen only at 0.5 T.

a.

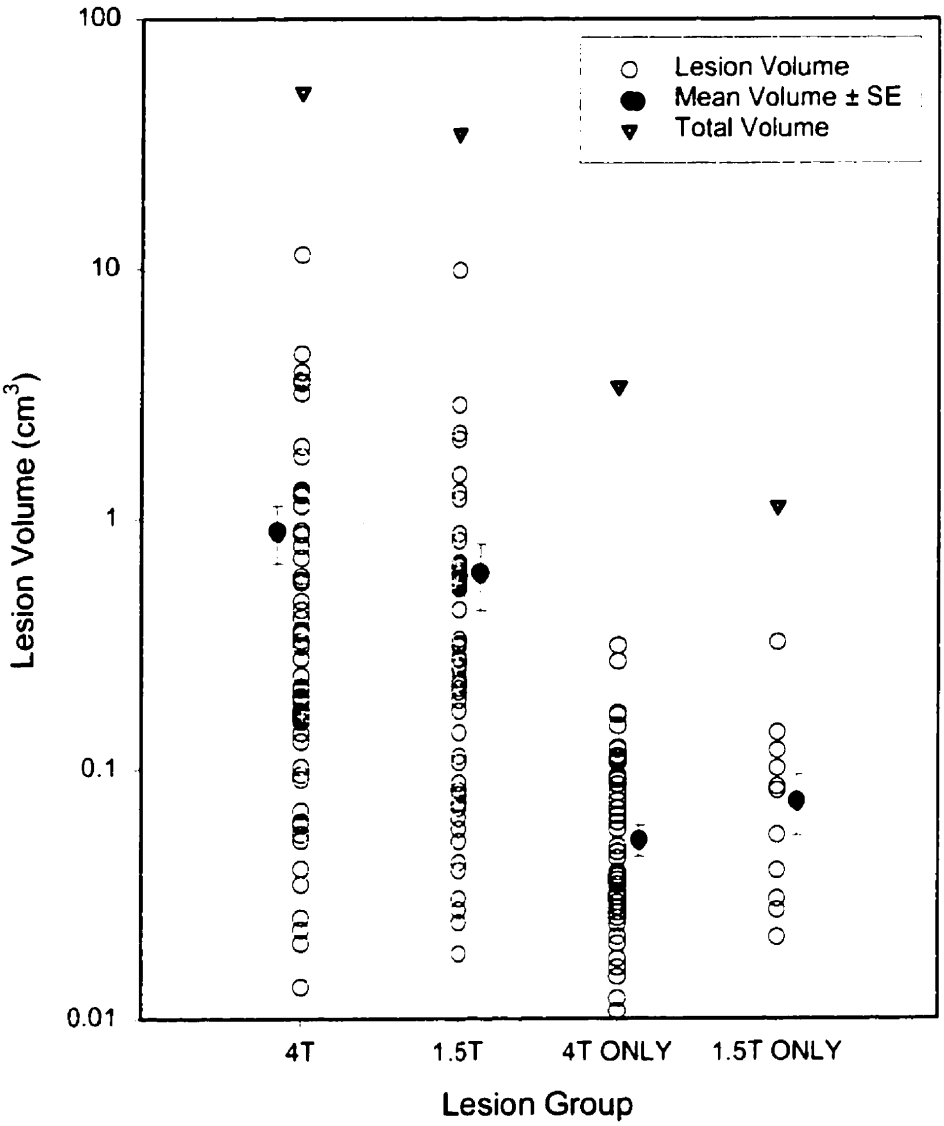

Figure 5.18 Per Group Analysis of Individual Lesion Volumes as Measured at High and Low Field.

(a) Comparison of the 4 T volumes and 1.5 T volumes of 57 lesions seen at both field strengths in patient group 1, as well as of the volumes of the lesions seen only at 4 T and the volumes of the lesions seen only at 1.5 T. Although the volume of some individual lesions decreased when measured at 4 T as compared to 1.5 T, there was a 47% increase in both the mean volume (0.898 ± 0.233 cm^3 vs. 0.612 ± 0.181 cm^3) and total volume (51.209 cm^3 vs. 34.858 cm^3) of lesions measured at 4 T. A total of 64 lesions, with a mean volume of 0.053 ± 0.007 cm^3 and a total volume of 3.366 cm^3, were detected at 4 T and missed at 1.5 T. Fifteen lesions, with a mean volume of 0.075 ± 0.020 cm^3 and a total volume of 1.123 cm^3 were not identified at 4 T and seen only at 1.5 T.

b.

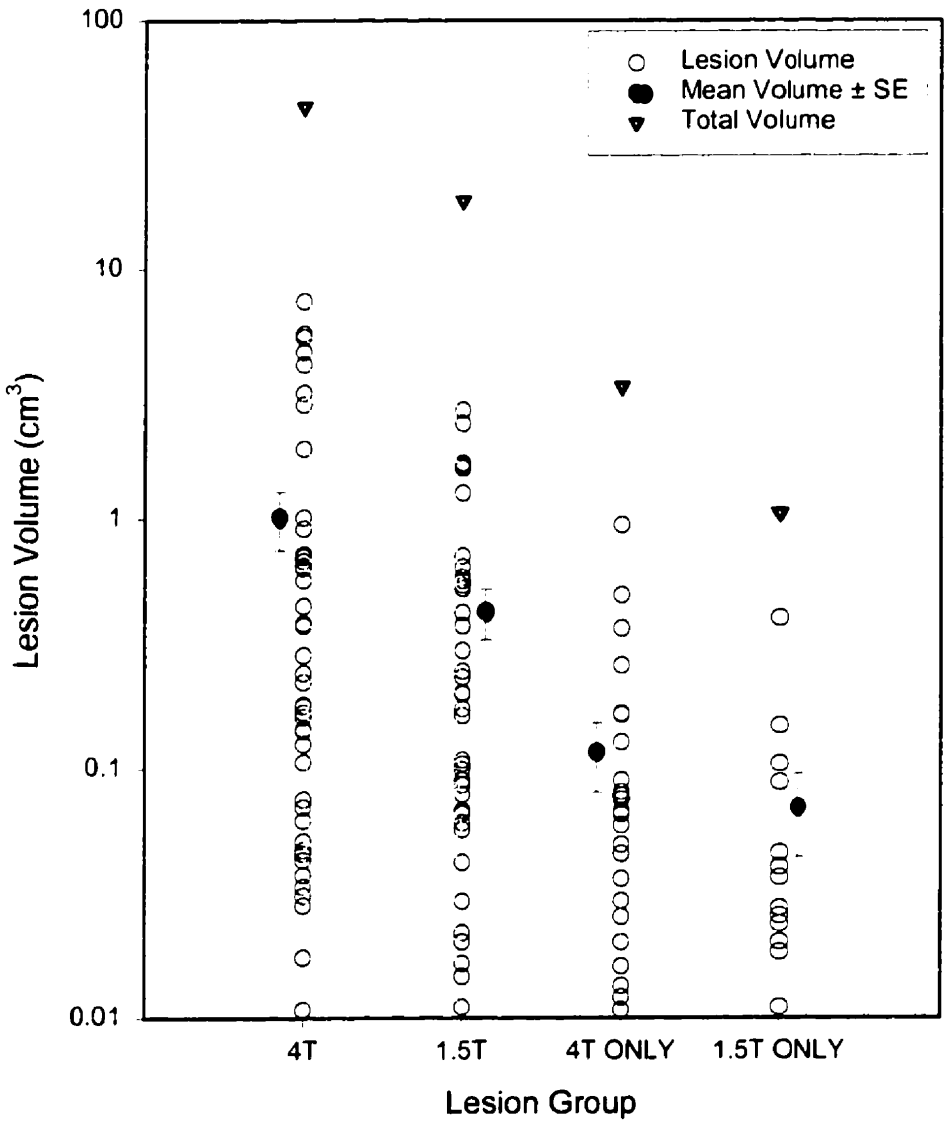

Figure 5.18 (Continued): (b) Comparison of the 4 T volumes and 1.5 T volumes of 44 lesions seen at both field strengths in patient group 2, as well as of the volumes of the lesions seen only at 4 T and the volumes of the lesions seen only at 1.5 T. Although the volume of some individual lesions decreased when measured at 4 T as compared to 1.5 T, there was a 139% increase in both the mean volume (1.014 ± 0.267 cm^3 vs. 0.424 ± 0.097 cm^3) and total volume (44.625 cm^3 vs. 18.675 cm^3) of lesions measured at 4 T. A total of 29 lesions, with a mean volume of 0.116 ± 0.036 cm^3 and a total volume of 3.377 cm^3, were detected at 4 T and missed at 1.5 T. Fifteen lesions, with a mean volume of 0.070 ± 0.025 cm^3 and a total volume of 1.044 cm^3 were not identified at 4 T and seen only at 1.5 T.

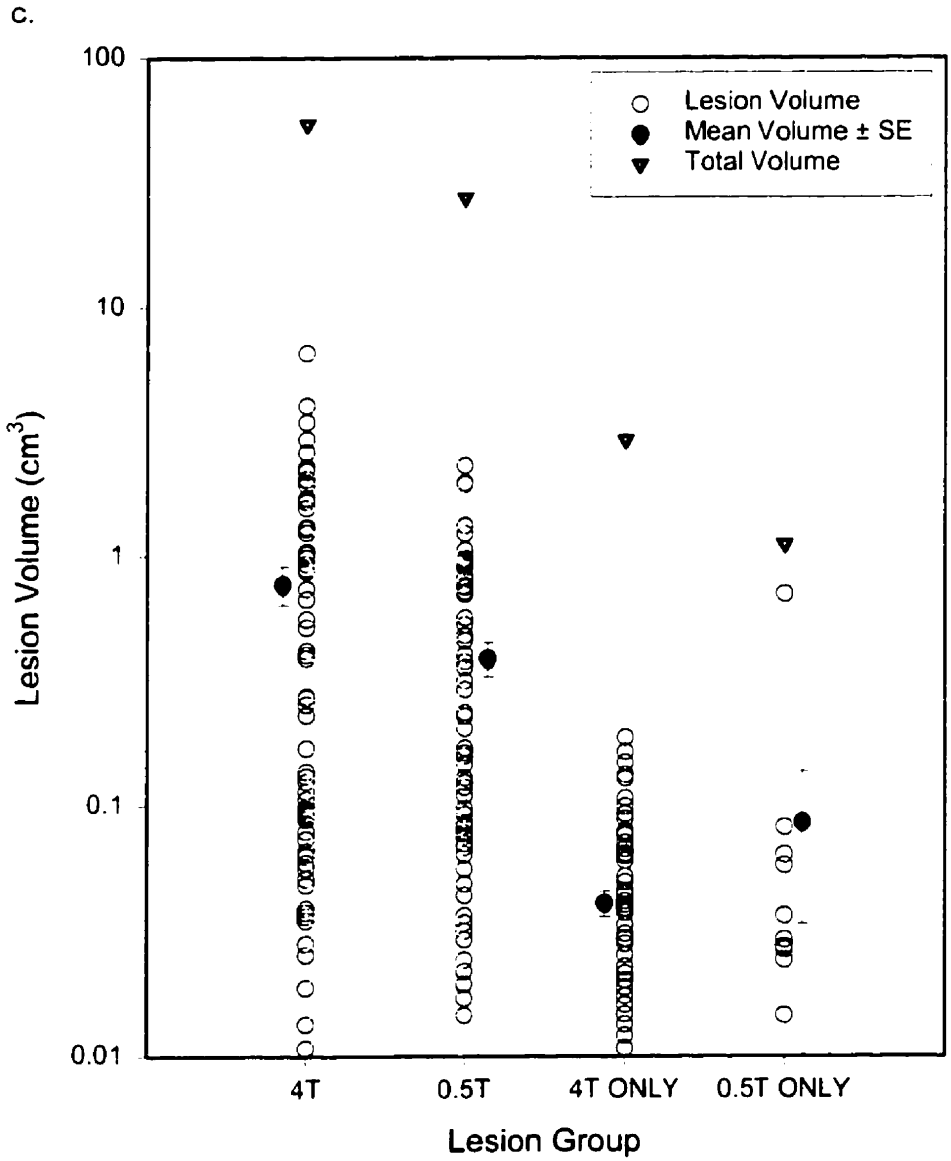

Figure 5.18 (Continued): (c) Comparison of the 4 T volumes and 0.5 T volumes of 70 lesions seen at both field strengths in patient group 3, as well as of the volumes of the lesions seen only at 4 T and the volumes of the lesions seen only at 0.5 T. Although the volume of some individual lesions decreased when measured at 4 T as compared to 0.5 T, there was a 97% increase in both the mean volume (0.772 ± 0.137 cm^3 vs. 0.391 ± 0.062 cm^3) and total volume (54.021 cm^3 vs. 27.393 cm^3) of lesions measured at 4 T. This difference was statistically significant (Mann-Whitney, p=0.046). A total of 71 lesions, with a mean volume of 0.041 ± 0.005 cm^3 and a total volume of 2.909 cm^3, were detected at 4 T and missed at 0.5 T. Thirteen lesions, with a mean volume of 0.086 ± 0.052 cm^3 and a total volume of 1.116 cm^3 were not identified at 4 T and seen only at 0.5 T.

d.

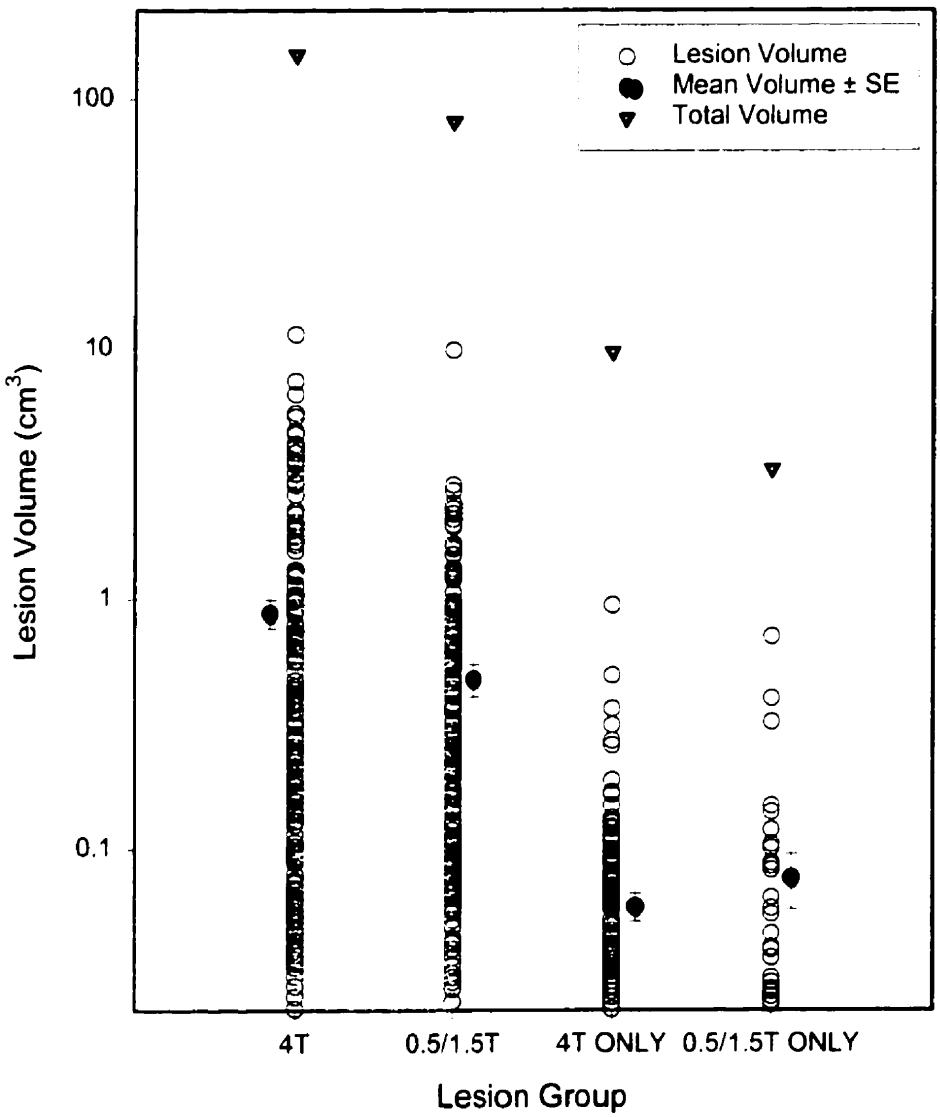

Figure 5.18 (Continued): (d) Comparison of the 4 T volumes and 0.5/1.5 T volumes of 171 lesions seen at both field strengths in all patients, as well as of the volumes of the lesions seen only at 4 T and the volumes of the lesions seen only at 0.5/1.5 T. Although the volume of some individual lesions decreased when measured at 4 T as compared to 0.5/1.5 T, there was a 85% increase in both the mean volume (0.876 ± 0.117 cm^3 vs. 0.473 ± 0.070 cm^3) and total volume (149.855 cm^3 vs. 80.926 cm^3) of lesions measured at 4 T. This difference was statistically significant (Mann-Whitney, p=0.024). A total of 164 lesions, with a mean volume of 0.059 ± 0.008 cm^3 and a total volume of 9.652 cm^3, were detected at 4 T and missed at 0.5 T. Forty-three lesions, with a mean volume of 0.076 ± 0.019 cm^3 and a total volume of 3.283 cm^3 were not identified at 4 T and seen only at 0.5/1.5 T.

both high and low field strengths. On average, using data from the twelve patients for whom lesion-to-lesion comparison was possible, 88% of the increase in total lesion load as measured at 4 T came from an increase in the volume of individual lesions when measured at 4 T as opposed to 0.5 or 1.5 T. The remaining 12 % of the increase was accounted for by the volume of lesions identified at 4 T that were not seen at the lower field strengths. Very similar results were obtained when the data were analysed by patient group based on the time elapsed between high-field and low-field imaging exam and the strength of the low-field exam. An increase in individual lesion volume was responsible for 83%, 89% and 90% of the increase in total lesion load observed in Groups 1, 2, and 3, respectively (Figure 5.19). When analysed on a patient by patient basis,

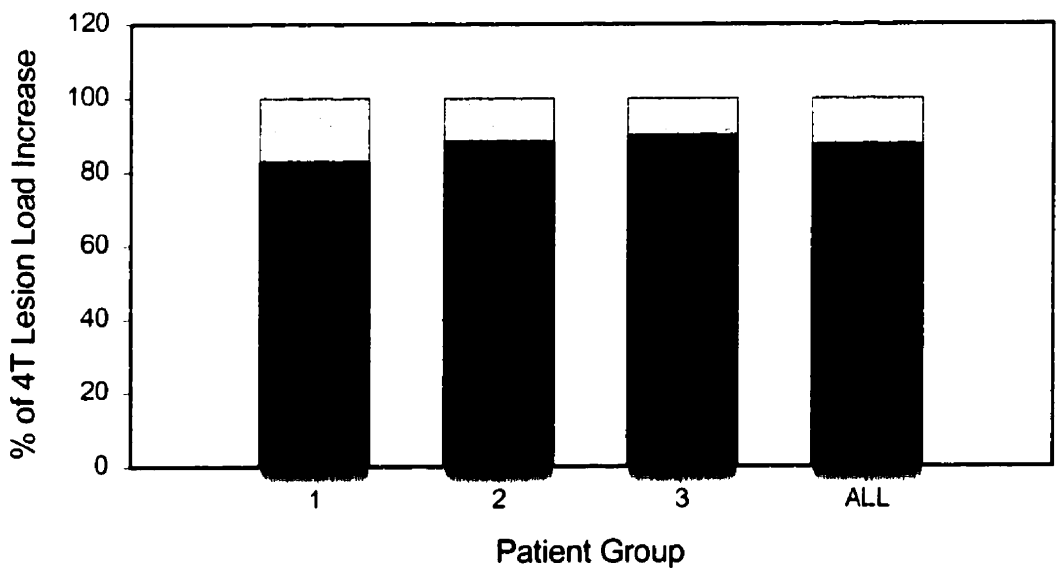

Figure 5.19 Origin of Increased 4 T Lesion Load by Patient Group

Most of the increase in the overall 4 T lesion load per patient group can be attributed to the larger 4 T volumes of lesions detected at both 4 T and 0.5 or 1.5 T (■). The contribution from lesions that were detected at 4 T but missed at 0.5/1.5 T (□) is small and very similar in all patient groups, ranging from 9.85% in group 3 to 17.07% in group 1. When all lesions are considered together, regardless of patient or patient group, lesions missed at the lower fields make up only 12.28% of the increase in lesion load measured at 4 T.

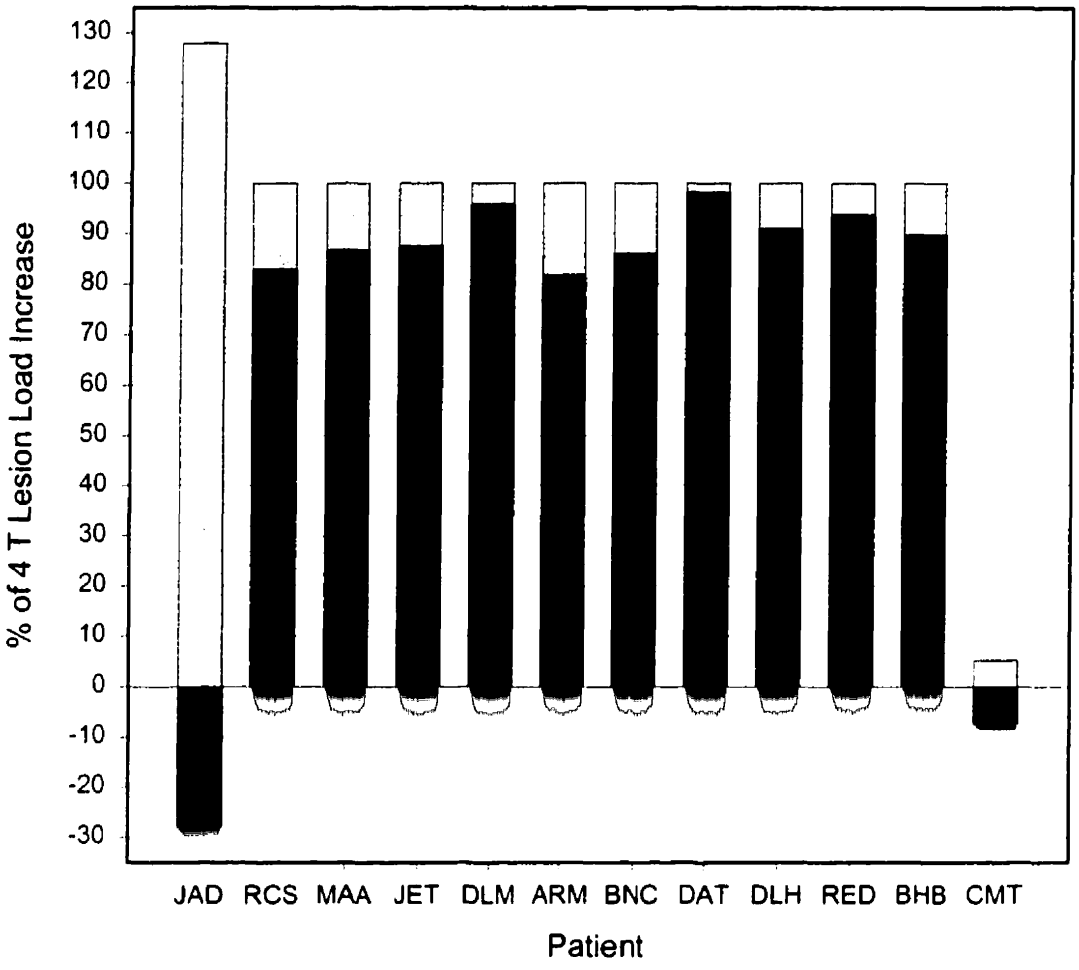

Figure 5.20 Per Patient Origin of Increased 4 T Lesion Load

Most of the increase in 4 T lesion load can be attributed to the larger 4 T volumes of lesions detected at both 4 T and 0.5 or 1.5 T (■). The contribution to the per patient increase in 4 T lesion load from lesions that were detected at 4 T but missed at 0.5/1.5 T (□) is small, ranging from 1.86% to 18.25%. There are two notable exceptions to this trend: Lesions that went undetected in JAD at 1.5 T but were seen at 4 T made up 128% of the increase in 4 T lesion load seen in this patient, while the 4 T volume of lesions seen at both 4 T and 1.5 T actually decreased by 28%. In the case of CMT, there was an overall decrease of 2.19% in the lesion load measured at 4 T as compared with 0.5 T. This decrease was caused by a 7.44% drop in the total 4 T volume of lesions detected at both 4 T and 0.5 T, which was partially offset by a 5.25% increase in 4 T lesion load from lesions that were not seen at 0.5 T.

the percent contribution of increased lesion volume to the increase in total lesion load was variably present in all subjects for whom data were available with the exception of patients JAD and CMT (Figure 5.20). That contribution ranged from 82% to 98%. In JAD and CMT, the mean volume of lesions was less at 4 T than at 0.5 or 1.5 T, resulting in a negative contribution to the increase in 4 T lesion

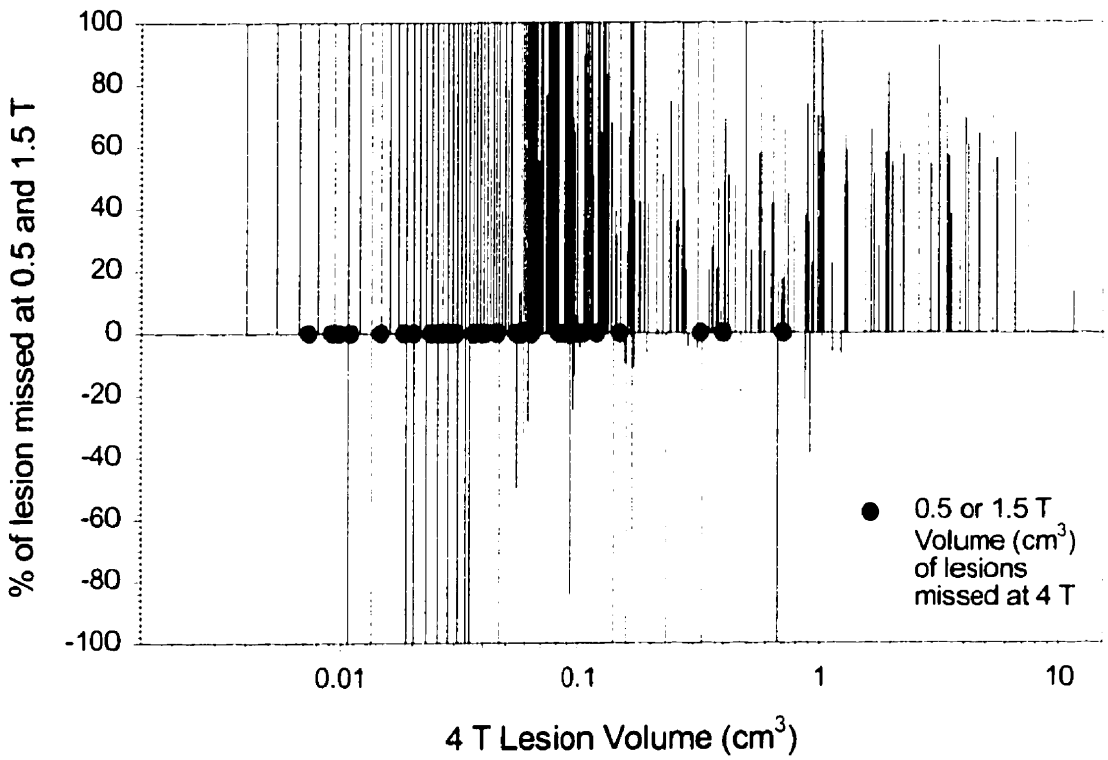

Figure 5.21 Relationship Between 4 T Lesion Volume and Percentage of Lesion Volume Missed at 0.5 T and 1.5 T

This graphical representation of the relationship between 4 T lesion volume and the percentage of lesion volume that is missed at 0.5 and 1.5 T demonstrates that the difference between lesion volumes at the two field strengths increases as the lesion volume measured at 4 T decreases. Below a 4 T volume of 1 cm^3 ( ), 0.5 T and 1.5 T measurements can yield corresponding volumes ranging from 0% to 7536% of the 4 T value. 378 lesion are represented by this graph, 40 of which were not detected at 4 T.

load. This negative contribution was more than offset in patient JAD by the large positive contribution of volume from lesions identified at 4 T that were not identified at 1.5 T, but was only partially offset by lesions seen at 4 T and missed at 0.5 T in CMT, producing a net decrease in 4 T lesion load in the latter patient.

An analysis of the relationship between lesion size, as measured at 4 T, and the number of lesions that went unidentified on either the high or low field images demonstrated that the difference between lesion volumes at 4 T and 0.5/1.5 T increases as the lesion volume decreases. Below a 4 T volume of 1 cm^3, 0.5 T and 1.5 T measurements can yield corresponding volumes ranging from 0% to 7536% of the 4 T value (Figure 5.21).

No significant differences were found between the mean signal-to-noise ratios of white matter, gray matter or CSF on the T1-/PD-weighted images obtained at 1.5 and 4 T. However, the greater mean lesion SNR on the 1.5 T T1-/PD-weighted images did reach statistical significance when compared to the 4 T T1-weighted images. The mean SNR of the T1W images at 4 T was greater than that of the PD-weighted 0.5 T images for all tissues, with the exception of CSF, for which there was no significant difference between field strengths (Figure 5.22). T2-weighted images also demonstrated no significant differences between the mean SNR of CSF at 4 T and 0.5/1.5 T. While there were no significant differences between the mean SNR measured for WM, GM, and lesion on T2W images at 0.5 T and 4 T, and on Group Two 1.5 T and 4 T images, the Group 1 1.5 T images did have larger signal-to-noise ratios for these tissues, which reached statistical significance when compared to the 4 T T2-weighted images (Figure 5.23).

Contrast-to-noise ratios were also calculated and no significant differences were found between the values for white matter and lesion, gray matter and lesion, and CSF and lesion on T2-weighted images obtained at 4 T versus

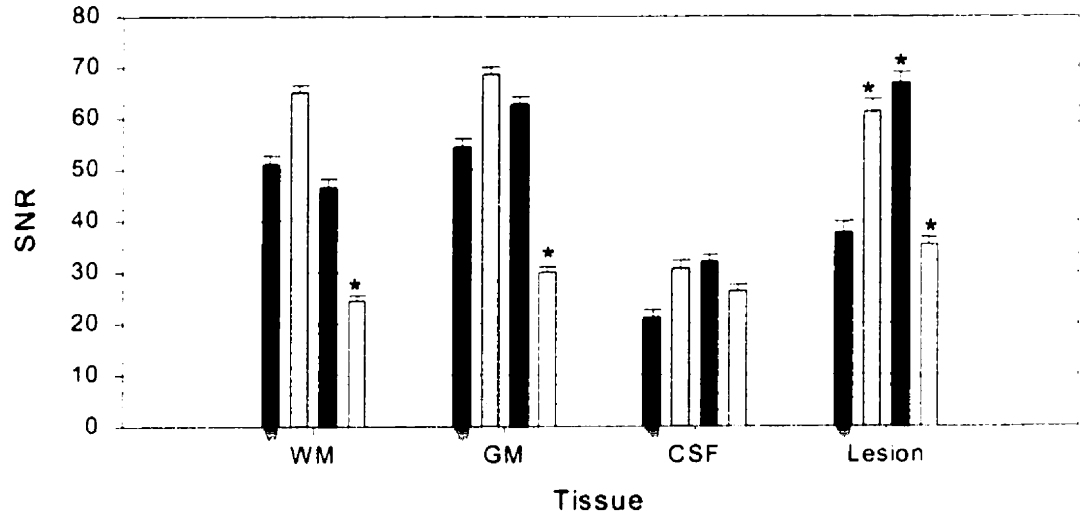

Figure 5.22 Mean T1-/PD-Weighted Image SNR ± Average SD of the Mean

No significant differences were found between the mean SNRs of WM, GM or CSF on the T1W ( ) or PDW ( ) images obtained at 1.5 and 4 T ( ). However, the greater mean lesion SNR on the 1.5 T T1W/PDW images did reach statistical significance when compared to the 4 T T1W images. The mean SNR of the T1W images at 4 T was greater than that of the PDW 0.5 T images ( ) for all tissues, with the exception of CSF, for which there was no significant difference between field strengths. (* $p < 0.05$, Dunnett's test)

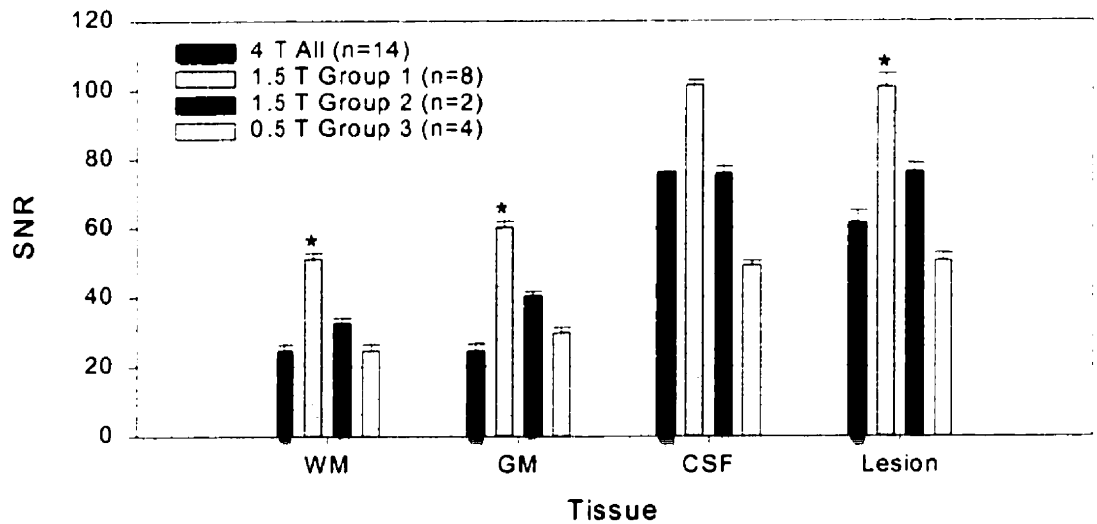

Figure 5.23 Mean T2-Weighted Image SNR ± Average SD of the Mean

No significant differences were found between the mean SNRs of WM, GM, CSF, and lesion on T2W images at 0.5 T and 4 T, or on Group Two 1.5 T and 4 T images. With the exception of CSF, group 1 T2W 1.5 T images did have larger SNRs for these tissues, which reached statistical significance when compared to the 4 T T2W images. (* $p < 0.05$, Dunnett's test)

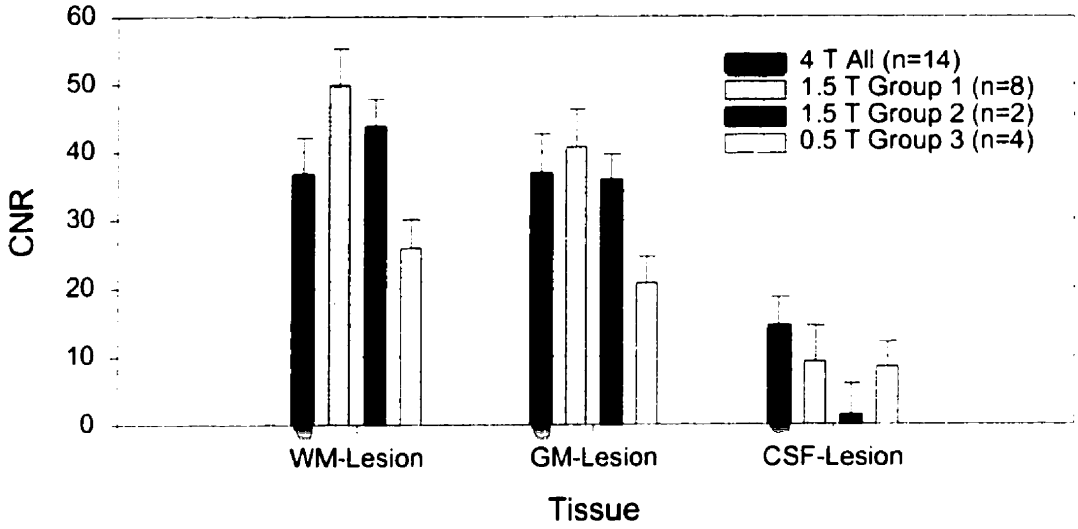

Figure 5.24 Mean T2-Weighted Image CNR ± Average SD of the Mean

No significant differences were found between the contrast-to-noise ratios for white matter-lesion, gray matter-lesion, and CSF-lesion on T2-weighted images obtained at 4 T versus those obtained at 0.5 and 1.5 T.

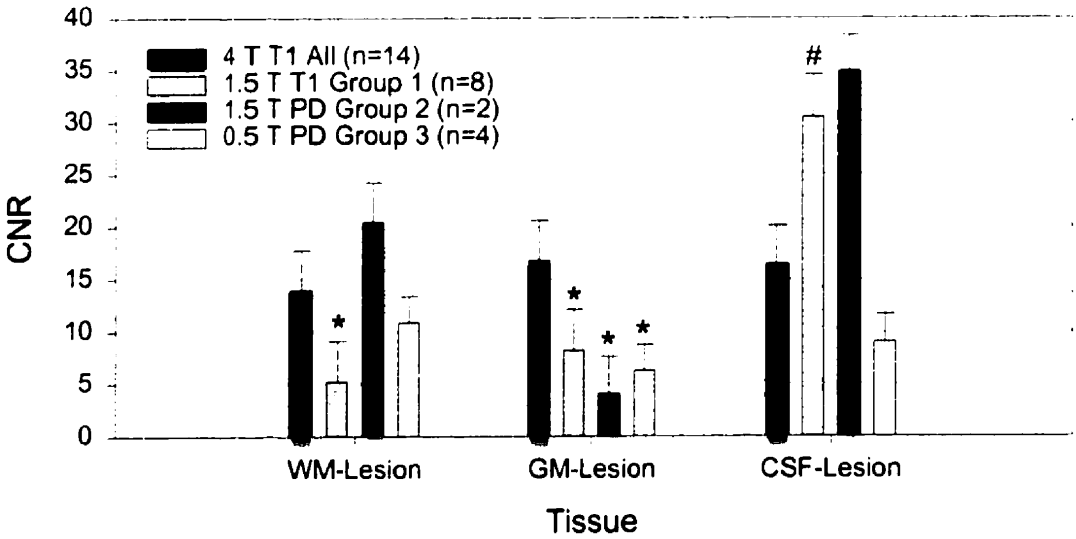

Figure 5.25 Mean T1-/PD-Weighted Image CNR ± Average SD of the Mean

The CNR for WM-lesion and GM-lesion was significantly higher on the 4 T T1W images than on the Group 1 1.5 T images. Conversely, the CSF-lesion CNR was higher on the Group 1 images than it was on the 4 T images. While the GM-lesion CNR on the 0.5 T PDW images and 1.5 T Group Two T1W images was significantly lower than that on the 4 T T1W images, no significant differences between the WM-lesion and CSF-lesion CNR values were present between these image sets. (* $p < 0.05$, Dunnett's test; # $p < 0.05$, Dunn's test)

those obtained at 0.5 and 1.5 T (Figure 5.24). However, the CNR for WM-lesion and GM-lesion was significantly higher on the 4 T T1W images than on the 1.5 T Group 1 T1-weighted images. Conversely, the CSF-lesion CNR was higher on the Group 1 T1-weighted images acquired at 1.5 T than it was on the T1W 4 T images. While the GM-lesion CNR on the 0.5 T PD-weighted images and Group Two 1.5 T T1-weighted images was significantly lower than that on the 4 T T1-weighted images, no significant differences between the WM-lesion and CSF-lesion CNR values were present between these image sets (Figure 5.25).

6

Discussion

This study demonstrates that it is possible to detect greater lesion loads using high-resolution 4 T imaging than can be measured using standard clinical imaging examinations of similar duration. The increase in lesion load observed at 4 T is caused by both the detection of small lesions that go unidentified on lower resolution images, and the increase in the measured volume of most lesions when viewed at high-resolution. Previous studies have demonstrated that the lesion load that is not detected by standard MRI is far from insignificant (Barbosa *et al.*, 1994; Filippi *et al.*, 1995b): Barbosa and co-workers found multiple small areas, often of only one or two pixels, of abnormal tissue in normal-appearing white matter. These lesions, which were only detected by using pixel-by-pixel relaxation time mapping, made up a significant portion of the NAWM (average 36% for T1 and 27% for T2 estimates). Filippi and colleagues found that the magnetization transfer ratio in the NAWM adjacent to lesions increased progressively with distance from the lesion. This pattern, indicating a "demyelinating penumbra" around visible lesions, was typical for more disabled

patients. Since both of these problems (i.e., undetected small lesions and poorly defined edges of visible lesions) are reduced as the voxel size is decreased, it is not surprising that both the number of lesions, and the average lesion volume increased when measured on the high-resolution 4 T images thereby producing an overall increase in the calculated lesion load. The use of 0.8 mm^3 voxels at 4 T, as compared to voxel volumes ranging from 2.6 mm^3 to 5.3 mm^3 at 0.5 and 1.5 T, resulted in a 65% increase in the total number of lesions detected, an 85% increase in the mean lesion volume measured, and an 84% increase in total lesion load.

Analysis of the increased 4 T lesion load revealed that, on average, 88 % of the increase can be attributed to the larger 4 T volumes of lesions identified at both 4 T and 0.5 or 1.5 T. Only a small fraction (12%) of the total increase in 4 T lesion load was produced by the added volume from newly detected lesions that were not seen on the lower resolution images. Considering the small size of these "new" lesions, the mean volume of which was 0.061 ± 0.008 cm^3, it is not surprising that their contribution to the total increase in volume was minimal. Provided that a substantial number of larger lesions is present, a very large number of these small, previously undetected, lesions would be necessary to produce a major impact on the total increase in lesion load calculated from the high-resolution images. These results are similar to those obtained by Wang and coworkers (Wang *et al.*, 1997), who studied twenty-eight patients with CDMS and found that 80% of all the lesions detected had volumes less than 0.180 cm^3. The contribution of these lesions to the total lesion load varied considerably between patients (range, 0% - 6%; mean, 1 %) and was correlated inversely with the total lesion volume (Spearman coefficient of correlation $r = -0.65$, $p < 0.001$, DF=27).

Despite the fact that these small lesions did not have a large impact on the increase in lesion load measured at 4 T, they comprised 49% of the lesions

detected on the high-resolution images. If small lesions such as these are located in critical areas of the brain, they could have very important biological consequences. The identification of this large group of "micro-lesions" could also be important for future studies investigating the natural history of multiple sclerosis. Previous relaxation time and magnetization transfer studies of NAWM have yielded conflicting results. Most studies of T1 and/or T2 relaxation times in patients with MS have found increased mean relaxation times in NAWM when compared with controls (Lacomis *et al.*, 1986; Ormerod *et al.*, 1987; Brainin *et al.*, 1989; Kesserling *et al.*, 1989, Miller *et al.*, 1989, Sappey-Marinier *et al.*, 1990, Armspach *et al.*, 1991; Rumbach *et al.*, 1991). It has also been reported that the magnetization transfer ratio of NAWM in MS patients is significantly lower than that of white matter in controls (Dousset *et al.*, 1992) and there appears to be a consensus that the white matter is diffusely abnormal in MS. However, some investigators have been unable to show significant differences between the relaxation times in their patients and controls (Larsson *et al.*, 1988), or have found abnormalities in some, but not all, regions of interest within NAWM (Haughton *et al.*, 1992), and in a subsequent MT study, differences in magnetization transfer ratios between NAWM of controls and MS patients were not reproduced (Gass *et al.*, 1994). In addition, small samples of NAWM have been shown to have normal characteristics upon MR spectroscopic examination (Bruhn *et al.*, 1992). While there are several possible explanations for this discrepancy, such as the MR methodology, the extent of white matter disease, and the clinical characteristics of the patients, these variable findings, as well as the large number of small lesions identified in the current study, make it likely that the impression of a diffuse white matter abnormality is simply an artifact of the resolution of the MR technique employed. If so, when NAWM is studied, the results will vary significantly in relation to the number and size of voxels that are

involved in the pathologic process within the region of interest.

Based on the observed relationship between 4 T lesion volumes and the percentage of those volumes that go undetected at 0.5 and 1.5 T, the lesion volumes measured using standard-resolution images for lesions with volumes between 7 cm^3 and 1 cm^3 can be expected to be about 60% lower than the actual volumes detected on high-resolution images. For lesions with volumes below 1 cm^3, standard-resolution images yield volumes ranging from 0% to 7536% of the volume measured on the 4 T images. The results of this study therefore suggest that standard clinical MRI examinations cannot accurately detect the volume of lesions which have 4 T volumes of less than 1 cm^3. It would also appear that the volumes calculated for lesions with 4 T volumes between 1 cm^3 and 7 cm^3 using these lower resolution images tend to be substantially less than the volumes that would be measured using higher resolution images. The significance of this finding is underscored by the above-mentioned work of Wang and colleagues who found that 80% of all lesions detected in their study had volumes less than 0.180 cm^3 (Wang *et al.*, 1997). Although forty-three lesions that were seen on the 0.5/1.5 T images were not identified on the high-resolution 4 T images, this number is about one quarter of the number of lesions missed on the lower resolution images and most likely reflects operator error, or differences in image contrast characteristics or slice positioning, rather than a resolution-dependent detection limit.

While analysis of the pooled data in the current study demonstrated strong positive correlations between low-field derived lesion numbers, volumes and lesion loads and those calculated using high-field images, there was considerable variation between subjects. The increase in the number of lesions seen at 4 T, measured as the percentage of the total number of 4 T lesions not detected at lower field, ranged from a low of 6% in patient ARM to a high of 62%

in patient JET. The variability in the 4 T increase in total lesion load is even more striking, ranging from a high of 282% in patient JET to a low of –2% in patient CMT. Given the fact that multiple sclerosis is characterized by a high degree of variability both within and between patients, markedly different results are to be expected from patient to patient. This is especially true in the case of lesion load estimates, as the calculated volume will depend on the number and size distribution of the lesions within a given patient, as well as on the exact three-dimensional shape and orientation of those individual lesions relative to the imaging plane, and the position of the slices relative to the lesions. If there is even a small error in the estimated volume of each lesion, the total error in lesion load will increase with the number of lesions detected. Since small lesions are often missed on low-resolution images, while lesions between 1 cm^3 and 7 cm^3 appear to be underestimated when identified on standard 0.5 T and 1.5 T imaging exams, the size distribution of lesions will also effect the change in estimated lesion load for a given patient. The in-plane resolution of MR images is much higher than the out-of-plane resolution, consequently, the size and shape of individual lesions in relation to the orientation of the imaging plane and the position of the slices can have a large impact on volume estimates due to substantial partial volume effects. Small lesions or small portions of lesions divided between voxels can go undetected, while the same lesion or part of a lesion located in the middle of a voxel may be easily identified. Thus, given the biological heterogeneity among patients and the relation between volume estimates and lesion characteristics, it is of no surprise that a large degree of interpatient variability was seen in the results of this study.

The fact that 22% of the lesions identified on both the 4 T and 0.5/1.5 T images in this study had larger volumes on the low-resolution images as opposed to the high-resolution images, which, in the case of patient CMT, resulted in a net

decrease in the lesion load calculated at 4 T is a result of the complicated relationship that exists between lesion size, shape, and orientation and imaging plane, slice position, and slice thickness. A similar decrease in the volume of some lesions was observed in a study by Molyneux and coworkers in which the mean lesion volume increased from 23.4 cm^3 when 5 mm thick slices were used to 25.3 cm^3 when 3 mm slices were used, but then decreased to 25.1 cm^3 when measured on 1 mm thick slices (Molyneux *et al.*, 1998). These observations can be explained by the research of Filippi and colleagues who used an idealized spherical lesion model to investigate the effects of reducing slice thickness on partial volume effects, and noted that lesion volumes tend to be overestimated when lesion dimensions are of the order of the slice thickness (Filippi *et al.*, 1995c). Therefore, a patient with a large number of convex lesions with dimensions similar to the slice thickness used on a given imaging examination would demonstrate a marked decrease in lesion load when the slice thickness was reduced.

In addition to determining the increase in the number of lesions, lesion volumes, and total lesion load detected on high-resolution 4 T images, as well as the manner in which the increased lesion load comes about, be it via "new" lesions or improved detection of existing lesions, the third objective of this research was to explore the relative contributions of improved in-plane and out-of-plane resolution versus different image SNR and CNR to the improvement in lesion detection. The quality of an image acquired with a given voxel size depends on the signal-to-noise ratio of the tissues in the image, with a higher SNR resulting in an image that is less grainy, and the tissue contrast, which determines lesion conspicuity. Previous research has demonstrated that improvements in image SNR, arising from the use of 3D acquisitions (Filippi *et al.*, 1996), and contrast, due to the use of FLAIR (fluid attenuated inversion

recovery) sequences (Filippi *et al.*, 1996b; Mastronardo *et al.*, 1998) result in increased lesion detection. Thus, the SNR and CNR of the 4 T and 0.5/1.5 T images were compared in order to determine to what degree changes in image SNR or contrast, resulting from differences in pulse sequences, field strength, or acquisition parameters such as TR, TE and receiver gain, contributed to the resolution-dependent improvement in lesion detection.

If magnetic field strength and voxel size were the only parameters that differed between the images from the various patient groups, the mean SNR of the 4 T images would be expected to be 2.08 times greater than the Group 3 0.5 T mean image SNR, and 0.59 times as great as the Group 1 1.5 T mean image SNR. When the ratios of 4 T SNR to 1.5 T SNR from WM, GM, CSF, and lesion on both the T2W and T1W images were averaged, the mean 4 T image SNR was found to be 0.64 times that of the Group 1 1.5 T image SNR. Similarly, the ratios of 4 T SNR to Group 3 0.5 T SNR were also averaged for all tissues, and the mean 4 T image SNR was found to have increased by a factor of 1.29 over the Group 3 0.5 T mean image SNR. Both of these values are close to the predicted values of 0.59 and 2.08, respectively. Thus, it would appear that, in general, the use of different imaging hardware and pulse sequences had only a minor impact on overall mean image SNR. However, some differences between the SNR values of individual tissues were detected.

No significant differences were observed between the signal-to-noise ratios of white matter, gray matter or CSF of the T1-weighted 4 T images, and the T1- and PD-weighted images obtained at 1.5 T. There was, however, a significant increase in the lesion SNR on both the T1-weighted and proton density 1.5 T images, indicating that, despite the fact that the signal-to-noise ratios were comparable in the 4 T and 1.5 T images, both the T1-weighted and PD-weighted 1.5 T images had less T1 weighting than the 4 T images. The SNR

of the 0.5 T proton density-weighted images was significantly lower for all tissues, except CSF, when compared to the 4 T T1W images. Considering the fact that all tissues generally appear somewhat bright on PD-weighted images, this difference in SNR is probably a result of the lower signal strength present at 0.5 T. While no significant differences in SNR were observed between the T2W images at high field and low field in group 2 and 3 patients, there was a statistically significant increase in the SNR of three out of four tissues in the group 1 1.5 T T2W images. It would appear that the overall increase in signal strength and doubling of NEX at 4 T did not completely compensate for the reduction in voxel size between imaging exams of group 1 patients. Thus, the possibility that differences in image SNR contributed to the difference in lesion load estimates at 4 T and 0.5/1.5 T in groups 1 and 3 cannot be ruled out. However, since all the images used in the present study were of good quality upon visual inspection, it is unlikely that differences in image SNR had a large impact on volume estimates.

Of perhaps greater importance in terms of potential influence on lesion identification and outlining, the decrease in contrast between the 4 T and 1.5 T T1-weighted images on one hand and the 0.5 T proton density-weighted images on the other, did not reach statistical significance. The lower CSF-Lesion CNR on 1.5 T images also did not reach significant levels when compared with the 4 T T1W images. Thus, the relatively lower T1-weighting in the 0.5 and 1.5 T images that was indicated by the SNR results does not appear to have been sufficient to significantly alter the contrast between tissues on any of the images, regardless of field strength, pulse sequence, or acquisition parameters. More variability in CNR was present on the T2W images than on the T1W and PDW images. Although gray matter-lesion contrast was significantly higher on the 4 T images, considering that most MS lesions are surrounded by white matter, this difference

is not expected to have had a major influence on the outcome of this study. Likewise, while there was a trend towards higher CSF-Lesion contrast at 1.5 T, this increase only reached significance for group 1 data. The white matter-lesion contrast in images from group 1 patients was also significantly different from the that of the 4 T images, however no differences were present between the WM-lesion contrast at high- versus low-field in groups 2 and 3. The fact that the CSF-Lesion contrast was greater and WM-lesion contrast was smaller on the group 1 1.5 T images than on the group 1 4 T images suggests that the 4 T T2-weighted images had a higher degree of T2-weighting than the group 1 T2W images. Although contrast differences on T2-weighted images may have made lesions more conspicuous on 4 T images compared to group 1 1.5 T images, thereby influencing the increase in lesion load seen in those eight patients, as with T1W/PDW image contrast, differences in T2W image contrast do not appear to have been significant in groups 2 and 3.

Despite the fact that differences in image SNR were observed between high- and low-field images in groups 1 and 3, and contrast differences may have facilitated lesion detection on T2W 4 T images in group 1, the great majority of the increase in 4 T lesion load can be attributed to the increased resolution of the 4 T images. While differences in image SNR and CNR effect the conspicuity of lesions, they have less of an influence on the number of pixels that appear abnormal within a given lesion, and hence, have little impact on lesion volume estimates. If the signal-to-noise ratio or contrast between tissues were so poor that it interfered with the identification of lesions or lesion boundaries, lesion load estimates would obviously be affected. However, since all images seemed to be of similar quality in terms of SNR and CNR upon qualitative inspection, it is not likely that these factors had a large influence on lesion volume estimates in this study.

One factor, aside from the improved in-plane and out-of-plane resolution, that may have effected the increase in 4 T lesion load however, was the interslice gaps present in the imaging data from patients in group 3. These 2 mm gaps (0.5 mm in the case of patient DLH) resulted in an extra 28 mm (7 mm for DLH) of tissue being imaged at 4 T. Hence, the 0.5 T lesion data from group three may be slightly underestimated producing a greater apparent increase at 4 T. Since the number of "new" lesions seen only at 4 T, the degree of individual lesion volume increase, and the increase in total lesion load on the high-resolution 4 T images did not vary significantly between groups, the effects of this possible underestimation would seem to be insignificant, or at least too small to be detected due to interpatient variations in lesion load among the small number of subjects in each group. This is not surprising considering that only small lesions that were positioned with the majority of their volume completely within the interslice gap would go totally undetected, while larger lesions would be seen, at least in part, in the neighbouring slices.

Despite differences in SNR and CNR between the high-field and low-field images within certain patient groups, and the variation in the volume of tissue analysed for patients in group 3, increased image resolution, both in the imaging plane and out-of-plane, appears to be primarily responsible for the improved lesion detection at 4 T. While it is clear that the smaller voxel size used at 4 T was the major factor in the increase in the number of lesions, volume of lesions, and total lesion load identified on the high-resolution images, the relative contribution of decreased slice thickness versus smaller pixel area cannot be determined from the data obtained in this investigation. Since the in-plane resolution was improved to a lesser degree than the out-of-plane resolution in this experiment, it seems logical to assume, however, that a greater portion of the increase in lesion load resulted from the use of thinner slices rather than from the

decreased pixel size.

The results of the current study seem to support previously published work on the effect of image resolution on lesion volume estimates in patients with multiple sclerosis. Filippi and associates observed a 9% (range, 1% - 33%) increase in lesion load when voxel volumes were reduced by 40% (from 3.7 mm^3 to 2.2 mm^3) by means of decreasing the slice thickness from 5 mm to 3 mm (Filippi *et al.*, 1995c). The same researchers also found a 42% increase in the mean volume of hypointense lesions on T1W images when slice thickness was reduced from 5 mm to 3 mm, and a 58% increase in mean lesion volume when data from 1 mm thick slices was compared with that from 5 mm thick slices (Filippi *et al.*, 1998). In the current study, voxel volumes were reduced by an average of 77% (range, 69% - 85%), resulting in a mean increase in lesion load of 84%. While, as expected, the number of lesions, lesion volumes, and total estimated lesion load detected was greater on the high-resolution 4 T images with increases variably present in all patients, the extent of the increase in lesion load was quite large in comparison to that observed by Filippi and coworkers (Filippi *et al.*, 1995c; 1998). However, even when Filippi and colleagues decreased the slice thickness of the images used in their study from 5 mm to 1 mm thereby reducing the voxel size used by 80%, their reduced voxel volume of 1.27mm^3 remained 57% larger than the 4 T voxels used in this study. Thus, although the percentage decrease in voxel size was similar in the two studies, the final resolution achieved was substantially better in the current experiment, possibly explaining the larger observed increase in mean lesion volume. It is important to note that the work of Filippi and associates was performed using a single MR scanner and a single pulse sequence. The author does not know of any previously published study in which the combined benefits of a state-of-the-art MR scanner, which include new or updated pulse sequences and improved

image resolution due to increased SNR available at higher magnetic fields, were compared with the results produced by standard clinical imaging technologies. What follows is a discussion of the possible sources of error in the present study and the limitations inherent to all lesion load estimates that make comparisons between studies problematic at best.

While quantitative measurement of lesion load in MS is a widely used marker of disease progression, it has been difficult to measure lesion load with a high degree of reproducibility. It has already been shown that several factors markedly influence lesion volume estimates in MS, including intrapatient biological variations (Stone *et al.*, 1995), the use of multiple MR scanners (Filippi *et al.*, 1997), different pulse sequences (Filippi *et* al., 1996; 1996b; 1998; 1998b; Rovaris *et al.*, 1997), acquisition parameters (Filippi *et al.*, 1995c; 1998), segmentation techniques (Filippi *et al.*, 1995d; 1998b; Grimaud *et al.*, 1996), operator training (Filippi *et al.*, 1998c), and accuracy of patient repositioning (Gawne-Cain *et al.*, 1996: Filippi *et al.*, 1997b). Because the magnitude of the variability introduced by all of these factors may make it impossible to reliably detect lesion load change, several strategies to reduce the effect of these sources have been developed (Stone *et al.*, 1995; Filippi *et al.*, 1995; 1997b; 1998d; Miller *et al.*, 1996). Ironically, however, the goal of the current study, which was to compare high-resolution 4 T MRI exams representative of the highest quality imaging achievable in a clinically reasonable timeframe using current technology with standard clinical MRI exams performed at 1.5 and 0.5 T, dictated the use of different scanners, different pulse sequences, and different acquisition parameters, thereby contravening many of the strategies developed to reduce the inherent variability of lesion load estimates. Scheduling constraints and limited patient availability necessitated the inclusion of data from a relatively small number of subjects obtained from imaging exams that, in some cases,

were separated in time on the order of months, rather than hours, thereby further increasing the potential for error in estimates of lesion load change. The possible effects of these factors on the data used in this study and their significance in terms of the interpretation of that will now be discussed.

Sources of variation in lesion load estimates include the scanners, pulse sequences, patients, techniques and operators used in the study. These factors influence the quality (i.e. SNR, contrast and spatial resolution) of the resultant images and the results of quantification. Since different scanners were used in this study, it is possible that differences between equipment and techniques resulted in changes in lesion volume estimates that were erroneously attributed to the increased 4 T image resolution. A previous study by Filippi and associates in which patients were scanned on the same day on two different scanners using the same imaging techniques and acquisition parameters found that, on average, estimated lesion volumes varied by 6% (Filippi *et al.*, 1997). The scanners used in the above-mentioned study varied only in manufacturer. Changes in lesion volumes can therefore be attributed to image inhomogeneity due to different receiver coils and receiver electronics, different lesion conspicuity caused by variations in image SNR and CNR as a result of minor variations in the pulse sequences used by different manufacturers, intraobserver variability, and the effect of even minor repositioning errors. Even when a single MR scanner is used, changes in image quality can result from minor differences in flip angle and magnetic field homogeneity, which must be reset for each patient, as well as from drift in system performance over time (Filippi *et al.*, 1998d). Thus, in this study, as with all studies comparing images obtained from different scanners, a relatively small percentage of the observed change in lesion volumes may be attributable to differences in system performance unrelated to the pulse sequences, acquisition parameters, or patients studied.

While changes in image resolution, contrast, and SNR resulting from different pulse sequences and acquisition parameters are of major importance in the estimation of lesion load, patient repositioning is also a critical factor in determining volume estimate accuracy. As discussed previously, lesion load estimates depend on the three-dimensional shape and orientation of individual lesions relative to the imaging plane, and the position of the slices relative to the lesions. Hence, in order to accurately compare the lesion load in a given patient using images obtained during separate examinations, the imaging plane and position of the slices must match as closely as possible. Despite the great efforts that are made to reduce any variation in lesion volume by accurate repositioning, errors in the alignment of the slices from different imaging exams inevitably exist. This fact was particularly so in the case of the current study, where, despite following the repositioning technique recommended by the ad hoc European Community Committee (Miller *et al.* 1991), accurate repositioning was complicated by the previously described deficiencies in the 4 T planning tools.

The mean percentage change in lesion load that can be expected due to imprecise repositioning is on the order of 7% when 5 mm thick slices are used and 3% when 3 mm thick slices are used (Filippi *et al.*, 1997b). This is despite the use of the well standardized repositioning technique employed in the current study and used in several clinical trials. In another study of repositioning errors conducted using two image sets in which the quality of the repositioning was judged by a radiologist to be "very good", two sets in which the repositioning was judged to be "moderate", and one set that was judged to have "poor" repositioning, a 15% (range, 9% - 32%) difference in lesion load was detected (Gawne-Cain *et al.*, 1996). It is interesting to note that the image set that produced the 32% difference in lesion load was judged by the radiologist to have "very good" repositioning. This apparent discrepancy might be explained by the

fact that the same study also found that the repositioning error will vary with patient, as the difference in lesion volume between the rating of each scan increased with mean lesion load. Although the different lesion volumes obtained in the above studies are not due solely to repositioning errors, since intraobserver variability must also be considered, they nonetheless indicate that the effect of repositioning errors cannot be ignored when evaluating the results of this, or any other lesion load study. Despite the impediment to accurate repositioning encountered in the current study, the variability introduced by this factor is probably lower than would be predicted based on the results of the work by Gawne-Cain and associates, which was conducted using 5 mm thick slices, due to the very thin 2.2 mm slice thickness used at 4 T.

As mentioned in the preceding paragraph, intraobserver variability also contributes to errors in lesion load estimates. Since the degree of intraobserver variability changes with the segmentation method used and the experience of the observer, these subjects will be addressed together. Currently employed image analysis methods are time consuming and prone to operator-induced errors as ambiguities often arise in identifying lesions and evaluating their size and extent (Filippi *et al.*, 1998d). These difficulties arise from the fact that MS lesions are inherently fuzzy with "soft" rather than "hard" boundaries, there is significant variation in the conspicuity of lesions on MR images, and lesions tend to be small in size and large in number. A considerable number of methods for quantifying lesion load have been described (Evans *et al.*, 1997). These methods can be divided into two broad categories: manual outlining and semiautomated local thresholding techniques. This classification system is misleading however, as manual outlining is performed with the aid of a computer, and semiautomated techniques, like the one used in the current study, require significant operator input. A previous comparison of manual versus semiautomated techniques

found the semiautomated method to be more reliable than manual outlining, with the semiautomated technique resulting in an intraobserver lesion load variability of 6 % compared to 12% - 33% variability for the manual technique (Wicks *et al., 1992).* Similar results have been observed in subsequent comparisons (Filippi *et al.*, 1995d; 1998c; Grimaud *et al.*, 1996; Mitchell *et al.*, 1996).

Although the intraobserver variability in lesion volume estimates is relatively low when a semiautomated segmentation tool such as Segtool (Mitchell *et al*, 1994) is used, the degree of vacillation will depend on operator experience and characteristics of the image sets under analysis. As operators gain experience in lesion identification and outlining, they may subconsciously modify their criteria for identifying lesions and lesion boundaries. A 10% reduction in lesion loads in a recent clinical trial was attributed to a systematic change in the technique applied by the single observer who performed the measurements (Paty *et al.*, 1993), and a recent study of lesion quantification shows that experienced observers are more conservative in lesion identification and outlining than inexperienced observers (Barkhof *et al.*, 1997). However, recent evidence demonstrates that even experienced observers exhibit intraobserver variability in lesion load estimates as high as 8% and may disagree about the identification and extent of individual lesions (Filippi *et al.*, 1998c). In addition to personal experience, image characteristics also influence the fluidity of volume estimates. The high lesion-to-white matter contrast present in FLAIR images has been shown to improve both intra- and interobserver variability (Filippi *et al.*, 1998b), and it can be assumed that images with superior in-plane resolution also result in less inconsistency. However, the effect of increased out-of-plane resolution on intraobserver variability is less clear. Repositioning and partial volume errors are reduced by the use of thinner slices and a recent study showed a decrease in both intraobserver and interobserver variability when 3 mm thick slices were used

to measure lesion volumes instead of 5 mm thick slices (Rocca *et al.*, 1998). The greater number of images in each exam causes an increase in analysis time, however, which may result in increased instability in volume estimates due to operator fatigue (Filippi *et al.*, 1998b). Also, it is conceivable that intraobserver variability may decrease with increasing lesion load, as overestimation and underestimation of individual lesion volumes may cancel each other out when large numbers of lesions are present (Filippi *et al.*, 1998b). Lesion size has an effect on intraobserver variability as well, with volume estimates from small focal lesions being less variable than those from large diffuse lesions (Mitchell *et al*, 1996).

Since all images in the current study were analysed using a semiautomated technique and reviewed by a single operator over a relatively short period of time, intraobserver variability was kept to a minimum. While it is possible that the lower in-plane and out-of-plane resolution of the 0.5/1.5 T images resulted in less reliable volume estimates than those measured from the 4 T images, operator fatigue caused by the increased amount of time required to analyse the larger number of slices in each 4 T image set may have partially offset any difference in intraobserver inconsistency. It can therefore be assumed that, as with other studies, approximately 6% of the increased lesion volume observed on the 4 T images may be due to intraobserver variability in lesion volume estimates. Of course, since the observer was not blinded as to the origin of the images used in this study, the possibility that unintentional bias influenced intraobserver inconstancy cannot be ruled out. While it is likely that intraobserver variability in lesion volume estimates had a relatively minor effect on the results of the current study, quantification techniques, operator experience, and image characteristics also influence interobserver variability, further complicating the comparison of the results from the current study with previous studies. A

different observer evaluating the images used in the current study could be expected to produce lesion volume estimates that varied by as much as 25% from those reported here (Filippi *et al.*, 1998c). When this difference is added to the heterogeneity produced by the use of different hardware, pulse sequences, acquisition parameters, patients, segmentation software, and observers the difficulty in comparing lesion load estimates between studies becomes clear.

In addition to the uncertainty in lesion volume estimates introduced by the use of different MR scanners and image segmentation software, and variations in the manner in which this equipment is operated, biological diversity also plays a major role in influencing the results of lesion load studies. As discussed previously, multiple sclerosis is a disease characterized by variability. Although there is a trend toward accumulation of lesions over time, marked fluctuations in lesion load are observed in patients from month to month (Stone *et al.*, 1995). While the intrapatient and interpatient differences in lesion load that occur over the short and long term appear to be much higher than the measurement errors caused by methodological deficiencies, the impact of the many sources of measurement error on sample size requirements has not been fully evaluated (Filippi *et al.*, 1998d).

Although the natural history of MS is toward a gradual increase in lesion load, for example, on the order of 7% to 13% per annum in relapsing-remitting MS (IFNB Study Group *et al.*, 1995; Stone *et al.*, 1995), there appears to be a natural 15% - 20% oscillation in T2 lesion load as new lesions wax and wane (Stone *et al.*, 1995). Neither a gradual increase in lesion load nor an oscillation in new lesion volumes would have effected the results obtained from patients in group 1 of the current study, from whom images were obtain at both field strengths less than 48 hours apart. The data from groups 2 and 3, however, was susceptible to influence from both of these factors, with the per-patient risk of

changes in lesion pathophysiology skewing results increasing with the time elapsed between imaging exams. If the data from these two groups had indeed been influenced by an increase in lesion volume during the interscan delay, due either to a graduai increase in lesion load or oscillation in lesion volumes, the increase in individual lesions volumes, number of lesions detected, or total lesion load should be greater in groups 2 and 3 than observed in group 1. Since no significant differences in the total lesion load increase was observed between groups, it does not appear that the time elapsed between 0.5/1.5 T imaging and 4 T imaging in groups 2 and 3 had a significant impact on the results of the current study. It is possible, however, that an increase in lesion load due to the natural progression of multiple sclerosis did occur in some patients during the interscan delay, but this increase was offset by an oscillatory decline in new lesion volume at the time of the second scan. Since the number of "new" lesions seen only at 4 T and the degree of individual lesion volume increase did not vary significantly between groups, this possibility also seems unlikely. It is more likely, though, that any small differences in lesion load that did occur in group 2 and 3 patients between imaging scans was outweighed by interpatient variability, thereby obscuring any differences between groups caused by interscan changes in patient pathophysiology. These hypothetical differences might have become apparent if a larger number of patients were scanned from each group.

The interpatient variability that characterizes multiple sclerosis was highlighted in the current study by the range of results observed when the data were analysed on a per patient basis. Patients were recruited for this study based only on their willingness to participate and their availability for a 4 T scan immediately prior to, or following, their visit to the MS clinic. Their clinical history, including duration of disease, EDSS score, current lesion load and lesion characteristics were not considered in the recruitment process. As previously

discussed, lesion load estimates will vary by patient according to the size distribution, number, and location of lesions, thus it is not surprising that the increase in lesion load detected on the high-resolution images varied greatly between patients. The large interpatient variability observed in multiple sclerosis makes the results of lesion load studies such a this one, in which a small number of patients are used, difficult to reproduce and even harder to accurately compare with other studies. However, an increase in the number of lesions detected on the high-resolution images was observed in *every* patient and total lesion load increased in all but a single subject. This demonstrates that the improvements in lesion detection afforded by 4 T imaging apply to a wide range, if not all, MS patients, regardless of differences in disease course and lesion characteristics.

Lesion load estimates are inherently variable due to the biological heterogeneity of multiple sclerosis both within and between patients, and the many variables involved in both the acquisition and analysis of images including imaging hardware, pulse sequences, image acquisition parameters, patient repositioning, segmentation method and operator and observer experience. Owing to this wide variability, while single-patient analysis may provide insight into the natural history of multiple sclerosis, it remains essential to look at pooled data such as total lesion load from multiple patients (Evans *et al.*, 1997). Although there was a significant, though not unexpected, amount of variability between the results from individual patients in this study, a clear pattern of improved lesion detection at 4 T emerged upon analysis of the pooled data. Due to the large increase in the number of lesions, volume of lesions, and total lesion load detected on the high-resolution 4 T images as compared to the lower-resolution 0.5 T and 1.5 T images, although possible, it is highly improbable that the improvement in lesion detection was simply an artifact of the inherent variability of lesion load estimates. In fact, the possible error in lesion load

estimates introduced by the interslice gap and interscan delay present in some of the data sets, and by discrepancies in image SNR and CNR between the high-resolution and lower resolution images appears to be negligible. While the exact effect of the small sample size in undetermined, the number of patients used in the current study is comparable to that used in previous studies of lesion load estimates. Even when the estimated percent error in lesion load volumes due to the use of different MR scanners (≈6%), repositioning error (≈15%), and intraobserver variability (≈6%) are summed, the resultant total estimated error is 37%. Since intraobserver error contributes to both the interscanner error and repositioning error estimates, and likewise, repositioning error contributes to interscanner error estimates, this total error value in likely overestimated. Nevertheless, even if 37% of the increase in lesion load seen in this study was in fact due to measurement uncertainty, this fact would account for less than half of the observed increase, leaving little doubt that, based on the assumptions discussed above, a substantial increase in lesion detectability did occur as a result of the improved resolution of the 4 T images.

7

Conclusion

7.1 Summary of Results

High-resolution magnetic resonance imaging of multiple sclerosis patients at 4 Tesla results in dramatically improved lesion detection which may have important implications for the study of MS and the design and monitoring of treatment trials. The increase in intrinsic signal-to-noise ratio afforded by the use of a 4 T magnetic field permits the acquisition of images with increased in-plane and out-of-plane resolution in times comparable to those used in current clinical settings to obtain lower-resolution images at 0.5 T and 1.5 T. This improvement in image quality generally results in a large increase in both the number and volume of MRI-visible lesions, with a subsequent increase in total lesion load detected. In the current study, the use of 0.8 mm^3 voxels at 4 T, as compared to voxel volumes ranging from 2.6 mm^3 to 5.3 mm^3 at 0.5 and 1.5 T, resulted in a 65% increase in the total number of lesions detected, an 85% increase in the mean lesion volume measured, and an 84% increase in total lesion load. While

the degree of per patient increase in lesion load still depends on the number, size distribution and location of lesions in any given individual, the decrease in partial volume effects that accompanies the use of high-resolution images should reduce the variations in lesion load estimates produced by inaccurate repositioning. Thus, high-resolution 4 T imaging has the potential to substantially increase the accuracy of large-scale multi-center clinical trials and serial studies of MS in which partial volume effects can lead to large variations in estimated lesion loads. Improved lesion detection may in turn permit the earlier diagnosis of clinically definite MS, increase the prognostic value of MRI lesion load estimates, and lead to a better understanding of the underlying pathological process of the disease.

While high-resolution imaging at 4 T enables a large number of small, previously MRI-invisible lesions to be visualized, these small lesions have a minor impact on the increase in total lesion load, with an average of 88% of the observed increase arising from the greater 4 T volume of lesions that are detected, albeit with smaller volumes, on lower-resolution images. The identification of these small lesions, however, and the fact that standard-resolution images appear to produce surprisingly variable and unreliable volume estimates for lesions with volumes below 1 cm^3 could have great significance for the selection and monitoring of subjects in treatment trials aimed at the early stages of disease. The detection of large numbers of these small lesions, which in the current study represented 49% of all the lesions identified at 4 T (but only accounted for 6% of the total lesion volume), may also help to explain the discrepancies observed in studies of normal-appearing white matter and the poor correlation that has been found between lesion load and clinical disability to date.

7.2 Future Directions

This study represents an important first step in the evaluation of the benefits of high-field, high-resolution imaging. Although the objectives of the current study dictated the use of different pulse sequences and different imaging parameters at high and low-field, now that it appears clear that lesion detection is substantially improved on high-resolution 4 T images, future studies in which the differences between image sets are reduced will allow for a more detailed investigation of the relative contribution of increased field strength, decreased slice thickness, smaller pixel size, and pulse sequence to the observed increase in estimated lesion load. While measurement errors due to interscanner variations, imprecise repositioning, and intraobserver variability are unavoidable in field strength studies comparing lesion volume estimates, other sources of uncertainty can probably be eliminated, or at least reduced, in future work. Hardware permitting, it would be highly desirable to compare images from 4 T and 0.5 or 1.5 T scanners that were acquired using similar pulse sequences. Although the exact implementation of imaging pulse sequences is manufacturer specific, modification of the manufacturer-provided software and careful selection of imaging parameters should permit the acquisition of images with similar T1 and T2 weighting, thereby reducing the possible influence of variations in image contrast on the results. The comparison of image sets with similar slice thicknesses and interslice gaps would also yield interesting data. For instance, if increases in lesion detection similar to those observed in this study could be achieved through the use of very thin slices without a simultaneous increase in matrix size, the time required to acquire relatively high-resolution images could be reduced. A serial study employing both standard resolution 1.5 T imaging as well as high-resolution 4 T imaging should also be conducted in order to

ascertain whether the short-term fluctuations observed in lesion volumes using standard 1.5 T images are a result of the relatively poor resolution of these images or reflect actual changes in lesion morphology. If lesion volumes turn out to be more stable when measured at 4 T, the variability in lesion load estimates would be reduced and our understanding of lesion pathophysiology would be improved.

Considering that variation in disease progression and lesion characteristics both between and within patients is a hallmark of multiple sclerosis, future comparison of lesion detection at high and low field would benefit from an increase in the number of patients studied. Since using a large number of patients presents economic, as well as logistical difficulties, perhaps selection criteria could be developed for the recruitment of suitable subjects. Not only would the number of participants eliminated due to claustrophobia and bladder incontinence be reduced, but patients with specific levels of functional disability or lesion loads could also be selected, thereby possibly reducing the interpatient variability in results. Every effort should be made to minimize the delay between imaging exams in order to avoid unnecessarily complicating the analysis of results. Keeping in mind the considerable time and resources required to conduct a clinical study, as well as the ever-present biological heterogeneity among patients and the time-consuming and subjective nature of current image segmentation techniques, a study employing a "lesion" phantom is perhaps the next logical step in the investigation of high-resolution 4 T imaging. Such a phantom study, where the "truth" is known, would allow the accuracy and precision of volume measurements of small objects under ideal conditions to be compared at high and low field. In this way, the factors that contribute to the increase in lesion number and volume detected on high-resolution 4 T images can be investigated under more controlled conditions. The results of this

research and those of subsequent studies will hopefully encourage the use of high resolution 4 T imaging, a technique that clearly has the potential to significantly improve our understanding and management of multiple sclerosis.

References

Adams CW: Pathology of multiple sclerosis: progression of the lesion. *Br Med Bull* **33**:15-20, 1977.

Allen IV, and McKeown SR: A histological, histochemical and biochemical study of the macroscopically normal white matter in multiple sclerosis. *J Neurol Sci* **41**:81-91, 1979.

Armspach JP, Gounot D, Rumbach L., and Chambron J: In vivo determination of multiexponential T2 relaxation in the brain of patients with multiple sclerosis. *Magn Reson Imaging* **9**:107-13, 1991.

Arnold DL, Matthews PM, Francis G, and Antel J: Proton magnetic resonance spectroscopy of human brain *in vivo* in the evaluation of multiple sclerosis: assessment of the load of disease. *Magn Reson Med* **14**:154-9, 1990.

Barbosa S, Blumhardt LD, Roberts N, Lock T, and Edwards RHT: Magnetic resonance relaxation time mapping in multiple sclerosis: Normal Appearing White Matter and the "invisible" lesion load. *Magn Reson Imaging* **12**:33-42, 1994.

Barkhof F, Filippi M, van Waesberghe JH, Molyneux P, Rovaris M, Lycklama a Nijeholt G, *et al.*: Improving interobserver variation in reporting gadolinium-enhanced MRI lesions in multiple sclerosis. *Neurology* **49**:1682-8, 1997.

Barkhof F, Scheltens P, Freguin ST, Nauta JJ, Tas MW, Valk J, *et al.*: Relapsing-remitting multiple sclerosis: sequential enhanced MR imaging vs clinical findings in determining disease activity. *AJR Am J Roentgenol* **159**:1041-7, 1992.

Bastianello S, Pozzilli C, Bernardi S, Bozzao L, Fantozzi LM, Buttinelli C, *et al.*: Serial study of gadolinium-DTPA MRI enhancement in multiple sclerosis. *Neurology* **40**:591-5, 1990.

Bilaniuk LT, Zimmerman RA, Wehrli FW, *et al.*: Cerebral magnetic resonance: comparison of high and low filed strength imaging. *Radiology* **153**:409-14, 1984a.

Bilaniuk LT, Zimmerman RA, Wehrli FW, *et al.*: Magnetic resonance imaging of pituitary lesions using 1.0 to 1.5 T field strength. *Radiology* **153**:415-8, 1984b.

Bloch F, Hansen WW, and Packard ME: Nuclear induction. *Phys Rev* **70**:460-73, 1946.

Bottomley PA, and Andrew ER: RF magnetic field penetration, phase shift and power dissipation in biological tissue: implications for NMR imaging. *Phys Med Biol* **23**:630-43, 1978.

Brainin M, Neuhold A, Reisner T, Maida E, Lang S, and Deecke L: Changes within the "normal" cerebral white matter of multiple sclerosis patients during acute attacks and during high dose cortisone therapy assessed by means of quantitative MRI. *J Neurol Neurosurg Psychiatry* **52**:1355-9, 1989.

Bruhn H, Frahm J, Merboldt KD, Hanicke W, Hanefield F, Christen HJ, *et al.*: Multiple sclerosis in children: cerebral metabolite alterations monitored by localised proton magnetic resonance spectroscopy in vivo. *Ann Neurol* **32**:140-50, 1992.

Chen CN, Sank VJ, Cohen SM, and Hoult DI: The field dependence of NMR imaging, I. Laboratory assessment of signal-to-noise ratio and power deposition. *Magn Reson Med* **3**:722-9, 1986.

Crooks LE, Arakawa M, Hoenninger J, *et al.*: Nuclear magnetic resonance whole-body imager operating at 3.5 kGauss. *Radiology* **143**:169-74, 1982.

Crooks LE, Arakawa M, Hoenninger J, *et al.*: Magnetic resonance imaging: effects of magnetic field strength. *Radiology* **151**:127-33, 1984.

Davie CA, Hawkins CP, Barker GJ, Brennan A, Tofts PS, Miller DH, *et al.*: Serial proton magnetic resonance spectroscopy in acute multiple sclerosis lesions. *Brain* **117**:49-58, 1994.

Dousset V, Grossman RI, Ramer KN, *et al.*: Experimental allergic encephalomyelitis and multiple sclerosis: lesion characterization with magnetization transfer imaging. *Radiology* **182**:483-91, 1992.

Ebers GC and Sadovnick AD: Epidemiology. In Paty DW and Ebers GC (eds.): *Multiple Sclerosis*, pp 1-28. F.A. Davis Company, Philadelphia, 1998.

Evans AC, Frank JA, Antel J and Miller DH: The role of MRI in clinical trials of multiple sclerosis: comparison of image processing techniques. *Ann Neurol* **41**:125-32, 1997.

Filippi M, Campi A, Dousset V, Baratti C, Martinelli V, Canal N, *et al.*: A magnetization transfer imaging study of normal-appearing white matter in multiple sclerosis. *Neurology* **45**:478-82, 1995b.

Filippi M, Gawne-Cain ML, Gasperini C, van Waesberghe JH, Grimaud J, Barkhof F, *et al.*: Effect of training and different measurement strategies on the reproducibility of brain MRI lesion load measurements in multiple sclerosis. *Neurology* **50**:238-244, 1998c.

Filippi M, Horsfield MA, Ader HJ, Barkhof F, Bruzzi P, Evans A, *et al.*: Guidelines for using quantitative measures of brain magnetic resonance imaging abnormalities in monitoring the treatment of multiple sclerosis. *Ann Neurol* **43**:499-506, 1998d.

Filippi M, Horsfield MA, Bressi S, Martinelli V, Baratti C, Reganati P, *et al.*: Intra- and inter-observer agreement of brain MRI lesion volume measurements in multiple sclerosis a comparison of techniques. *Brain* **118**:1593-1600, 1995d.

Filippi M, Horsfield MA, Campi A, Mammi S, Pereira C, and Comi G: Resolution-dependent estimates of lesion volumes in magnetic resonance imaging studies of the brain in multiple sclerosis. *Ann Neurol* **38**:749-54, 1995c.

Filippi M, Horsfield MA, Morrissey SP, MacManus DG, Rudge P, McDonald WI, *et al.*: Quantitative brain MRI lesion load predicts the course of clinically isolated syndromes suggestive of multiple sclerosis. *Neurology* **44**:635-41, 1994.

Filippi M, Horsfield MA, Rovaris M, Yousry T, Rocca MA, Baratti C, *et al.*: Intraobserver and interobserver variability in schemes for estimating volume of brain lesions on MR images in multiple sclerosis. *AJNR Am J Neuroradiol* **19**:239-44, 1998b.

Filippi M, Horsfield MA, Tofts PS, Barkhof F, Thompson AJ, and Miller DH: Quantitative assessment of MRI lesion load in monitoring the evolution of multiple sclerosis. *Brain* **118**:1601-12, 1995d.

Filippi M, Marciano N, Capra R, Rocca MA, Prandini, Gasparotti R, *et al.*: The effect of imprecise repositioning on lesion volume measurement in patients with multiple sclerosis. *Neurology* **49**:274-6, 1997b.

Filippi M, Paty DW, Kappos L, Barkhof F, Compston DA, Thompson AJ, *et al.*: Correlations between changes in disability and T2-weighted brain MRI activity in multiple sclerosis. A follow-up study. *Neurology* **45**:255-60, 1995.

Filippi M, Rocca MA, Horsfield MA, Rovaris M, Pereira TA, Yousry TA, *et al.*: Increased spatial resolution using a three-dimensional T1-weighted gradient-echo MR sequence results in greater hypointense lesion volumes in multiple sclerosis. *AJNR Am J Neuroradiol* **19**:235-8, 1998.

Filippi M, van Waesberghe JH, Horsfield MA, Bressi S, Gasperini C, *et al.*: Interscanner variation in brain MRI lesion load measurements in MS: implications for clinical trials. *Neurology* **49**:371-377, 1997.

Filippi M, Yousry Y, Baratti C, *et al.*: Quantitative assessment of MRI lesion load in multiple sclerosis: a comparison of conventional spin-echo with fast-fluid-attenuated inversion recovery. *Brain* **119**:1349-55, 1996b.

Filippi M, Yousry T, Horsfield MA, Alkadhi H, Rovaris M, Campi A, *et al.*: A high-resolution three-dimensional T1-weighted gradient echo sequence improves the detection of disease activity in multiple sclerosis. *Ann Neurol* **40**:901-7, 1996.

Francis GS, Evans AC, and Arnold DL: Neuroimaging in multiple sclerosis. *Neurol Clin* **13**:147-71, 1995.

Friebolin, H: *Basic One- and Two-Dimensional NMR Spectroscopy: Second, enlarged edition*, pp V. VCH Publishers, New York, 1993.

Gareau PJ, Mitchell JR, Karlik SJ, and Rutt BK: In vivo multi-component T2 relaxation of normal guinea pig brain at 1.5T and 4T. *Proceedings of the ISMRM, Sixth Scientific Meeting and Exhibition*, Sydney, Australia, p 1339, 1998.

Gasperini C, Horsfield MA, Thorpe JW, Kidd D, Barker GJ, Tofts PS, *et al.*: Macroscopic and microscopic assessments of disease burden by MRI in multiple sclerosis: relationship to clinical parameters. *J Magn Reson Imaging* **6**:580-4, 1996.

Gass A, Baker GJ, Kidd D, Thorpe JW, MacManus D, Brennan A, *et al.*: Correlation of magnetic transfer ratio with clinical disability in multiple sclerosis. *Ann Neurol* **36**:62-7, 1994.

Gawne-Cain ML, Webb S, Tofts P, and Miller DH: Lesion volume measurement in multiple sclerosis: how important is accurate repositioning? *J Magn Reson Imaging* **6**:705-13, 1996.

Grimaud J, Lai M, Thorpe J, Adeleine P, Wang L, Barker GJ, *et al.*: Quantification of MRI lesion load in multiple sclerosis: a comparison of three computer-assisted techniques. *Magn Reson Imaging* **14**:495-505, 1996.

Hader WJ, Elliot M, and Ebers GC: Epidemiology of multiple sclerosis in London and Middlesex County, Ontario, Canada. *Neurology* **38**:617-621, 1988.

Hansson LG, Westesson PL, Katzberg RW, *et al.*: MR imaging of the temporomandibular joint: comparison of images of autopsy specimens made at 0.3 T and 1.5 T with anatomic cryosections. *AJR Am J Roentgenol* **152**:1241-4, 1989.

Harris JO, Frank JA, Patronas N, McFarlin DE, and McFarland HF: Serial gadolinium-enhanced magnetic resonance imaging scans in patients with early, relapsing-remitting multiple sclerosis: implications for clinical trials and natural history. *Ann Neurol* **29**:548-55, 1991.

Hart HR Jr., Bottomley PA, Edelstein WA, *et al.*: Nuclear magnetic resonance imaging: contrast-to-noise ratio as a function of strength of magnetic field. *AJR Am J Roentgenol* **141**:1195-201, 1983.

Haughton VM, Yetkin FZ, Rao SM, Rimm AA, Fisher ME, Papke RA, *et al.*: Quantitative MR in the diagnosis of multiple sclerosis. *Magn Reson Med* **26**:71-8, 1992.

Henkelman RM: Measurement of signal intensities in the presence of noise in MR images. *Med Phys* **12**:232-3, 1985.

Hiehle JF Jr., Lenkinski RE, Grossman RI, Dousset V, Ramer KN, *et al.*: Correlation of spectroscopy and magnetization transfer imaging in the evaluation of demyelinating lesions and normal appearing white matter in multiple sclerosis. *Magn Reson Med* **32**:285-93, 1994.

Hoult DI, Chen CN, and Sank VJ: The field dependence of NMR imaging, II. Arguments concerning an optimal strength. *Magn Reson Med* **3**:730-46, 1986.

IFNB Study Group, and University of British Columbia MS/MRI Analysis Group: Interferon beta-1b in the treatment of multiple sclerosis: final outcome of the randomized, controlled trial. *Neurology* **45**:1277-85, 1995.

Inman, RP: Disability indicies, the economic costs of illness, and social insurance: The case of multiple sclerosis. *Acta Neurol Scand Suppl* **70**:46-55, 1984.

Isaacs C, Li DK, Genton M, Jardine C, Grochowski E, Palmer M, *et al.*: Multiple sclerosis: A serial study using MRI in relapsing patients. *Neurology* **38**:1511-5, 1988.

Jack CR, Berquist Th, Miller GM, Forbes GS, Gray JE, Morin RL, *et al.*: Field strength in neuro-MR imaging: A comparison of 0.5 T and 1.5 T. *J Comput Asst Tomog* **14**:505-513, 1990.

Keller JS, Lo Vetri J, Barberi E, and Rutt BK: Optimization of field uniformity for arbitrarily shaped birdcage resonators. *Proceedings of the ISMRM, Fifth Scientific Meeting and Exhibition*, Vancouver, Canada. 1500, 1997.

Kermode AG, Thompson AJ, Tofts P, MacManus DG, Kendall BE, *et al.*: Breakdown of the blood-brain barrier precedes symptoms and other MRI signs of new lesions in multiple sclerosis. *Brain* **113**:1477-1489, 1990.

Kesserling J, Miller DH, MacManus DG, Johnson G, Milligan NM, Scolding N, *et al.*: Quantitative magnetic resonance imaging in multiple sclerosis: the effect of high dose methylprednisolone. *J Neurol Neurosurg Psychiatry* **52**:14-7, 1989.

Lacomis D, Osbakken M, and Gross G: Spin lattice relaxation (T1) times of cerebral white matter in multiple sclerosis. *Magn Reson Med* **3**:194-202, 1986.

Lai M, Hodgson T, Gawne-Cain M, Webb S, MacManus D, McDonald WI, *et al.*: A preliminary study into the sensitivity of disease activity detection by serial weekly magnetic resonance imaging in multiple sclerosis. *J Neurol Neurosurg Psychiatry* **60**:339-41, 1996.

Larsson HB, Frederiksen J, Kjaer L, Henriksen O, and Olesen J: In vivo determination of T1 and T2 in the brain of patients with severe but stable multiple sclerosis. *Magn Reson Med* **7**:43-55, 1988.

Larsson HB, Thomsen C, Frederiksen J, Stubgaard M, and Henriksen O: In vivo magnetic resonance diffusion measurement in the brain of patients with multiple sclerosis. *Magn Reson Imaging* **10**:7-12, 1992.

Lauterbur P: Image formation by induced local interactions, examples employing nuclear magnetic resonance. *Nature* **242**:190-1, 1973.

Lee DH, Vellet AD, Eliasziw M, Vidito L, Ebers GC, Rice GP, *et al.*: MR imaging field strength: Prospective evaluation of the diagnostic accuracy of MR for diagnosis of multiple sclerosis at 0.5 and 1.5T. *Radiology* **194**:257-62, 1995.

Lee J, Garwood M, Menon R, Adriany G, Andersen P, Truwit C and Ugurbil K: High contrast and fast three-dimensional magnetic resonance imaging at high fields. *Magn Reson Med* **34**:308-12, 1995.

Loevner LA, Grossman RI, Cohen JA, Lexa FJ, Kessler D, and Kolson DL: Microscopic disease in normal-appearing white matter on conventional MR images in patients with multiple sclerosis: assessment with magnetization-transfer measurements. *Radiology* **196**:511-5, 1995.

Mastronardo G, Rocca MA, Rovaris M, Origgi D, Reganati P, Comi G, *et al.*: A comparison of the sensitivity of monthly unenhanced and enhanced MRI techniques in detecting new multiple sclerosis lesions. *Proceedings of the ISMRM, Sixth Scientific Meeting and Exhibition*, Sydney, Australia, p 1314, 1998.

McDonald WI: The pathological and clinical dynamics of multiple sclerosis. *J Neuropathol Exp Neurol* **53**:338-43, 1994.

McDonald WI and Sears TA: The effects of experimental demyelination on conduction in the central nervous system. *Brain* **93**:583-598, 1970.

Miller AE: Clinical Features. In Cook SE (ed.): *Handbook of Multiple Sclerosis*, pp 201-221. Marcel Dekker, Inc., New York, 1996.

Miller DH, Albert PS, Barkhof F, Francis G, Frank JA, Hodgkinson A, *et al.*: Guidelines for the use of magnetic resonance techniques in monitoring the treatment of multiple sclerosis. *Ann Neurol* **39**:6-16, 1996.

Miller DH, Barkhof F, Berry I, Kappos L, Scotti G, and Thompson AJ: Magnetic Resonance Imaging in monitoring the treatment of multiple sclerosis: concerted action guidelines. *J Neurol Neurosurg Psychiatry* **54**:683-8, 1991.

Miller DH, Grossman RI, Reingold SC, and McFarland HF: The role of magnetic resonance techniques in understanding and managing multiple sclerosis. *Brain* **121**:3-24, 1998.

Miller DH, Johnson G, Tofts PS, MacManus D, and McDonald WI: Precise relaxation time measurements of normal-appearing white matter in inflammatory central nervous system disease. *Magn Reson Med* **11**:331-6, 1989.

Miller DH, Rudge P, Johnson G, Kendall BE, MacManus DG, Moseley IF, *et al.*: Serial gadolinium enhanced magnetic resonance imaging in multiple sclerosis. *Brain* **111**:927-39, 1988.

Mitchell JR, Karlik SJ, Lee DH, and Fenster A: Computer-assisted identification and quantification of multiple sclerosis Lesions in MR imaging volumes in the brain. *J Magn Reson Imaging* **4**:197-208, 1994.

Mitchell JR, Karlik SJ, Lee DH, Eliasziw M, Rice GP, and Fenster A: The variability of manual and computer assisted quantification of multiple sclerosis lesion volumes. *Med Phys* **23**:85-97, 1996.

Molyneux PD, Tubridy N, Parker GJM, Barker GJ, MacManus DG, Tofts PS, *et al.*: The effect of slice thickness between 1 and 5mm with #D fast-FLAIR on MRI lesion detection and quantification in multiple sclerosis. *Proceedings of the ISMRM, Sixth Scientific Meeting and Exhibition*, Sydney, Australia, p 1321, 1998.

Morrissey SP, Miller DH, Kendall BE, Kingsley DP, Kelly MA, Francis DA, *et al.*: The significance of brain magnetic resonance imaging abnormalities at presentation with clinically isolated syndromes suggestive of multiple sclerosis. A 5-year follow-up study. *Brain* **116**:135-46, 1993.

O'Riordan JI, Thompson AJ, Rudge P, McDonald WI, and Miller DH: The long term risk of multiple sclerosis following clinically isolated syndromes of the central nervous system [abstract]. *J Neurol* **243**:Suppl 2:S33, 1996.

Ormerod IE, Johnson G, MacManus D, and du Boulay EP: Relaxation times of apparently normal cerebral white matter in multiple sclerosis *Acta Radiol* **369**:382-4, 1986.

Ormerod IE, Miller DH, McDonald WI, de Boulay EP, Rudge P, Kendall BE, *et al.*: The role of NMR imaging in the assessment of multiple sclerosis and isolated neurological lesions: a quantitative study. *Brain* **110**:1579-616, 1987.

Orrison WW, Stimac GK, Stevens EA, *et al.*: Comparison of CT, low-field-strength MR imaging, and high-field-strength imaging. *Radiology* **181**:121-7, 1991.

Pan JW, Hetherington HP, Vaughan JT, Mitchell G, Pohost GM, and Whitaker JN: Evaluation of multiple sclerosis by 1H spectroscopic Imaging at 4.1 T. *Magn Reson Med* **36**:72-7, 1996.

Paty DW, Li DK, UBC MS/MRI Study Group, and IFNB Multiple Sclerosis Study Group: Interferon beta-1b is effective in relapsing-remitting multiple sclerosis. II. MRI analysis results of a multicenter, randomized, double-blind, placebo-controlled trial. *Neurology* **43**:641-3, 1993.

Paty DW and Ebers GC: Clinical Features. In Paty DW and Ebers GC (eds.): *Multiple Sclerosis*, pp 135-191. F.A. Davis Company, Philadelphia, 1998.

Posin JP, Arakawa M, Crooks LE, *et al.*: Hydrogen MR imaging of the head at 0.35 T and 0.7 T: effects of magnetic field strength. *Radiology* **157**:679-83, 1985.

Purcell EM, Torrey HC, and Pound RV: Resonance absorption by nuclear magnetic moments in a solid. *Phys Rev* **69**:37-8, 1946.

Rinck RA, Fischer HW, Vander Elst L, Van Haverbeke Y, and Muller RN: Field-cycling relaxometry: medical applications. *Radiology* **168**:843-9, 1988.

Rocca MA, Rovaris M, Sormani MP, Horsfield MA, Comi G, and Filippi M: Intra- and inter-observer variability in measuring lesion volume changes on serial brain MR scans in patients with multiple sclerosis. *Proceedings of the ISMRM, Sixth Scientific Meeting and Exhibition*, Sydney, Australia, p 1317, 1998.

Rovaris M, Gawne-Cain ML, Wang L, and Miller DH: A comparison of conventional and fast spin-echo sequences for the measurement of lesion load in multiple sclerosis using a semi-automated contour technique. *Neuroradiology* **39**:161-5, 1997.

Rumbach L, Armspach JP, Gounot D, Namer IJ, Chambron J, *et al.*: Nuclear magnetic resonance T2 relaxation times in multiple sclerosis. *J Neurol Sci* **104**:176-81, 1991.

Rumsby, MG: Organization and structure in central-nerve myelin. *Biochem Soc Trans* **6**:448-62, 1978.

Sadovnick AD, Ebers GC, Wilson RW, and Paty, DW: Life expectancy in patients attending multiple sclerosis clinics. *Neurology* **42**:991-4, 1992.

Sappey-Marinier D: High resolution NMR spectroscopy of cerebral white matter in multiple sclerosis. *Magn Reson Med* **15**:229-39, 1990.

Seidenwurn D, Meng TK, Kowalski H, *et al.*: Intracranial hemorrhagic lesions: evaluation with spin-echo and gradient-refocused MR imaging at 0.5 and 1.5 T. *Radiology* **172**:189-94, 1989.

Sheldon JJ, Siddharthan R, Tobias J, *et al.*: MR imaging of multiple sclerosis: comparison with clinical and CT examinations of 74 patients. *AJNR Am J Neuroradiol* **6**:683-690, 1985.

Steinberg HV, Alarcon JJ, and Bernadino ME: Focal hepatic lesions: Comparative MR imaging at 0.5 and 1.5 T. *Radiology* **174**:153-6, 1990.

Stewart WA, Hall LD, Berry K, and Paty DW: Correlation between NMR scan and brain slice data in multiple sclerosis [letter]. *Lancet* **2**:412, 1984.

Stone L, Albert PS, Smith ME, *et al.*: Changes in the amount of diseased white matter over time in patients with relapsing-remitting multiple sclerosis. *Neurology* **45**:1808-14, 1995.

Strupp JP: Stimulate: A GUI based fMRI analysis software package. *NeuroImage* **3**:S607, 1996.

Thompson AJ, Kermode AG, Wicks D, MacManus DG, Kendall BE, Kingsley DP, *et al.*: Major differences in the dynamics of primary and secondary progressive multiple sclerosis. *Ann Neurol* **29**:53-62, 1991.

Thompson AJ, Miller D, Youl B, MacManus D, Moore S, Kingsley D, *et al.*: Serial gadolinium-enhanced MRI in relapsing/remitting multiple sclerosis of varying disease duration. *Neurology* **42**:60-3, 1992.

Tomiak MM, Rosenblum JD, Prager JM and Metz CE: Magnetization transfer: a potential method to determine the age of multiple sclerosis lesions. *AJNR Am J Neuroradiol* **15**:1569-74, 1994.

Verhoye MR, Gravenmade EJ, Raman ER, Van Reempts J, and Van der Linden A: In vivo noninvasive determination of abnormal water diffusion in the rat brain studied in an animal model for multiple sclerosis by diffusion-weighted NMR imaging. *Magn Reson Imaging* **14**:521-32, 1996.

Wang L, Lai HM, Thompson AJ, and Miller DH: Survey of the distribution of lesion size in multiple sclerosis: implication for the measurement of total lesion load. *J Neurol Neurosurg Psychiatry* **63**:452-5, 1997.

Weiner, HL: A 21 point unifying hypothesis on the etiology and treatment of multiple sclerosis. *Can J Neurol Sci* **25**:93-101, 1998.

Wicks DAG, Tofts PS, Miller DH, du Boulay GH, Feinstein A, Sacares RP, *et al.*: Volume measurement of multiple sclerosis lesions with magnetic resonance images: a preliminary study. *Neuroradiology* **34**:475-9, 1992.

Wiloughby EW, Grochowski E, Li DK, Oger J, Kastrukoff LF, and Paty DW: Serial magnetic resonance scanning in multiple sclerosis: a second prospective study in relapsing patients. *Ann Neurol* **25**:43-9, 1989.

Wolinsky JS, Narayana PA, and Fenstermacher MJ: Proton magnetic resonance spectroscopy in multiple sclerosis. *Neurology* **40**:1764-9, 1990.

Young IR, Hall AS, Pallis CA, Legg NJ, Bydder GM, and Steiner RE: Nuclear magnetic resonance imaging of the brain in multiple sclerosis. *Lancet* **ii**:1063-6, 1981.

Zelaya FO, Chalk JB, Mullins P, Brereton IM, and Doddrell DM: Localized 1H NMR spectroscopy of rat spinal cord in vivo. *Magn Reson Med* **35**:443-8, 1996.

Appendix A

A.1 Ethics Approval for Research Involving Human Subjects

The UNIVERSITY of WESTERN ONTARIO

Vice-Provost • Health Sciences • Health Sciences Centre

REVIEW BOARD FOR HEALTH SCIENCES RESEARCH INVOLVING HUMAN SUBJECTS

1996-97 CERTIFICATION OF APPROVAL OF HUMAN RESEARCH

ALL HEALTH SCIENCES RESEARCH INVOLVING HUMAN SUBJECTS AT THE UNIVERSITY OF WESTERN ONTARIO IS CARRIED OUT IN COMPLIANCE WITH THE MEDICAL RESEARCH COUNCIL OF CANADA "GUIDELINES ON RESEARCH INVOLVING HUMAN SUBJECT."

1996-97 REVIEW BOARD MEMBERSHIP

1) Dr. B. Borwein, Assistant Dean-Research · Medicine (Chairman) (Anatomy/Ophthalmology)
2) Ms. S. Hoddinott, Assistant Director of Research Services (Epidemiology)
3) Dr. R. Richards, St. Joseph's Hospital Representative (Surgery)
4) Dr. F. Rutledge, Victoria Hospital Representative (Critical Care · Medicine)
5) Dr. D. Bocking, University Hospital Representative (Physician · Internal Medicine)
6) Dr. L. Heller, Office of the President Representative (French)
7) Mrs. E. Jones, Office of the President Representative (Community)
8) Mr. H.E. Fleming, Office of the President Representative (Legal)
9) Dr. D. Freeman, Faculty of Medicine Representative (Clinical)
10) Dr. D. Sim, Faculty of Medicine Representative (Basic)(Epidemiology)
11) Dr. M.I. Kavaliers, Faculty of Dentistry Representative (Dentistry-Oral Biology)
12) Dr. H. Laschinger, Faculty of Nursing Representative (Nursing)
13) Dr. S.J. Spaulding, Faculty of Applied Health Sciences Representative (Occup. Therapy)
14) Dr. R. Rice, Faculty of Kinesiology Representative (Kinesiology)
15) Dr. W. Khalil, Research Institutes Representative (Endocrinology & Metabolism)
16) Mrs. R. Yohnicki, Administrative Officer
Alternates are appointed for each member.

THE REVIEW BOARD HAS EXAMINED THE RESEARCH PROJECT ENTITLED:
"MRI and MRS of MS patients at 4T."

REVIEW NO: E5502

AS SUBMITTED BY: Dr. S. Karlik, Diagnostic Radiology, Victoria/University Hospital

AND CONSIDERS IT TO BE ACCEPTABLE ON ETHICAL GROUNDS FOR RESEARCH INVOLVING HUMAN SUBJECTS UNDER CONDITIONS OF THE UNIVERSITY'S POLICY ON RESEARCH INVOLVING HUMAN SUBJECTS.

APPROVAL DATE: August 30, 1996 (UWO Protocol, Letter of Information & Consent)

AGENCY:

TITLE:

Bessie Borwein

Bessie Borwein, Chairman

c.c. Hospital Administration

London, Ontario • Canada • N6A 5C1 • Telephone (519) 661-3036

A.2 Letter of Explanation

LETTER OF EXPLANATION

Magnetic Resonance Imaging and Spectroscopy of Multiple Sclerosis Patients at 4 Tesla

In this study, patients with multiple sclerosis (MS) will undergo a magnetic resonance imaging scan (MRI) and magnetic resonance spectroscopy (MRS):

a) to compare the sensitivity and specificity of brain imaging in magnetic fields of two different strengths
b) to use high Tesla field strength to characterize myelin related proteins in the brain
c) to use high Tesla field strength to characterize myelin related proteins in the spinal fluid.

The purpose of this form is to ask for your consent to take part in this study. Magnetic resonance imaging is an important diagnostic tool. You have previously had an MRI at London Health Sciences Centre. Magnetic scanners differ in the field strength and image quality.

London Health Sciences Centre/Robarts Research Institute has acquired a new magnetic scanner which will probably afford tremendous new insights into many diseases. In the current study, we are going to compare the image quality of the new scanner, compared to your previous scan done on the 1.5T scanner. It will probably take approximately 1.5 hours of your time. Information derived from the scan will be used to study myelin chemistry, to determine if there are unique features about brain and spinal fluid chemistry of patients with multiple sclerosis. This will be obtained from the scan and not require any further testing, beyond the time spent in the scanner.

Taking part in this study is voluntary. You may refuse to participate or withdraw from the study at any time with no effect on your future care. The information recorded is confidential: a number will be used by your doctor to identify your case. Your doctor can decide to take you out of the study at any time if he thinks that it is best for you. If you do not feel well or have any other medical problems during the study period, you should contact Dr. S. Karlik (519-663-3648), Dr. G. Rice or Jane Lesaux (Research Nurse) at (519-663-3456). If you have questions concerning this research or your rights as a patient please contact any of the above.

Telephone (519) 663-3000
University Campus • 339 Windermere Road, London, Ontario, Canada, N6A 5A5

A.3 Consent Form

CONSENT FORM

Magnetic Resonance Imaging and Spectroscopy of Multiple Sclerosis Patients at 4 Tesla

I have carefully read and understood all the information provided to me and I have received a copy of the consent form.

_____ _____

PATIENT'S SIGNATURE DATE

I confirm that the patient has freely agreed to participate in this study.

_____ _____

WITNESS SIGNATURE DATE

Telephone (519) 663-3000
University Campus • 339 Windermere Road, London, Ontario, Canada N6A 5A5

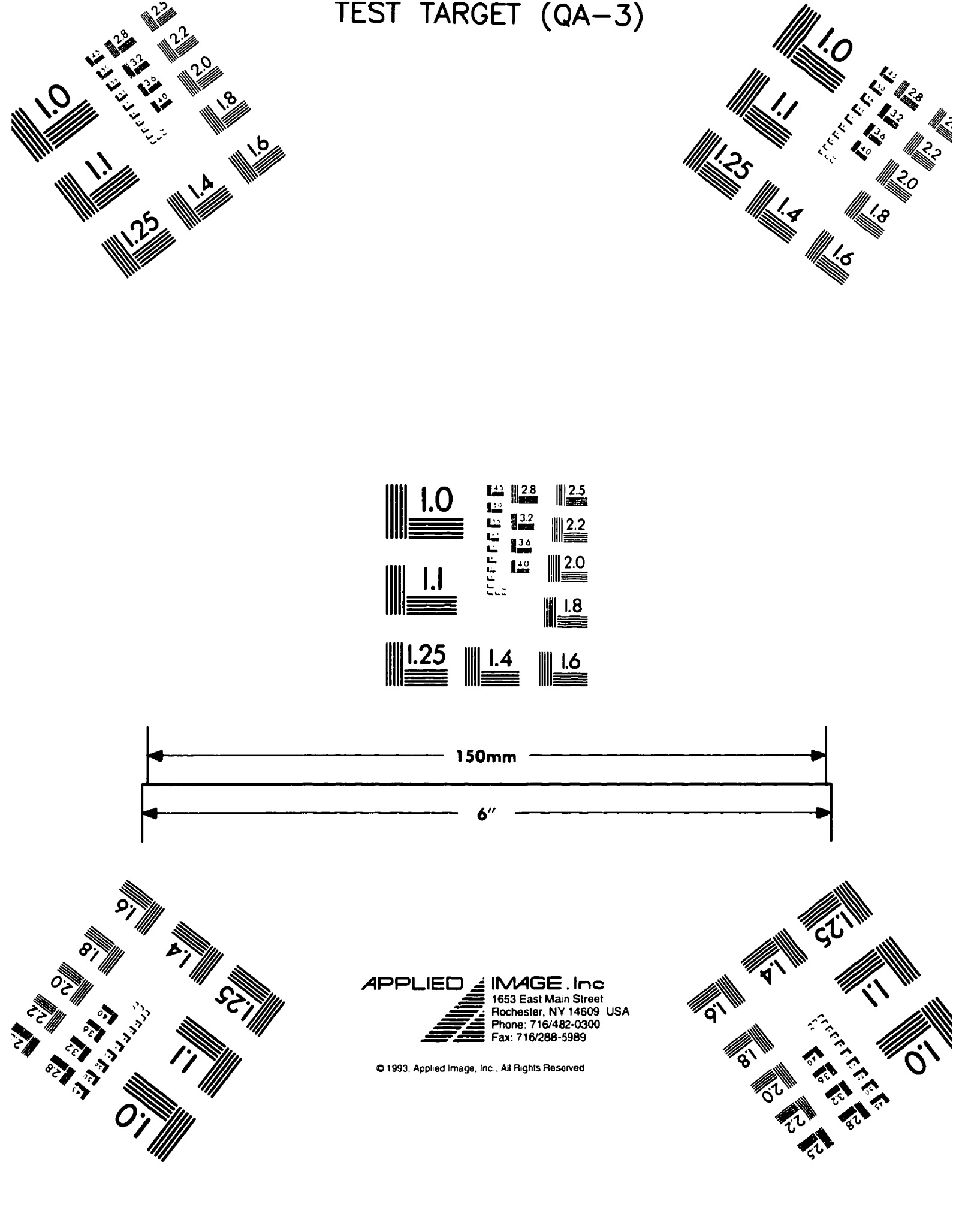
TEST TARGET (QA-3)
1.0
1.1
1.25
1.4
1.6
1.8
2.0
2.2
2.5
2.8
3.2
3.6
4.0
150mm
6"
APPLIED IMAGE, Inc
1653 East Main Street
Rochester, NY 14609 USA
Phone: 716/482-0300
Fax: 716/288-5989
© 1993, Applied Image, Inc., All Rights Reserved